STUDIES ON DAYLIGHT-RESPONSIVE DYNAMIC LIGHTING SYSTEM

Thesis submitted by

Pradip Kr Maiti

Doctor of Philosophy (Engineering)

Electrical Engineering Department
Faculty Council of Engineering & Technology
Jadavpur University
Kolkata, India

2019

JADAVPUR UNIVERSITY
KOLKATA - 700 032, INDIA

INDEX NO.: 14/16/E

1. Title of the Thesis: **STUDIES ON DAYLIGHT-RESPONSIVE DYNAMIC LIGHTING SYSTEM**

2. Name, Designation & Institution of the Supervisor:

Dr. Biswanath Roy
Professor
Electrical Engineering Department
Jadavpur University
Kolkata - 700032, India

3. List of Publication:

I. Journal publications:

i) **Maiti PK**, Roy B. 2019. Evaluation of a daylight-responsive, iterative, closed-loop light control scheme. *Lighting Research & Technology*. (*SAGE*). DOI: 10.1177/1477153519853318.

ii) **Maiti PK**, Roy B. 2018. Evaluation of a light controller for a LED-based dynamic light source. *Lighting Research & Technology*. (*SAGE*). 50(4): 571–582. DOI: 10.1177/1477153517690798.

iii) **Maiti PK**, Roy B. 2017. Development and performance assessment of white LED dimmer. *Journal of The Institution of Engineers (India): Series B*. (*Springer*). 98(5): 461-466. DOI: 10.1007/s40031-017-0275-7.

iv) **Maiti PK**, Roy B. 2015. Development of dynamic light controller for variable CCT white-LED light source. *LEUKOS: The Journal of the Illuminating Engineering Society of North America*. (*Taylor & Francis*). 11(4): 209-222. DOI:10.1080/15502724.2015.1011784.

II. International conference proceedings:

i) **Maiti PK**, Roy B. November 2015. Performance evaluation of developed LED dimmer on WLED parameters: Photometric. *In: Lux Pacifica 2015 Proceedings*; Kolkata (India). p. 312-319.

III. National conference proceedings:

i) **Maiti PK**, Singh AD, Roy B. 2017. Design and development of daylight responsive RF light controller. *In: 2017 IEEE Calcutta Conference (CALCON)*; Kolkata (India). p. 309-313.

4. List of Patents: Nil

5. List of Presentations in National/ International/ Conferences/ Workshops:

I. International conferences:

i) **Maiti PK**, Roy B. 27-29th November 2015. Performance evaluation of developed LED dimmer on WLED parameters: Photometric. *In: Lux Pacifica 2015*; Kolkata (India).

II. National conferences:

i) **Maiti PK**, Singh AD, Roy B. 2-3 December 2017. Design and development of daylight responsive RF light controller. *In: 2017 IEEE Calcutta Conference (CALCON)*; Kolkata (India).

Certificate from the Supervisor

This is to certify that the thesis entitled **Studies on daylight-responsive dynamic lighting system** submitted by **Shri Pradip Kr Maiti**, who got his name registered on **21st September, 2016** for the award of **Ph.D. (Engg.)** degree of Jadavpur University, is absolutely based upon his own work under the supervision of **Dr. Biswanath Roy** and that neither his thesis nor any part of the thesis has been submitted for any degree/ diploma or any other academic award anywhere before.

Date: Signature of the Supervisor

Office Seal

ACKNOWLEDGEMENT

This dissertation would not have been possible without the guidance and the help of several individuals who in one way or another contributed and extended their valuable assistance in the preparation and completion of this study.

First and foremost, with immense gratitude, I acknowledge the support and help extended by my supervisor, Dr. Biswanath Roy, whose encouragement, supervision and support from the preliminary to the concluding level enabled me to develop an understanding of the research problem. Apart from academic aspects, I would cherish all the moments shared in discussions with him, which helped me grow as a more matured person and also to develop the understanding about the lessons of life from different perspectives, more precisely and in an assertive way.

I consider it my privilege to express my sincere respect to Late Prof. (Dr.) Sunil Ranjan Bandyopadhyay, the Founder Professor of Illumination Engineering Laboratory at Electrical Engineering Department, Jadavpur University.

I owe my deepest gratitude to Dr. Manika Saha and Ms. Sarmistha Patel, who always stood beside me as my elder sister and sometimes as parent and also motivated me to study this subject as well as to complete this research work.

I wish to acknowledge the Government of West Bengal for providing the Senior Research Fellowship under State Government Fellowship Scheme to carry out the research work.

I am grateful to Head of the Department and all the faculty members and staff of the Electrical Engineering Department, specially Illumination Engineering Section, Jadavpur University for their direct and indirect cooperation and assistance towards completion of this work. I sincerely acknowledge the support and help received from all the research fellows and students working in the lab dur-

ing this period.

I wish to acknowledge the technical discussions and support received from Mr. Aniruddha Sengupta and Mr. Amit Majumder.

I wish to convey my thanks to Vineet K. Rohatgi, Director of Binay Opto Electronics Pvt. Ltd. for helping me to fabricate the LED luminaire used in this work.

This thesis would not have been possible without the support of my parents and my family, specially my elder brother, who took the pain all through these years of sacrificing the time they wanted to spend with me for the sake of my research. Last but not the least, I am thankful to the Supreme power for giving me the strength to plod on despite all my insecurities and troubles.

Date: (Pradip Kr Maiti)

Dedicated
to
My Parents

Nomenclature and Abbreviations

List of Symbols

x, *y*	CIE 1931 chromaticity
u',v'	CIE 1976 chromaticity
D_{uv}	Deviation in chromaticity
ΔE^*_{uv}	CIE 1976 CIELUV color difference
T_C	Correlated color temperature (*K*)
Φ	Luminous flux (*Lumen, lm*)
E	Illuminance (*Lux, lx*)
R_a	General color rendering index
R_9	Specific color rendering index for 9^{th} (saturated red) color sample
X,Y,Z	Tristimulus value
R,G,B	Response signal of RGB color sensor
P_i	Coefficient of curve-fitting equation
T	Tristimulus matrix
S	Sensor response matrix
C	Correlation matrix
T_{PWM}	Time period of PWM signal
DC	Duty cycle of PWM signal
Δ	Deviation
M	Blending ratio

Superscripts

W	WW LED array
C	CW LED array
b	Blended color
$mean$	Mean value
std	Standard deviation value
α	Internal light scene due to DLS
β	External daylight scene
H	Upper limit
L	Lower limit
T	Target value

Subscripts

$high$	Upper limit
low	Lower limit
avg	Average value
R	Required value
M	Measured value
MOD	Modified value
δ	Percentage variation

List of Abbreviations

CCT	Correlated color temperature
DLS	Dynamic lighting system
DLC	Dynamic light controller
WW	Warm white
CW	Cool white
LED	Light emitting diode
WLED	White light emitting diode
UDI	Useful daylight illuminance

Contents

List of Figures

List of Tables

Chapter 1

General Introduction

It is estimated that one third of the global consumption of electricity is utilised for lighting [Mirvakili and Koomson 2012]. Due to continuous increase in energy cost [Pinho et al. 2013], and the global need to reduce CO_2 emission [Jung et al. 2010; Pinho et al. 2013], the improved utilization of electrical energy is urgently needed. To comply with these demands, utilization of daylight is rapidly increasing for indoor illumination to reduce the amount of electric lighting load through energy efficient adaptive lighting system [Dong and Sanderson 2014]. It minimizes associated energy consumption required to meet lighting requirements. However, it would be impractical to rely entirely on daylight, because daylight is dynamic in quality (spectrum) and quantity. The spectral power distribution (SPD) and light level of daylight vary with time of a day, day of a month and season to season for a location [de Kort and Smolders 2010; Pinho et al. 2013]. Moreover, this dynamic pattern is location-specific. Therefore, adaptive integration of daylight with electric light is required to maintain the desired level of illumination and quality of overall lighting ambience within the work environment.

Conventional electric lamps have constant color appearance whereas color of daylight is dynamic as the spectral composition of daylight changes as a result of weather conditions and position of the sun [Ashdown 2002]. Most commonly used metric to describe the color appearance of a white light source is correlated color temperature (CCT) [Hernández-Andrés et al. 1999]. The CCT of daylight can vary from 2000K at sunrise through 5000K for direct daylight at noon and can exceed 10000K in overcast conditions [Gilman et al. 2013; Hernández-Andrés et al. 2001].

In natural environment, the transition in color of daylight is often not noticeable as only daylight is present and our visual system adapts to this smooth changing color of daylight. But in case of daylight integrated lighting system, the daylight and electric light will be simultaneously present and illuminate the areas of the work environment adjacent to the respective sources. As the CCT of electric light remains constant [Albu et al. 2013] and CCT of daylight varies with time of a day, light with two colors are si-

multaneously present in same work environment. Therefore, our visual system has to adapt continuously to a color somewhere between the colors of two light sources [Ashdown 2002; Gilman et al. 2013]. The difference in color beyond the tolerance limit is undesirable for visual task performance [Gilman et al. 2013] unless it is closed to the minimum-perceptible-color-difference (MPCD) [MacAdam 1985] which is represented by Δuv and

$$\Delta uv = \sqrt{(u - u_0)^2 + (v - v_0)^2}$$

where (u,v) is the source color coordinate and (u_0,v_0) is the required coordinate [MacAdam 1985]. Hence the system demands tunable or dynamic electric light source who's CCT can be varied in consonance with daylight and also light output can be varied to compensate the daylight level in the work environment. This dynamic electric light source meets the above mentioned requirements of a daylight integrated lighting system.

Recent research findings indicate that lighting has an impact on human biological and psychological systems [Anonymous 2004a; Belia et al. 2011; Boyce 2010, 2014; Curcio et al. 2016; Lin and Lin 2015; Mills et al. 2007; Rüger et al. 2006; Webb 2006]. Light can influence the regulation of the biological clock and the secretion of hormones, viz., melatonin and cortisol [Webb 2006]. During daytime, the secretion of melatonin is low and during dark period secretion is high [Reiter 1991]. Hence the exposure to light of suitable color and quantity at night time strongly suppresses the secretion of melatonin [Belia et al. 2011; Brainard et al. 2001; Heschong 2002; Lewy et al. 1980]. Whereas, the level of cortisol increases when exposed to high light levels in the morning, but not in the afternoon or evening [Rüger et al. 2006; Scheer and Buijs 1999]. These biological effects depend on the color temperature, light level, duration and the timing of exposure as well as on the size and position of the light sources [Morita and Tokura 1998; Rea et al. 2002; van Bommel 2006].

Recent research outcomes also indicate that the absence/ insufficiency of daylight in greenhouse cultivation can be effectively replenished with tunable artificial light sources and thus significantly

contributed to the improvements in the productivity of certain crops [Pinho et al. 2013]. The growth and development of plants are influenced by the quality (spectral composition), quantity (irradiance) and periodicity (time duration) of light exposure. The light quality mainly affects the morphological variables of plants while light quantity affects mostly the productivity of plants [Pinho et al. 2013].

The dynamic lighting has significant effect on ambience perception [Li et al. 2016; Lu et al. 2019; Wang et al. 2013]. In the study [Lu et al. 2019], the two dimensions of ambience perception were obtained and identified as coziness and liveliness using factor analysis for both illuminance and CCT change. This study shows that for illuminance changes, light of higher CCT is used to create liveliness and it increases with the increase of light level whereas the coziness increases with the linear variation of illuminance. On the other hand, variation of the CCT at higher illuminance level or variation from lower CCT to higher CCT creates the liveliness whereas the linear and quadratic variation of CCT offer the coziest ambience where quadratic variation results in the highest perceived evenness of change. The other study [Wang et al. 2013] shows that the dynamic lighting have a significant influence on ambience perception where more saturated light emitting diode (LED) light would lead to less tense, more cosy, more safe and more lively ambience perceptions and brighter lighting generates less tensed environment. If the speed of changing the ambience is increased then a more tense and less cosy ambience is created. So the medium speed creates the most lively and preferred ambience.

Another work [Canazei et al. 2014] indicates that the permanent morning shift workers, suffer from higher work-related psychophysiological stress due to advanced working hours and shortened sleep duration, could benefit from dynamic lighting scenarios. The authors found that the dynamic lighting had an acute psychophysiological calming effect and positively influenced sleep latency and anxiety/depression ratings.

The effects of dynamic lighting compared to static lighting on work-

ers' well-being, health and subjective performance in a longitudinal field was investigated [de Kort and Smolders 2010]. The results showed no significant differences in workers' need for recovery, vitality, sleep quality, mental health, headache and eyestrain, or subjective performance under both lighting conditions. But the workers reported that they are more satisfied in the dynamic lighting condition and at the same time they reported being disturbed by direct or reflected light.

The review of recent technical literatures explains the necessity of dynamic light source, i.e. an artificial light source of variable spectral composition or CCT and light output. Once the dynamic light source is practically realized, it can be applied for different purposes viz., daylight integration in case of indoor lighting and daylight simulation in case of greenhouse cultivation as well as indoor environment. Separate control algorithm is necessary for case specific applications. For a daylight integrated lighting system, the daylight is provided through openings such as windows and skylights that allow daylight into the building. But the daylight coming from the window is not always sufficient as the luminance of visible sky through window is variable throughout a day during the whole year. Apart from that the penetration of daylight into deep space through window is limited by the window height. Daylight pipe system is a good solution of this problem. The useful daylight illuminance (UDI) at the indoor space depends on the daylight availability at the window plane or the collector of daylight-pipe system. The daylight level higher than the UDI is available only near the windows or the emitter of the daylight-pipe system. So, energy savings through dimming can be achieved only for the luminaire adjacent to the windows or daylight pipe system. Hence, zone-specific control of light is required for the daylight integrated lighting system.

The limitation of practical implementation of a dynamic lighting system on the basis of economical and energy efficiency are-

- a dynamic lighting system requires special type of light source and additional control circuitry and hence imposes additional

cost to the system compared to any conventional lighting system. So, use of this system needs prior cost-benefit analysis

- for daylight-integrated lighting system, when the UDI is sufficiently greater than the required light level, then the dynamic lighting system can save a significant amount of energy by dimming of the light source. But when the UDI is less than the required light level, then the energy aspect of the dynamic lighting system is not viable.

For indoor illumination, the preferable color of illumination is white viz., warm white, neutral white and cool white and it can be produced by incandescent lamps, fluorescent lamps or LEDs [Albu et al. 2013]. These conventional electric light sources provide almost constant spectral composition [Albu et al. 2013; Webb 2006] and constant light output when operated at fixed supply voltage apart from the effect of depreciation due to aging [Royer 2014]. To meet time varying lighting requirements, light output of luminaires are to be controlled by using different dimming techniques. Dynamic pattern of spectral composition is to be achieved through blending of radiations from lamps of different spectral compositions by suitable control algorithm.

Recent advancements in white LED (WLED) technology have accelerated the trend of replacing conventional fluorescent light sources with WLEDs due to their higher energy efficiency, longer lifetime, compact size and environment friendliness [Chen et al. 2014; Protzman and Houser 2006]. WLEDs are also suitable as dimmable light source since these are current controlled light source and its light output varies approximately linear with its forward current [Schubert 2003; Žukauskas et al. 2002]. The variation of light output and color of the linear WLED array along its length is reported and analyzed in a recent research publication [Li et al. 2015]. Subjective visual perception of white illumination produced by light sources of different CCTs is studied [Rea and Freyssinier 2013] and performance of WLEDs to produce perceived white illumination is also experimentally evaluated [Houser et al. 2014]. Moreover, WLEDs show minimal reduction in luminous efficacy when compared to the conventional fluorescent light sources over a wide

dimming range [Albu et al. 2013]. These advantages establish the suitability of WLEDs for daylight integration.

Existing LEDs produce white light through one of the two means: ultra violet (UV) or blue LED with yellow phosphor [Chen et al. 2015; Lee et al. 2016]; by direct combination of three or more individual spectral emitters having peak spectrum emissions spaced across the visible spectrum [Dyble et al. 2005; Gilman et al. 2013]. These can include the application of red, green and blue (RGB) [Dyble et al. 2005; Muthu et al. 2002; Tang et al. 2014; Wang et al. 2010; Wu et al. 2014; Zhai et al. 2014] or red, yellow/amber, green and blue (RYGB) LEDs [Gilman et al. 2013]. Although the application of individual colored LED provides greater control on spectrum of emitted light, the green and yellow LEDs show significantly less efficiency than the blue and red LEDs [Crawford 2009; Gilman et al. 2013]. Apart from that these systems suffer from poor color rendering index (CRI), chromaticity shifts due to prolonged aging [Ng et al. 2014] and also required complex electronics [Gilman et al. 2013].

The effect of lamp lumen depreciation (LLD) on colorimetric shift [Royer 2014] is prominent due to variation of lumen depreciation rates for different colored LEDs used to produce white light. So the effect of LLD on colorimetric shift for phosphor-converted LEDs is less than mixed color LEDs. The phosphor-converted LEDs show lower colorimetric shift than above mixed color LED under both continuous current and pulse width modulation (PWM) dimming schemes [Dyble et al. 2005]. The SPD of LEDs varies with amplitude of current and the junction temperature [Dyble et al. 2005; Mirvakili and Koomson 2012]. In continuous current dimming scheme, the amplitude of continuous current is changed to vary the light output from LED. This variation of amplitude causes variation in junction temperature and hence SPD of emitted light changes. In case of PWM dimming topology, the amplitude of current remains constant, which results in stable SPD.

So, from the above discussions, the necessity of daylight-responsive dynamic light source is well explained. Dynamic light sources are

available commercially and also developed by various researcher but none of the products is daylight-responsive. Hence in the present work systematic approach is taken up to conceive suitable lighting control algorithm and subsequently to design and develop a daylight-responsive dynamic lighting system.

Problem Statement:

To design, develop and experimental evaluation of a dynamic lighting system which is capable of monitoring dynamic nature of daylight and hence tunes its spectral composition and lumen output in consonant to instantaneous available daylight to ensure visual comfort of occupants in an indoor space illuminated by daylight-integrated artificial lighting system.

Objective:

Development of a daylight-responsive dynamic lighting system.

Methodology:

A. System design and development:

A1. To obtain a composite light module, consisting of multiple sources of different spectral compositions, capable of meeting visual requirements of occupants in an indoor environment.

A2. To develop a sensor-based dynamic light controller to drive the developed composite light module as daylight-responsive dynamic lighting system.

B. Performance evaluation:

B1. To evaluate the desired photometric performance of the developed dynamic lighting system through

i) Laboratory experimentation and

ii) *In-situ* experimentation.

B2. To characterize the developed system in terms of
i) Electrical parameter and
ii) Photometric parameter.

Steps of Execution:

Step 1: Design and fabrication of composite WLED module

1.1. To measure spectral composition of commercially available white light emitting diode (WLED) of different CCTs (warm white, white, cool white).

1.2. To study the effect of dimming on electrical and photometric characteristics of above light sources with the variation of lamp input power through pulse width modulation (PWM) of lamp current.

1.3. To estimate required quantities of LED chips of different CCTs (spectral compositions) to design a LED module of specific electrical and photometric ratings.

Step 2: Design, development and testing of Dynamic Light Controller (DLC)

2.1. To design and develop a DLC and test under following purposes:

- to control light output of the developed composite WLED module at fixed CCT;
- to control CCT of the developed composite WLED module at fixed light output;
- to control both the CCT and light output of the developed composite WLED module under step variation and under continuous variation.

Step 3: Development of daylight-responsive Dynamic Lighting System (DLS)

3.1. To develop and calibrate a photo-sensor which is based on R-G-B color sensor, to monitor dynamic pattern of illuminance and CCT of available daylight.

3.2. To upgrade the developed DLC to open-loop daylight-responsive DLS by incorporating the developed photo-sensor.

3.3. To upgrade the above open-loop DLS to closed-loop daylight-responsive DLS.

Step 4: Evaluation of the developed daylight-responsive DLS

4.1. To evaluate the open-loop DLS under laboratory test set up and *in-situ* testing.

4.2. To evaluate the closed-loop DLS under laboratory test set up and *in-situ* testing.

4.3. To characterize electrical and photometric parameters of the developed DLS.

My Thesis:

Original Contribution:

The outcome of the present study is a WLED based daylight-responsive dynamic lighting system which is capable of tuning its lumen output as well as CCT by monitoring light level and CCT of instantaneous available daylight.

Organisation of the Thesis:

A brief description of existing publications on tunable LED lighting systems reported in reputed scientific and technical journals, technical datasheets of commercially available dynamic lighting system is presented in **Chapter 2**. The applications and necessities of such type of products and their limitations are also highlighted. At the end, research gap is identified and accordingly research questions are formulated.

The general descriptions on technical features and schemes of dynamic lighting system are discussed in **Chapter 3**. Working principles of commercially available dynamic lighting system are also briefly described highlighting their technical short comings. The salient features of the proposed dynamic lighting system, to overcome those short comings, are presented along with the background theory and scheme of the system.

Chapter 4 deals with the design and development of the composite LED module. The results of the study on photometric and colorimetric parameters of two types of phosphor-converted LED sources and the effect of dimming on these parameters are presented here. Layout of a typical WLED arrays are designed and a prototype is developed to obtain a composite LED module. The electrical and photometric parameters of the developed module are experimentally evaluated.

Chapter 5 describes the step-wise design and development of the DLC which is the primary component of DLS. The DLS is realised by connecting the developed DLC electrically with the developed composite LED module. The control logic embedded in the DLC can be modified accordingly to drive the DLS for three operational modes viz., (1) variable illuminance at fixed CCT, (2) variable CCT at fixed illuminance and (3) variable CCT and variable illuminance. The control logic can be modified to vary the CCT and illuminance of the DLS either in steps or continuously to follow a preset time varying pattern. Finally, results of the experimental evaluation of the developed system are presented.

Design and development of a daylight-responsive dynamic lighting system by means of two light control schemes- open-loop and closed-loop is presented in **Chapter 6**. One RGB color sensor, calibrated with *CL 200A* chromameter, is used to monitor the instantaneous daylight data at window plane. For closed-loop light control scheme, another calibrated RGB color sensor is used in the feedback path to monitor the output of the DLS and also to reduce the deviation between desired and measured data due to temperature variation and other physical process. Hardware prototype of both the light control schemes are developed, fabricated and subsequently performance is evaluated experimentally.

Chapter 7 contains the overall conclusions and the scope for future work.

The conceptual flow diagram of the Thesis is shown in **Figure 1.1**.

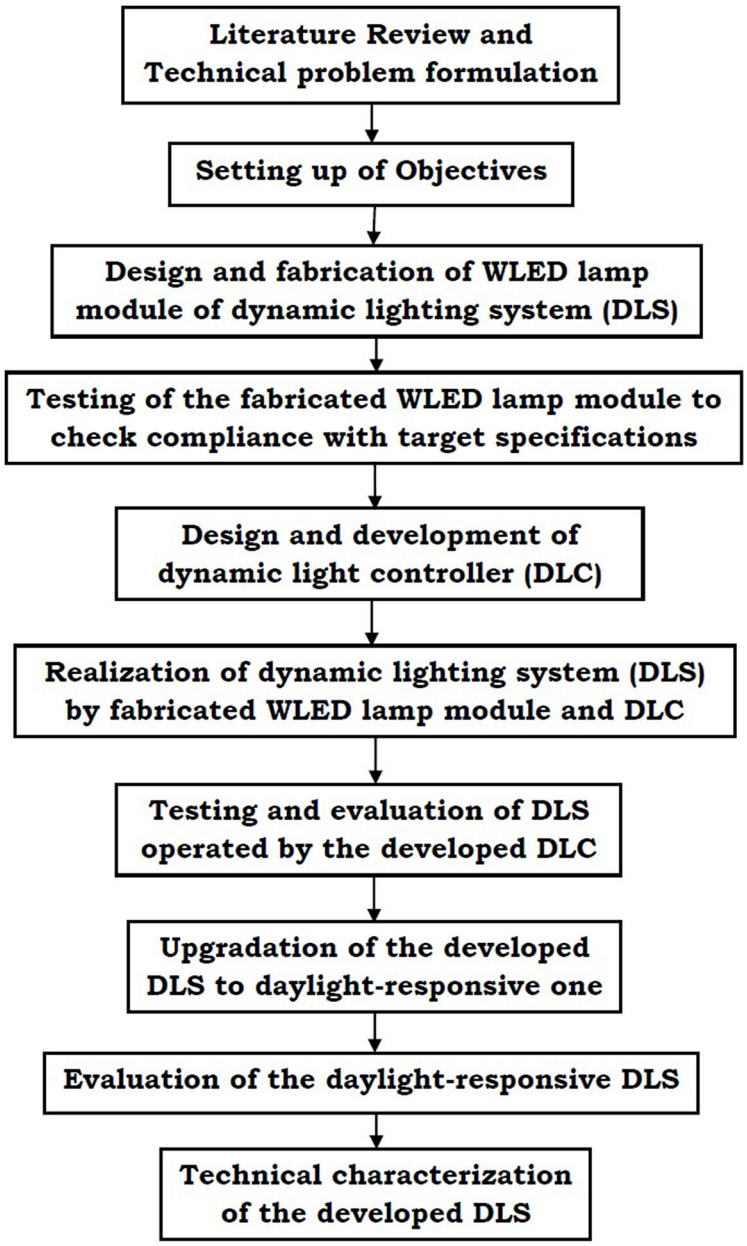

Figure 1.1: Conceptual flow diagram of the Thesis

Chapter 2

Literature Review

White light emitting diodes (WLEDs) are presently considered as most energy efficient light sources for indoor lighting applications [Cole et al. 2015; Kim et al. 2011; Kim and Schubert 2008; Mirvakili and Koomson 2012; Protzman and Houser 2006]. Apart from the energy efficiency, the most useful attribute of WLEDs lies in its tunability of spectral composition [Dyble et al. 2005; Gilman et al. 2013; Houser et al. 2014; Maiti and Roy 2015, 2018]. This aspect of WLED luminaires makes it technically compatible in daylight integrated artificial lighting system- an important component of modern building energy management system [Dikel et al. 2018; Koroglu and Passino 2014; Maiti and Roy 2017; Pandharipande and Caicedo 2013; Pandharipande et al. 2014; Tang et al. 2017; Uhm et al. 2010]. The spectral composition and light level of daylight is dynamic in nature which cause variation in CCT and illuminance with time of a day and sky condition [Ashdown 2002; de Kort and Smolders 2010; Pinho et al. 2013]. To make compatible a WLED luminaire with time-varying daylight scene within a room, its spectral composition is to be controlled and tuned accordingly [Gilman et al. 2013; Maiti and Roy 2015, 2018]. Thus, the applications of the tunable WLED luminaires eradicate the undesirable visual discomfort due to mismatch of time-varying CCT of daylight and time-invariant CCT of conventional artificial light sources [Maiti and Roy 2015]. With these attributes WLED luminaires can be considered as dynamic electric light sources.

In addition to the fulfilment of the requirements of modern building energy management system, tunable WLEDs are effective in greenhouse cultivation [Pinho et al. 2013] and also to meet biological and psychological requirements of human beings [Anonymous 2004a; Belia et al. 2011; Boyce 2010, 2014; Curcio et al. 2016; Lin and Lin 2015; Mills et al. 2007; Morita and Tokura 1998; Rüger et al. 2006; Scheer and Buijs 1999].

LED based dynamic light sources for indoor lighting applications are commercially available from a number of manufacturers viz., Lutron®, Telelumen®, Ketra®, LuxiTune^{TM}, lumenetix®. Technical and operational features of these products are available from the respective product datasheets. A brief description of these

products are given below-

Lutron® provides three types of color tuning facilities viz., *dim to warm*, *tunable white* and *full color tuning* [Anonymous 2016b]. Out of these products, *tunable white* resembles to the system developed in this research work and realized through two schemes. In one scheme, the LED light engines are controlled through dimmable drivers each with a separate control input generated from a single controller [Anonymous 2016b]. Here the LED drivers are the essential components of the system. In the other scheme, the LED light engine is controlled through a driver-cum-controller unit. Two separate control inputs are fed to the controller to control the intensity and color respectively [Anonymous 2016b]. However, these Lutron® products are incapable of following a custom made time varying pattern of intensity and color.

Telelumen® provides two multispectral LED luminaires viz., 16 channel *Light Replicator* and 5 channel *Penta* capable of produceing custom made spectral composition [Anonymous 2014b]. The operations of these products require optical spectrometer, LED luminaire and developer suit software [Anonymous 2014b]. Here also, driver-cum-controller is the integral part of the system.

Ketra® provides fully tunable LED product *S38 PAR* lamp. The lamp is a single source consists of both monochromatic and phosphor converted blue LED chip [Anonymous 2015a]. The driver and on-board wireless controller are the integral parts of the lamp. The on-board wireless controller controls the intensity and color according to the received signal [Anonymous 2015a].

LuxiTune^{TM} provides tunable light in a compact single emitter with two dimming modes viz., warm dimming and CCT tuning [Anonymous 2016c]. Here the compact single emitter consists of LED modules and driver-cum-controller. Two control signals are fed to the driver-cum-controller to control the intensity and color respectively [Anonymous 2016c]. LuxiTune^{TM} products are not also capable of following a custom made time varying pattern of intensity and color [Anonymous 2016c].

lumenetix® provides color tunable LED product to be realized by integrating araya[5] logic module (ALM) and araya[5] tunable color LED array of five different colors [Anonymous 2016d]. The ALM incorporates on-board driver electronics and control logic. Two control signals are needed for intensity and color variation [Anonymous 2016e]. Here also LED module and ALM are the integral parts of the system.

In all the above commercially available products, both the LED driver and controller are the integral part of the system. In some products control signals act directly on driver-cum-controller and in other products the control signals are fed to the dimmable driver to get desired color tuning.

The dynamic light sources, sometimes called as color tunable light sources, are also developed by various researchers. These dynamic light sources may be of two types viz., open-loop and closed-loop. The open-loop system has been developed by either red-amber-green-blue (RAGB) LED chips [Gilman et al. 2013] or phosphor-coated WLED [Chen et al. 2015; Kim et al. 2015; Malik et al. 2018, 2019].

The research work [Gilman et al. 2013] demonstrated a daylight-matched lamp with adjustable CCT where the CCT of the lamp is varied by blending the radiation from two sources of different CCTs viz., low CCT source and high CCT source. Each source comprises of RAGB LED chips with centre wavelengths of 464, 512, 598 and 634 nm and separately controlled to produce desired CCT point. PWM dimming scheme is incorporated in this work to reduce the colorimetric shift and binary PWM signal is used to generate the required spectral distribution for the given source where the power level of each of the four LEDs are controlled by their on-time. Using this method light of desired chromaticity can be produced but it requires complex algorithm and costly electronics to control the three or more different LEDs.

Another research works [Malik et al. 2018, 2019] demonstrated a

decoupled control schemes of CCT and illuminance of a LED based lamp where the radiation from a phosphor converted white LED is mixed with either blue or red LED chips to get CCT value higher or lower than that of the white LED respectively. This results in extra control circuitry. In Malik et al. [2018], PWM dimming is incorporated and the average forward voltages of active LEDs are measured at runtime to estimate the junction temperature and the luminous parameters which required additional time and cost. In Malik et al. [2019], the heat sink temperature is measured using three temperature sensors connected with each LED strings to estimate the junction temperature and fed to the control unit to mitigate the variation of luminous parameter due to junction temperature.

In the work [Chen et al. 2015], the CCT and illuminance of a bicolor WLED lamp is controlled by means of a nonlinear empirical luminous flux and CCT model of the LEDs which consider the thermal interdependence of the two constituting LEDs. A numerical solver is utilized to calculate the duty ratio of the two LEDs from the nonlinear empirical relations of CCT and flux.

Another research work [Kim et al. 2015] created various luminous environment by changing the luminous flux and CCT of a phosphor converted LED source consisting of four different CCT WLED chips viz., 2600K, 3500K, 4600K and 5600K. This LED luminaire is dimmed using a computer through dimming control software.

In the above works based on open-loop control scheme, some predefined CCT and illuminance points are achieved using step variation. However, the open-loop control scheme has some inherent limitations such as-

- incapable of monitoring the instantaneous achieved CCT and illuminance due to light source
- incapable of addressing the effect of ambient temperature as well as junction temperature variation on spectral composition and lumen output of WLEDs and also of lumen depreciation and spectral variation due to aging [Royer 2014].

So, for daylight responsive lighting system, a closed-loop scheme is essential to monitor the achieved light scene and also to compensate the above variations.

Different closed-loop control schemes, applied to control both the luminous flux output and CCT of bicolor or multicolor WLED lamp systems, are reported in earlier works [Chew et al. 2016; Lee et al. 2016]. In this work [Lee et al. 2016], a closed-loop dimming and color control scheme for a bicolor WLED module is reported where a non-linear relationship between duty cycle and luminous flux output is adopted which shows better performance compared to linear approximation. The empirical non-linear relationships are experimentally evaluated by considering the thermal interdependence of two color LEDs separately. A look-up table is then generated consisting of duty ratios for a finite set of required combination of luminous flux and CCT of tunable WLED source. This look-up table is embedded in the controller so that desired duty cycles of two LED arrays can be determined through piecewise linear interpolation to achieve a target light output and CCT. One RGB color sensor is used to obtain the feedback signal. Their proposed closed-loop control scheme works on an iterative cycle consists of two separate controls to be executed in turn- at first, flux control with constant CCT and then CCT control with constant flux. The reported maximum errors in luminous flux and CCT are 3% and 1.78% respectively. In another closed-loop control scheme [Chew et al. 2016], a spectral sensor is used to obtain the feedback signal. This control scheme is experimentally validated by a wireless communication system with three static target chromaticities. The reported maximum deviation of CCT is 5% and chromaticity deviation lies in 5-step $u'v'$ unit circle.

The above review indicates to the followings-

- the closed-loop control schemes are validated to achieve a set of target static combination of chromaticity and luminous flux
- control signals are directly fed to dimmable drivers- the essential component of the system

- the first work requires one look-up table to be generated from experimentally measured data which is product dependent
- the second work requires spectral composition data for each target spectrum.

These above features are not universally applicable to any commercial WLED luminaires to make it daylight responsive. So, to address this research gap, a dynamic light controller (DLC) is to be developed with the following additional technical features

- capable of varying the spectral composition and light output of the WLED to make it daylight-responsive
- compatible with a source of specific wattage range
- can control several sources connected to a constant current DC bus.

So, first research question originates from the above survey, is how to develop a dynamic light controller (DLC) with added technical features viz., compatible with a source of specific wattage range and electrically attachable between the LED module and its driver which are not available so far. This developed DLC can control several sources connected to a constant current DC bus. The second research question is how to upgrade the developed DLC technically to achieve daylight-responsive dynamic lighting system.

Chapter 3

Dynamic Lighting System: Schemes and Features

Necessities and applications of dynamic lighting system are described elaborately in **Chapter 2**. General descriptions on technical features and schemes of dynamic lighting system are presented here. Working principles of commercially available dynamic lighting system are also briefly described highlighting associated technical short comings. The salient features of the proposed dynamic lighting system, to overcome those short comings, are presented along with the background theory and technical scheme of the system.

3.1 Dynamic Lighting System (DLS)

Dynamic lighting system may be described by a lighting system of variable/ adjustable color appearance (CCT) and light output. In this sense, daylighting system is an example of natural dynamic lighting system. In this study, attempts have been made to obtain DLS by developing LED-based electric lamp system whose CCT and lumen output can be adjusted/varied by suitable control algorithm. Thus the primary components of DLS are the LED-based light source and dynamic light controller (DLC) as shown in **Figure 3.1**.

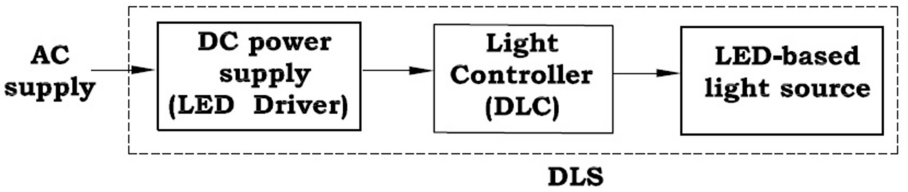

Figure 3.1: Block diagram of DLS

Theoretical as well as practical studies related to electrical energy savings that might be achieved by the integration of available daylight and artificial light have been carried out throughout the world by various lighting engineers and researchers. The spectral composition and light level of daylight vary throughout the day depending on the weather conditions and the position of the sun. This dynamic nature of daylight influences human physiology and psychology. There may be some spaces in offices and commercial buildings where available daylight is insufficient or even absent. The lack or absence of daylight may be compensated by a special electric light source which is able to simulate the ambience of dynamic nature of daylight. This special type of electric light source is referred to as a dynamic light source.

Conventional electric light sources provide almost constant spectral composition [Albu et al. 2013; Webb 2006] and constant light output when operated at fixed supply voltage apart from the ef-

fect of depreciation due to temperature variation and ageing [Royer 2014]. The light output of these traditional sources can be varied by using different dimming techniques. To achieve dynamic pattern of spectral composition, an unique feature of dynamic lamp, blending of radiation from multiple spectral emitters is done by suitable control algorithm. To follow daylight variation pattern, that support or enhance the natural rhythm of human's alertness, the CCT and light output of the DLS are to be varied with time of a day according to a preset protocol or as required.

Suitable light sources for daylight integration are white or cool white fluorescent lamp and WLED [Albu et al. 2013] which are to be dimmed accordingly to maintain constant illumination on the working plane. Recent advancements in WLED technology have accelerated the trend of replacing conventional fluorescent light sources with linear WLED arrays due to their higher energy efficiency, longer lifetime, compact size and environment friendliness [Chen et al. 2014; Protzman and Houser 2006]. However, the luminous flux and color parameters of linear WLED array vary due to current imbalance in the different parallel string along its length [Li et al. 2015]. It can be minimized with suitable wiring. Subjective visual perception of white illumination produced by light sources of different CCTs is studied [Rea and Freyssinier 2013] and performance of WLEDs to produce perceived white illumination is also experimentally evaluated [Houser et al. 2014]. Moreover, WLEDs show minimal reduction in luminous efficacy when compared to the conventional fluorescent light sources over a wide dimming range [Albu et al. 2013]. These advantages establish suitability of WLEDs for daylight integration.

Existing LEDs produce white light through one of the two means: ultra violet (UV) or blue LED with yellow phosphor; or by direct combination of three or more individual spectral emitters having peak spectrum emissions spaced across the visible spectrum [Dyble et al. 2005; Gilman et al. 2013]. These can include the application of red, green and blue (RGB) [Dyble et al. 2005]; or red, yellow, green and blue (RYGB) [Gilman et al. 2013] LEDs. Although the application of individual colored LED provides greater control on

spectrum of emitted light, the green and yellow LEDs show significantly less efficiency than the blue and red LEDs [Gilman et al. 2013]. Apart from that these systems suffer from poor color rendering index (CRI), chromaticity shifts due to prolonged aging [Ng et al. 2014] and also required complex electronics [Gilman et al. 2013].

The effect of lamp lumen depreciation (LLD) on colorimetric shift [Royer 2014] is prominent due to variation of lumen depreciation rates of different colored LEDs used to produce white light. In contrast, the effect of LLD on colorimetric shift for phosphor-converted blue LEDs is less than mixed color LEDs. The phosphor-converted LEDs also show lower colorimetric shift than above mixed color LED under both continuous current and pulse width modulation (PWM) dimming schemes [Dyble et al. 2005]. The SPD of LEDs varies with amplitude of current and the junction temperature [Dyble et al. 2005; Mirvakili and Koomson 2012]. In continuous current dimming scheme, the amplitude of continuous current is controlled to vary the light output from LED. This variation of amplitude causes variation in junction temperature and hence SPD of emitted light changes. In case of PWM dimming topology, the amplitude of current remains constant and this results in more or less stable SPD.

Like other semi-conductor diodes, LEDs have a non-linear relationship between forward current and voltage. If the forward voltage is varied even a small amount above the threshold voltage, the current through the LEDs and their light output are changed significantly. This imposes difficulty in precise control of light output. On the other hand, small changes in forward current cause small variation in light output. Therefore, current controlled method is preferred to drive and control the LEDs. The variation of light output of a $1W$ WLED chip with average forward current is represented by **Figure 3.2** [Maiti and Roy 2017] and it indicates that the light output of the LED varies almost linearly with forward LED current over a wide range. With the increment of forward current, the optical conversion non-linearity increases whereas photonic output efficiency decreases beyond the linear range [Schubert 2003;

Žukauskas et al. 2002].

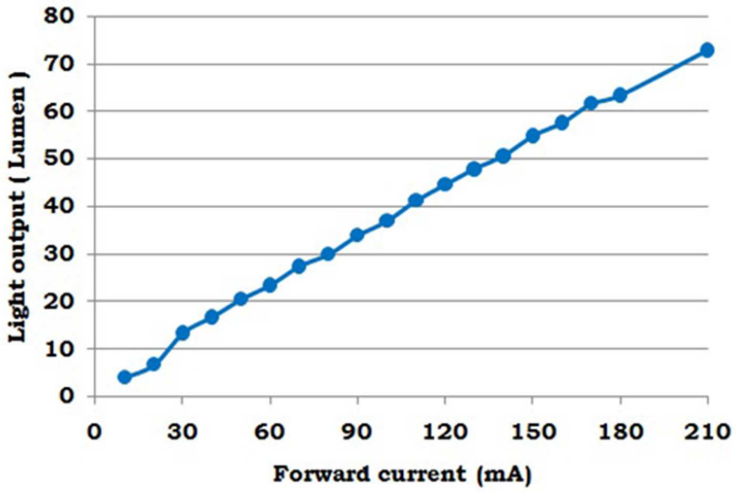

Figure 3.2: Variation of light output of a $1W$ WLED with forward current [Maiti and Roy 2017]

3.2 Commercial Dynamic Lighting System

Lutron® provides three types of color tuning facilities viz., *dim to warm*, *tunable white* and *full color tuning* [Anonymous 2016b]. Out of these products *tunable white* resembles to our proposed dynamic lighting system and is realized through two schemes -

i) Fixtures with two different CCT LED light engines: In this scheme, tunable white is achieved by separate control of two different CCT LED engines (e.g. $3000K$ and $5000K$) where the resulting color temperature and the intensity of the system is determined by the relative intensity of the two engines [Anonymous 2016b]. The CCT of the system is tuned within the bounds set by the CCT of individual LED engine. This is achieved with two dimmable LED drivers, each with a separate control input which can be phase control, 0 - $10V$ or digital. **Figure 3.3** depicts a Lutron® 0-$10V$

Energi Savr Node$_{TM}$ unit controlling a fixture with two independent 0 - 10V drivers with different CCT LED light engines [Anonymous 2016b]. In this scheme, the CCT and intensity of the fixture are not completely independent. In order to achieve a target CCT, the intensities of the individual LEDs must be set to specific values which will result in the overall intensity of the fixture.

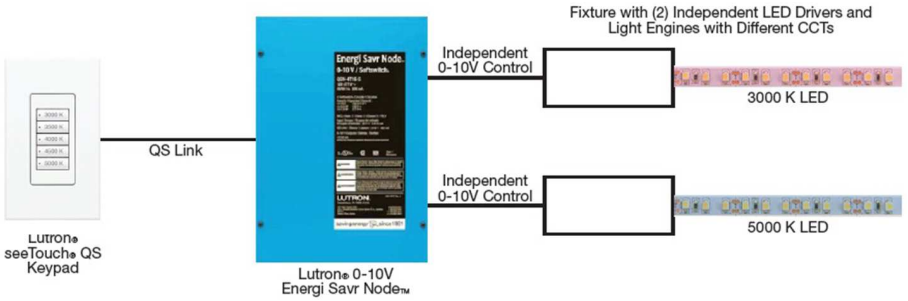

Figure 3.3: Lutron® Tunable white: independent control of CCT [Anonymous 2016b]

ii) Fixtures with separate intensity and CCT control inputs: In this scheme, the LED light engine uses one control signal for CCT control and a separate control signal for the intensity control as shown in **Figure 3.4** [Anonymous 2016b]. This scheme essentially required a controller, USAI controller, capable of dynamically mixing the output of two or more colors of the light engine for a required CCT and intensity by taking the two control signals which are typically either 0 - 10V or digital signal [Anonymous 2016b]. Two manual slide dimmers are provided to the user with manual control of CCT and intensity. One dimmer provides a 0 - 10V signal to the USAI controller for CCT control, while the other dimmer provides the intensity control signal to a Lutron® Hi-lume® 1% 3-wire LED dimming driver [Anonymous 2016b].

Telelumen® provides two multispectral LED luminaires viz., 16 channel *Light Replicator* and 5 channel *Penta* as variable spectrum light source [Anonymous 2014b]. Both these LED luminaires are

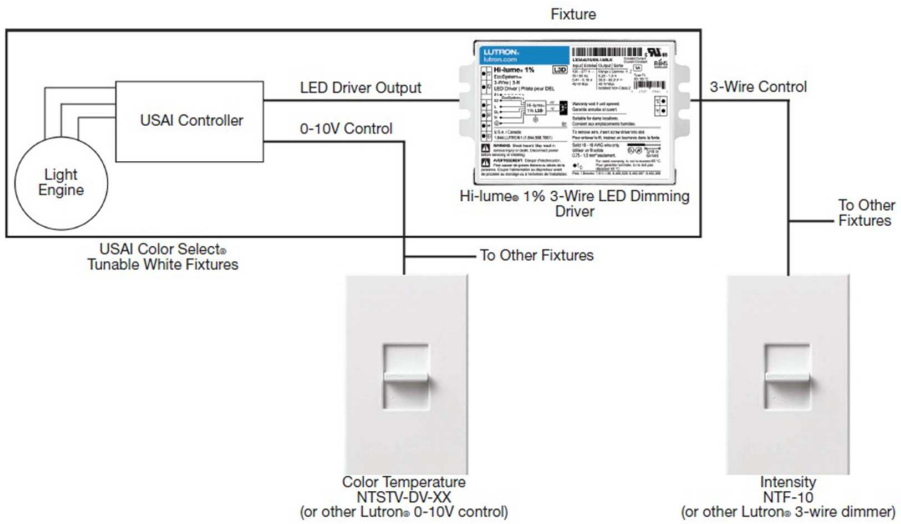

Figure 3.4: Lutron® Tunable white: independent control of CCT and intensity [Anonymous 2016b]

capable of producing either natural or custom made spectral compositions by controlling the each of the LED color channels independently [Anonymous 2014b]. The above system consists of an optional spectrometer, a luminaire (*Penta* or *Light Replicator*) and the developer suite software as shown in **Figure 3.5** where the spectrometer is used for controlling the luminaires, creating SPDs, recording, and storing data independently [Anonymous 2014b]. Here the driver-cum-controller is integrated with the luminare.

LuxiTune^{TM} provides a single tunable white light engine which is capable of simulating a halogen-style warm dimming and also CCT tuning. In the warm dimming, the CCT varies from 3000K to below 1600K as it dims halogen-style whereas in CCT tuning, it varies from 2100 - 4300K with independent brightness control [Anonymous 2016c]. Here the compact single light engine consists of multichannel LED emitter and driver-cum-controller as shown in **Figure 3.6**. Two control signals are fed to the driver-cum-controller to control the intensity and CCT respectively [Anonymous 2016c]. Although this product preciously follows a short distance below

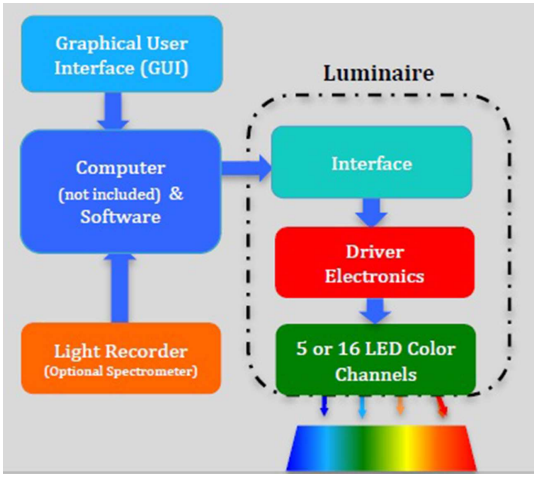

Figure 3.5: working of the Telelumen® multispectral LED luminaires [Anonymous 2014b]

the black body locus, not capable of following a custom made time varying pattern of intensity and color [Anonymous 2016c].

Ketra® provides fully tunable LED product *S38 PAR* lamp as shown in **Figure 3.7**. The lamp is a single source consists of both monochromatic and phosphor converted blue LED chip [Anonymous 2015a]. The lamp employs color and thermal feedback to maintain the color accuracy of <1 MacAdam ellipse. The driver and on-board wireless controller are the integral parts of the lamp. The on-board wireless controller controls the intensity and color according to the received signal [Anonymous 2015a]. The lamp is capable of producing any CCT between 2700 - 5000K along the black body curve and also dimmable upto 0.1% with wireless or line voltage dimming [Anonymous 2015a].

lumenetix® provides two color tunable LED products-

i) araya®^{5} logic module tunable color LED array: araya^5 logic module (ALM) integrated with araya^5 tunable color LED array of five different colors as shown in **Figure 3.8** to provide tunable

Figure 3.6: LuxiTune^{TM} tunable white light engine [Anonymous 2016c]

Figure 3.7: Ketra® *S38 PAR* lamp [Anonymous 2015a]

and dimmable white light from 1650 - 8000*K* [Anonymous 2016d]. The ALM incorporates on-board driver electronics and control logic along with closed loop thermal feedback and closed loop optical feedback to provide color consistency of <2 MacAdam ellipse across the tuning range [Anonymous 2016d]. The ALM is compatible with 0-10*V* wired controls and can be dimmed the light from 100 - 1% in step of 1% at constant CCT [Anonymous 2016d].

ii) araya®[5] color tuning module: Color tuning module (CTM), shown in **Figure 3.9**, mixes five colors of LEDs to provide tunable and dimmable white light in the range of 1650-4000*K* or 2700 - 6000*K* with 90+ CRI [Anonymous 2016e]. Similar to ALM, the CTM also incorporates on-board driver electronics and control logic

Figure 3.8: ALM and araya®^{5} tunable color LED array [Anonymous 2016d]

along with closed loop thermal feedback and closed loop optical feedback to provide color consistency of<2 MacAdam ellipse across the tuning range [Anonymous 2016e].

Figure 3.9: araya®^{5} color tuning module [Anonymous 2016e]

The CTM is compatible with the wireless light commissioning tool (LCT) and also 0 - 10V wired control as shown in **Figure 3.10**. The CCT and light output of CTM can be varied using two separate 0 - 10V controller.

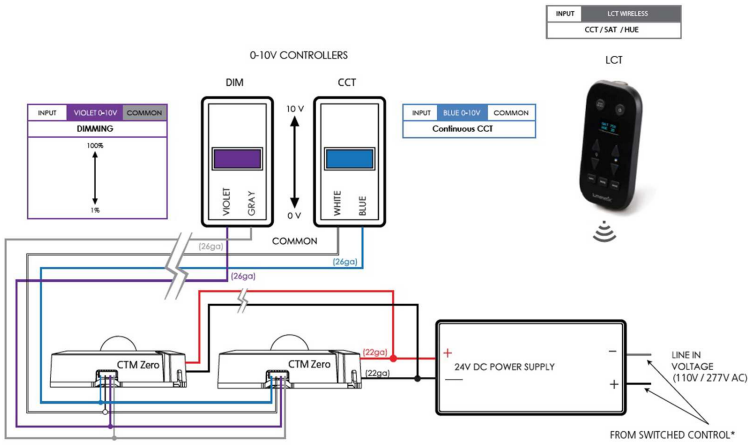

Figure 3.10: 0-10V control of continuous CCT and dimming [Anonymous 2016e]

3.3 Background Theory: Dimming and Color Mixing

3.3.1 Dimming scheme

Dimming of LEDs can be achieved by two dimming schemes

- analog dimming scheme
- digital dimming scheme.

Both dimming schemes control the time averaged current through LEDs, but differ in terms of advantages and disadvantages of the dimming circuits as discussed in following subsections.

Analog dimming scheme

Analog dimming is also known as amplitude modulation (AM) dimming. It is the adjustment of cycle-by-cycle LED current. More simply, it is the adjustment of the constant current level. This dimming scheme utilizes the linear region of the V-I characteristics of LED. Throughout this linear range, as forward current is reduced,

the light output of LED reduces proportionally. It is the simplest and cost effective dimming scheme and may be done by simply connecting a variable resistor in series with the LEDs as shown in **Figure 3.11** [Pousset et al. 2010]. The magnitude of current flowing through LEDs can be varied by varying this series resistance.

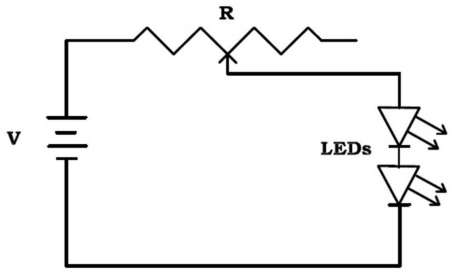

Figure 3.11: Analog dimming using variable resistor [Pousset et al. 2010]

The disadvantages of analog dimming are

1. Due to heat loss (I^2R) in the series resistance (R), the luminous efficacy of LEDs system significantly less.
2. The color (CCT) of the emitted light varies due to variation of the spectral power distribution (SPD) of LEDs with the amplitude of forward current [Dyble et al. 2005; Mirvakili and Koomson 2012].
3. Lower limit of dimming up to 10% is achievable [Dyble et al. 2005] but below 10% is difficult.

Digital dimming scheme

The digital method of dimming is the actual start and restart of LED current for short period of time. Digital dimming is the better choice for LED dimming since the amplitude of current supplied to LED is constant for all duty cycles. This constant current amplitude preserves the stability of the colorimetric parameters. Digital

dimming is of two types, viz., pulse width modulation (PWM) dimming and frequency modulation (FM) dimming.

In case of PWM dimming, LED is supplied with a pulse current which is made of fixed amplitude pulse of varying duty cycle i.e. the peak current is kept at a constant value and only the duty cycle (*DC*) is changed by changing the pulse width of the signal. The average current (I_{avg}) of a PWM signal shown in **Figure 3.12** can be related to peak current (I_p) by **Eqn. 3.1**.

$$I_{avg} = (DC).I_P$$
$$where \qquad DC = \frac{On\ time}{Time\ period} = \frac{T_{on}}{T} \tag{3.1}$$

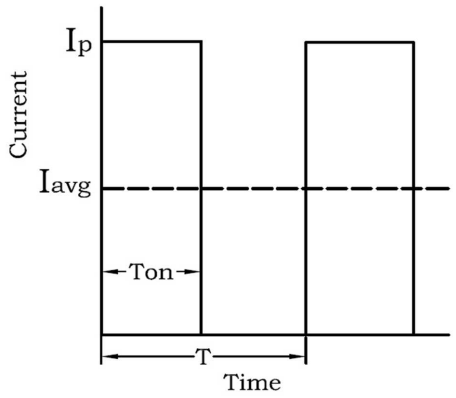

Figure 3.12: PWM Signal

In PWM dimming, usually a high modulation frequency (greater than 200 *Hz*) is set to prevent the perception of individual pulse, causing flickering effect [Gacio et al. 2010]. This dimming topology provides the ability to increase the dimming range by achieving lower current level and linear control of light output down to zero percent [Dyble et al. 2005].

On the other hand, in case of FM dimming, the duty cycle of the

dimming signal is varied by varying the time period (*T*) i.e. the frequency of the dimming signal. Hence, in this dimming scheme, frequency is to be lowered to obtain less light output. However, frequency can't be lowered below 200 *Hz* to avoid possible flickering effect. This imposes a technical constraint to achieve lower dimming levels.

Considering the above observations in the present study, dynamic lighting system uses phosphor-converted blue LEDs as white light source and PWM dimming is adopted to vary light output.

3.3.2 Color mixing scheme

The dynamic daylight pattern can be achieved by mixing the radiations from sources (emitters) having different spectral emission. Source color [Murdoch 1985] is specified in terms of its chromaticity coordinates (*x,y*) and the tristimulus value *Y* as [(*x,y*),*Y*] whereas white color is commonly reported in terms of CCT and D_{uv} [Ohno 2014]. According to Grassman's law of color mixing [Murdoch 1985], if the above values [(*x,y*),*Y*] of two source colors are known, then by adding them the chromaticity of the blended color can be obtained using **Eqn. 3.2**.

$$x^b = \frac{x_1\frac{Y_1}{y_1} + x_2\frac{Y_2}{y_2}}{\frac{Y_1}{y_1} + \frac{Y_2}{y_2}} \quad and \quad y^b = \frac{Y_1 + Y_2}{\frac{Y_1}{y_1} + \frac{Y_2}{y_2}} \tag{3.2}$$

The chromaticity coordinates (x^b, y^b) of this blended color will be somewhere on the straight line connecting the chromaticity coordinates of two colors on the CIE 1931 chromaticity diagram as shown in **Figure 3.13**. The tristimulus distribution function $\bar{y}_\lambda$ is exactly similar with the relative photopic spectral luminous efficiency curve $V(\lambda)$ as shown in **Figure 3.14**. Hence any photometric parameter like luminous flux (Φ), luminance (*L*), or illuminance (*E*) is proportional to *Y*. So color can be specified by chromaticity coordinates (*x,y*) and any photometric parameter. In this work the color of WLED is specified by (*x,y*) and Φ as [(*x,y*),Φ]. So the **Eqn.**

3.2 can be modified as-

$$x^b = \frac{x_1\frac{\Phi_1}{y_1} + x_2\frac{\Phi_2}{y_2}}{\frac{\Phi_1}{y_1} + \frac{\Phi_2}{y_2}} \quad and \quad y^b = \frac{\Phi_1 + \Phi_2}{\frac{\Phi_1}{y_1} + \frac{\Phi_2}{y_2}} \tag{3.3}$$

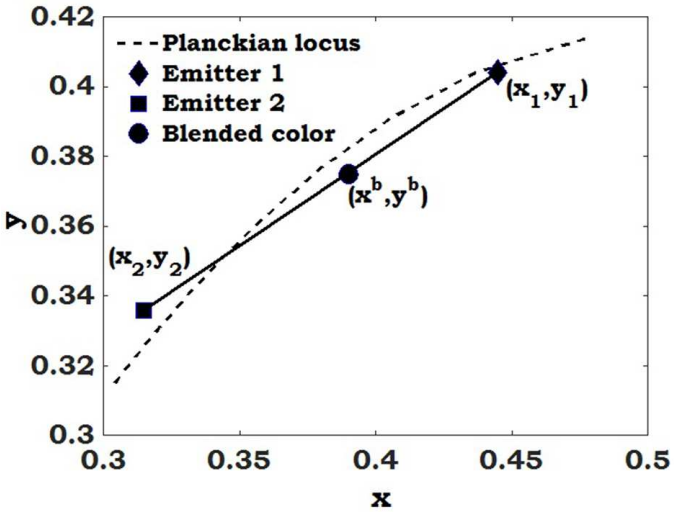

Figure 3.13: Blending concept of sources of two colors

3.4 Scheme and Features

3.4.1 Scheme

The CCT of daylight varies from 2000K at sunrise through 5000K for direct daylight at noon and can exceed 10000K in overcast conditions [Gilman et al. 2013]. The CCT of daylight varies between 5500K and 7500K over both clear and overcast conditions during a typical workday when solar elevation is greater than 10° [Hernández-Andrés et al. 2001]. The lower CCTs are experienced only during early morning or late evening when the solar elevation is less than 10° [Hernández-Andrés et al. 2001].

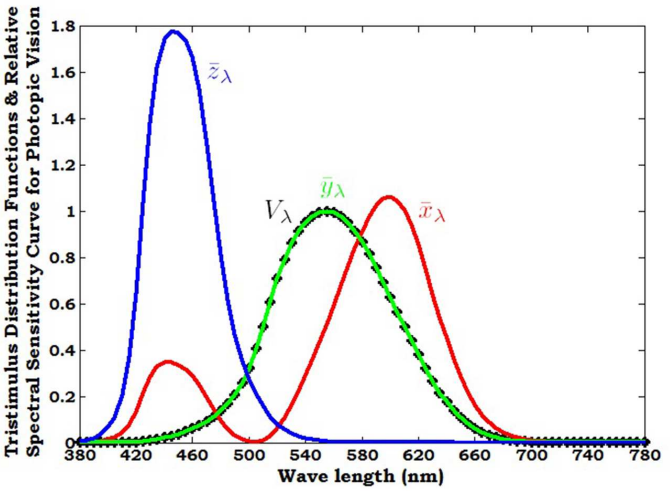

Figure 3.14: Tristimulus distribution functions and relative spectral sensitivity function for photopic vision

The scheme of dynamic lighting system developed in this work, is designed to follow the CCT variation of daylight from 2700*K* to 6000*K*. Hence it needs two white emitters, one having higher CCT (6000*K*)- cool white (CW) and the other having lower CCT (2700*K*)- warm white (WW). The light output of two white emitters are controlled and blended proportionally to follow the chromaticity coordinates of the dynamic daylight and also the illuminance level. So, along with the two white emitters, a light controller is required to achieve the dynamic lighting system. A light controller, named as dynamic light controller (DLC), drives the composite source (composite LED module) to achieve programmable variable CCT and variable light output artificial light source. This entire system is termed as DLS.

The single line diagram of the proposed scheme of DLS is shown in **Figure 3.15**.

In this scheme, the CCT and lumen values of WW (T_C^W, Φ^W) and CW (T_C^C, Φ^C) LED arrays are embedded in the controller of the DLC. The

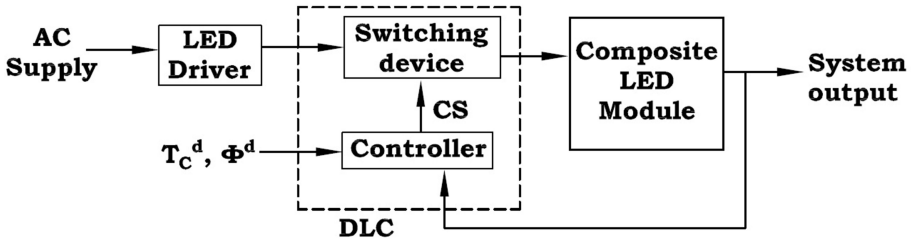

Figure 3.15: Proposed scheme of the DLS

controller generates control signal *CS* to control the composite LED module depending on the desired CCT and lumen values (T_C^d, Φ^d). This control signal is then fed to the switching device, connected between the LED driver and the composite module, to control the power fed to the composite LED module. The proposed DLC also takes feedback of the system output to monitor the output and also to minimize the deviation between desired and achieved value.

3.4.2 Features

The salient improvements of the proposed light control scheme over previous works are-

- light controller may be open-loop or closed-loop
- dimmable driver is not required which reduces the system cost
- even driver is not required provided power to LED module is fed directly from suitable constant current DC power source
- no measured data set is required for closed-loop system. Only manufacturers declared data on rated photometric quantities viz., luminous flux, CCT (chromaticity) and rated electrical quantities viz., current, voltage are required;
- developed closed-loop light controller is universally applicable to any WLED luminaire of compatible power rating

- it is capable of driving the WLED module to match the time-varying CCT of daylight and generates luminous flux according to the external daylight level in a reverse pattern. However, it may be programmed to follow a similar pattern of daylight variation
- it is capable of compensating for lumen depreciation due to aging of WLEDs
- it is capable of compensating for the variation of luminous flux and spectral composition due to a rise in ambient temperature as well as junction temperature of WLEDs.

Summary

In this chapter the features of the commercial dynamic lighting systems are elaborately described along with the general scheme of DLS. The background theory for the development of DLS is also presented. The technical scheme and features of the proposed DLS are described with the block diagram, which are utilised in subsequent works presented in the following chapters.

Chapter 4

Development of Composite LED Module

The proposed scheme of dynamic lighting system, described in **Chapter 3**, shows that the DLS comprises of two main functional blocks- composite LED module and DLC. This chapter deals with the design and development of the composite LED module. The results of the study on photometric and colorimetric parameters of two types of phosphor-converted LED sources and the effect of dimming on these parameters are presented here. Layout of a typical WLED arrays are designed and a prototype is developed to obtain a composite LED module. The electrical and photometric parameters of the developed module are experimentally evaluated.

4.1 Studies on Spectral Compositions

Before employing WLED chips to design a composite WLED module, it is necessary to know how light output, luminous efficacy and emitted spectral composition vary at different dimming levels under PWM dimming technique. The spectral compositions of phosphor converted warm white and cool white LEDs luminaires are measured using *JETI Specbos-1211* spectrometer at rated supply (230*V*, 50*Hz*) provided by the Agilent *6812B* AC power source and presented in **Figure 4.1**. The instruments used for the entire experimentation are listed in **Table 4.1** and their details are given in **Appendix A**.

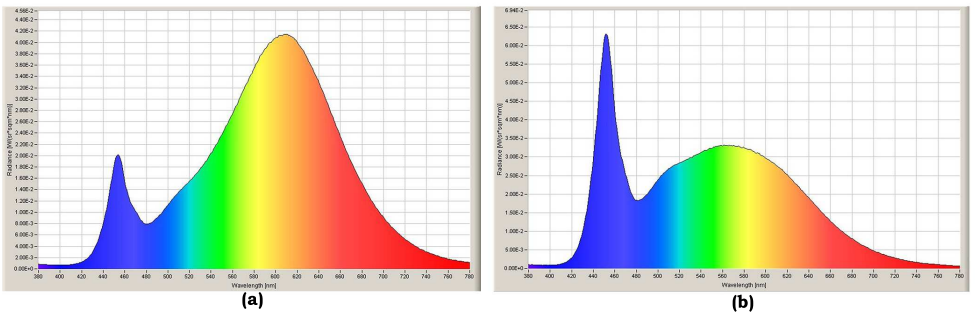

Figure 4.1: Measured SPD of LED luminaire (a) WW (2700K) and (b) CW (6000K) at rated supply

Table 4.1: Instruments used for the experimentation

Sl. No.	Name of the Instrument
1	Agilent *6812B* AC Power Source /Analyzer
2	Integrating Sphere
3	JETI *Specbos-1211* spectrometer
4	Konica Minolta (*CL-200*) chromameter
5	Yokogawa (*WT 210*) digital power meter

4.2 Studies on Effect of Dimming

The effect of dimming on the photometric and colorimetric parameters of both WW and CW LED luminaires are required to study at rated supply voltage because the dynamic lighting system requires variation of the light output of the constituting WLEDs of the composite source. For this purpose a developed LED dimmer is electrically connected between the WLED module and its driver as shown in **Figure 4.2**. The details description of the dimmer is given **Section 5.4**. The both LED modules are driven by a LED driver. The rated electrical specifications of the driver are given below:
Input: 230*V*, 50*Hz*; **Output:** 24*V* DC, 0.6 *A*, constant current source.

The measured electrical and photometric specification of both the WLED luminaires are given **Table 4.2**.

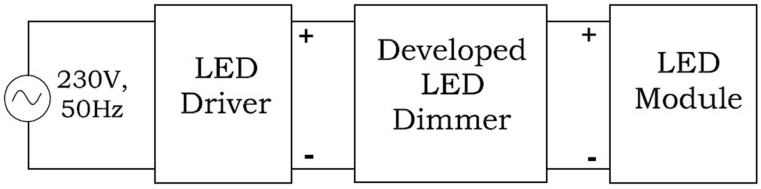

Figure 4.2: Connection block diagram of developed LED dimmer and LED luminaire

Four different dimming levels, viz., 25%, 50%, 75% and 100% with respect to light output from the WLED modules when driven by its driver at rated supply voltage are considered. The entire experimentation is done at 230*V*, 50*Hz* supply from Agilent *6812B* AC Power Source /Analyzer, in a dark room.

4.2.1 Photometric

The light output (Lumen) of the LED module is measured using integrating sphere of diameter 2.5*m* and presented in **Figure 4.3(a)**.

Table 4.2: Measured photometric and electrical parameters of both WLED module at rated supply voltage

Measured parameter		WW LED (2700K)	WW LED (6000K)
Photometric	T_C (K)	2714	5962
	Φ (lm)	607.3	644.1
Chromaticity	x	0.4519	0.3227
	y	0.3980	0.3346
Electrical	V_T (V)	24.3	24.3
	I (mA)	359.5	371.1
	P (W)	8.73	9.02

The electrical power input to the LED module is measured using Yokogawa (*WT 210*) digital power meter. The luminous efficacy (Lumen/W) of the both the LED modules are calculated from the measured light output and electrical power input to the LED module without dimmer (W/O Dimmer) and with dimmer at four dimming levels and presented in **Figure 4.3(b)**.

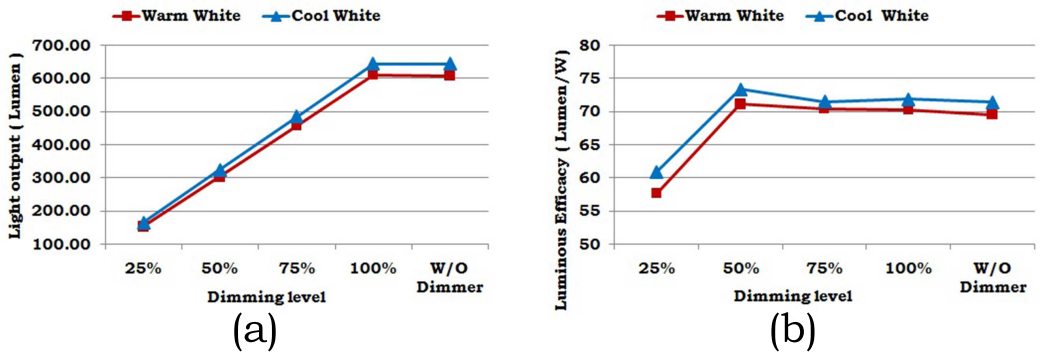

Figure 4.3: Variation of (a) light output and (b) luminous efficacy of both WW and CW LED module at four dimming levels [Maiti and Roy 2017]

Spectral power distribution (SPD) is measured using *JETI specbos-1211*. The SPD of WW and CW LED modules at different dimming levels are presented in **Figure 4.4**.

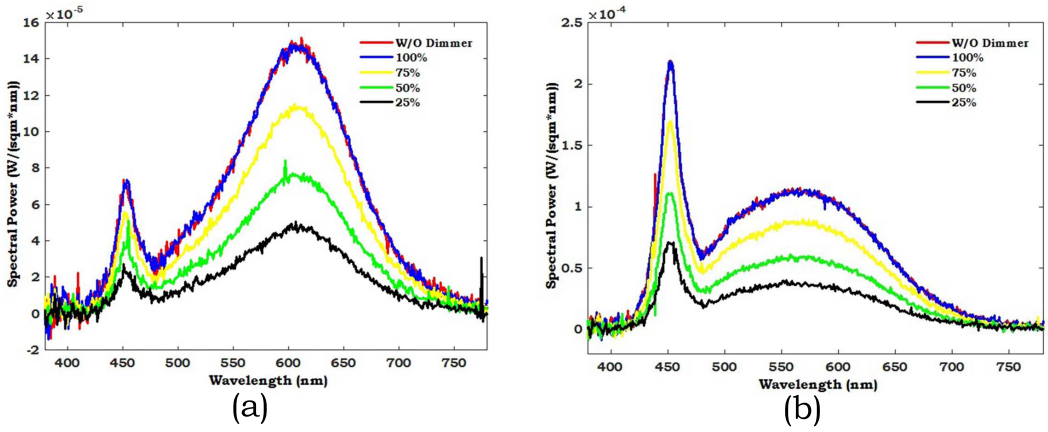

Figure 4.4: Measured SPD of (a) WW and (b) CW LED module at four dimming levels

4.2.2 Colorimetric

The colorimetric parameters viz., CIE 1931 chromaticity coordinates (*x*,*y*), correlated color temperature (CCT), general color rendering index (R_a) and one specific color rendering index (R_9) for saturated red color sample are also measured using the *specbos-1211*. The CIE 1931 chromaticity (*x*,*y*) of WW and CW LED modules at four dimming level are presented in **Table 4.3**. The variation of chromaticity is calculated using CIE 1976 CIELUV color difference ΔE^*_{uv} [Anonymous 2004b] and also presented in **Table 4.3**.

Variation of measured CCT of both WW and CW LED modules at four dimming levels is presented in **Figure 4.5**.

Variation of measured R_a and R_9 of both WW and CW LED at four dimming levels are presented in **Figure 4.6**.

Table 4.3: Chromaticity and CIELUV color difference ΔE^*_{uv} of WW and CW LED module at four dimming levels [Maiti and Roy 2017]

	WW LED module			CW LED module		
	x	y	ΔE^*_{uv}	x	y	ΔE^*_{uv}
W/O dimmer	0.4519	0.3980	-	0.3227	0.3346	-
100%	0.4500	0.3968	0.2145	0.3233	0.3357	0.1546
75%	0.4526	0.3996	0.1235	0.3233	0.3356	0.1197
50%	0.4516	0.3987	0.0780	0.3248	0.3390	0.5887
25%	0.4526	0.3996	0.1326	0.3245	0.3398	0.5482

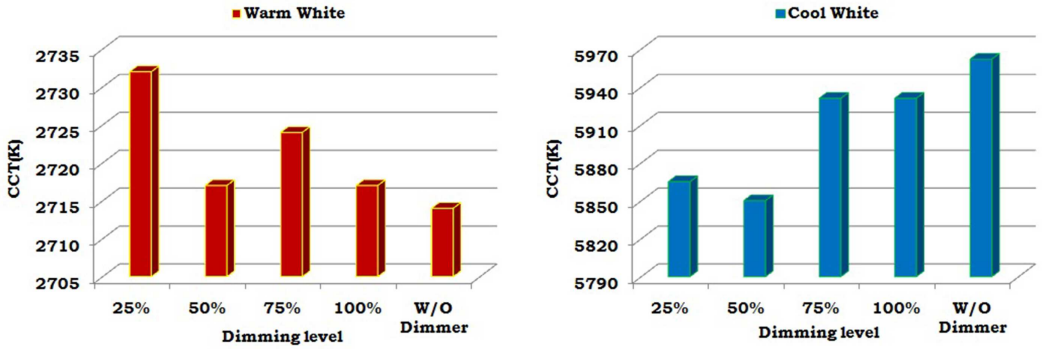

Figure 4.5: Variation of measured CCT of WW and CW LED module at four dimming levels [Maiti and Roy 2017]

Analysis of experimental results

The above experimental results show that variations of luminous efficacy are negligible at dimming level 100%, 75% and 50% for both the WLED modules. Only significant change occurs at 25% dimming level. Visual inspections of measured spectral power distribution diagrams also indicate insignificant variation at the four dimming levels for both LED modules. The maximum variation of measured CCT for WW and CW LED modules at four dimming level is $18K$ and $112K$ respectively. According to the study [Anonymous

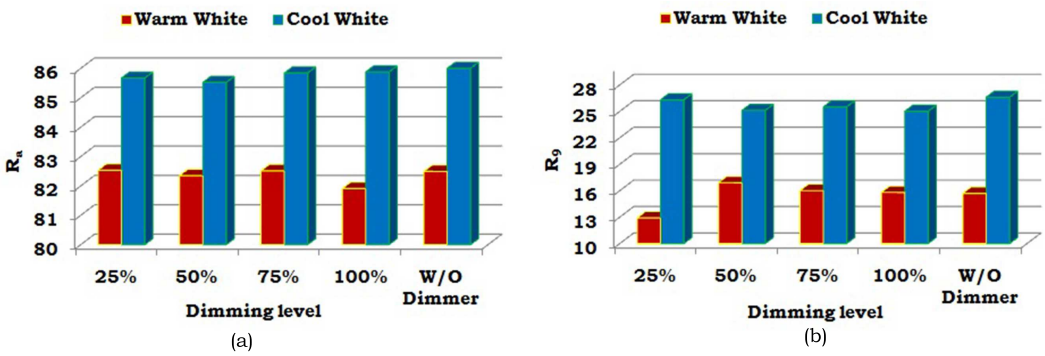

Figure 4.6: Variation of (a) general CRI (R_a) and (b) specific CRI (R_9) of both WW and CW LED at four dimming level [Maiti and Roy 2017]

2008a; Chen et al. 2014], for warm white LED (2700K), the CCT variation within 145K is acceptable. For cool white LEDs these acceptable variations are limited to 355K for 5700K source and 510K for 6500K source. It indicates that the observed variations in CCT are within acceptable limit. The maximum color difference for WW and CW LED modules at four dimming level is 0.2145 and 0.5887 respectively. The maximum percentage variation of General CRI (R_a) for WW and CW LED module at four dimming levels are 0.7% and 0.6% respectively.

From the above experimental findings it can be concluded that both the WW and CW LED modules show insignificant variation in their colorimetric parameters and luminous efficacy value (except for 25% dimming level).

Thus both the WLED modules at different dimming levels exhibit with insignificant variation in their color characteristics. About 17% and 14.7% reduction in luminous efficacy are observed for WW and CW LED module respectively at 25% dimming level. Thus WLED is found suitable as primary light source to design a dynamic lighting system.

4.3 Design of WLED Layout

It is seen that CCT of daylight varies from 2000-6000*K* for a typical sunny day, hence the CCT of a composite light source is to be variable within this range. Since the spectral composition of a phosphor-coated WLED does not vary at different dimming levels, hence to achieve variable spectral composition (CCT), more than one type of LED chip are necessary to achieve desired CCT range.

According to Grassman's color mixing law [Murdoch 1985] any intermediate color of light can be produced by mixing of two light sources of different color. Here the intended composite light module comprises of two types of white LED chips, viz., WW (2700*K*) and CW (6000*K*). The specifications of the WLED chips are listed in **Table 4.4**.

Table 4.4: Electrical and photometric specification of individual WLED chip

Declared parameter	WW LED chip	CW LED chip
Forward voltage (*V*)	3.0	3.0
Forward current (*mA*)	82.5	82.5
Power (*W*)	0.25	0.25
Luminous efficacy (*lm*/*W*)	90	95
T_C (*K*)	2700	6000

The number of LED chip is calculated for at least 600 *lm* light output from individual type of WLED.

4.3.1 WW LED array

Minimum light output required from WW LED array = 600 *lm*

Wattage of the system = $\frac{lumen\ output}{luminous\ efficacy}$ = $\frac{600}{90}$ W = 6.67 $W \approx 7W$

Number of chips required = $\frac{wattage\ of\ the\ system}{power\ of\ individual\ chip}$ = $\frac{6.67}{0.25}$ = 26.68

The number of chips is rounded up to 28 to get the system wattage as $7W$ ($28 \times 0.25W = 7W$). These 28 chips can be arranged either 4×7 or 7×4.

If 4 chips are connected in series then required terminal voltage = $4 \times 3V = 12V$

For 7 parallel paths required forward current = 7×82.5 mA = 577.5 mA

On the other hand, if 7 chips are connected in series then required terminal voltage = $7 \times 3V = 21V$

For 4 parallel paths required forward current = 4×82.5 mA = 330 mA

So, from the above discussion it is clear that the 7×4 combination required lesser current which is required to minimize the power loss due to heat in the circuit. Hence the 7×4 combination is selected for these 28 chips and the electrical specification of the WW LED array is $21V$, 330 mA, $7W$.

4.3.2 CW LED array

Minimum light output required from WW LED array = 600 lm

To maintain the system wattage as $7W$, number of chips required = $\frac{wattage\ of\ the\ system}{power\ of\ individual\ chip}$ = $\frac{7}{0.25}$ = 28

These 28 chips can be distributed in the same manner as discuss in case of WW i.e. four parallel strings with seven chips connected in series (7×4). So the electrical specification of the WW LED array is $21V$, 330 mA, $7W$.

4.4 Details of the Developed Composite LED Module

For proper mixing of light output emitted by the two arrays, the 4 parallel strings of each array are placed alternatively on a printed circuit board (PCB) as shown in **Figure 4.7(b)** and placed in a single luminaire covered with white diffuser as shown in **Figure 4.7(a)**.

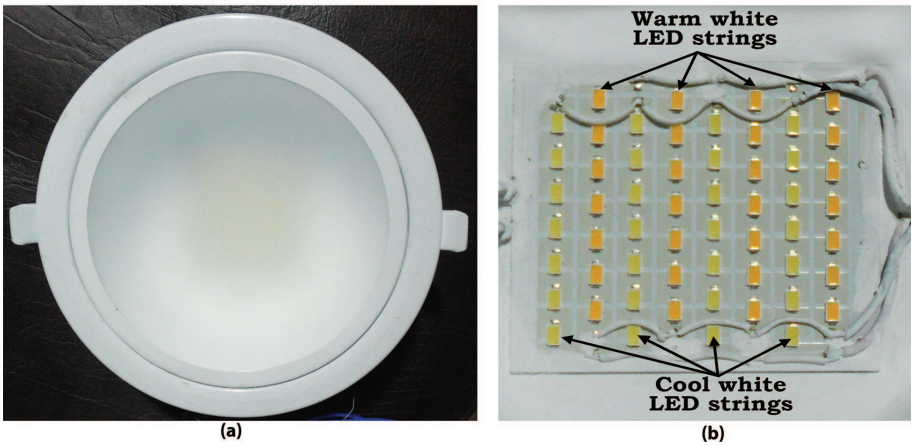

Figure 4.7: (a) Composite light module and (b) arrangement of WW and CW LED arrays [Maiti and Roy 2015]

This two WLED arrays are driven by two separate drivers. The electrical specification of the driver is given below-

Input: 230 *V*, 50*Hz*

Output: 24 *V* DC, 0.6 *A*, constant current source

The electrical and photometric parameters of the individual WLED array are measured with rated supply voltage and presented in **Table 4.5**. The electrical parameters viz., terminal voltage (V_T), forward current (*I*) and power consumption (*P*) are measured across the WLED array using Yokogawa *WT-210* digital power meter. The

luminous flux (Φ) of the individual WLED array is measured using integrating sphere of diameter 2.5m. The CCT and the chromaticity coordinates (x,y) are measured using Konica-Minolta *CL 200* chromameter.

Table 4.5: Measured photometric and electrical parameters of individual WLED array at rated supply voltage

Measured parameter		WW LED array	WW LED array
Photometric	T_C (K)	2840	5750
	Φ(lm)	648	681
Chromaticity	x	0.4483	0.3269
	y	0.4079	0.3363
Electrical	V_T(V)	24.2	24.2
	I (mA)	366	374.3
	P (W)	8.85	9.05

The spectral composition of the individual WLED array of the composite LED module are measured at rated condition and presented in **Figure 4.8**.

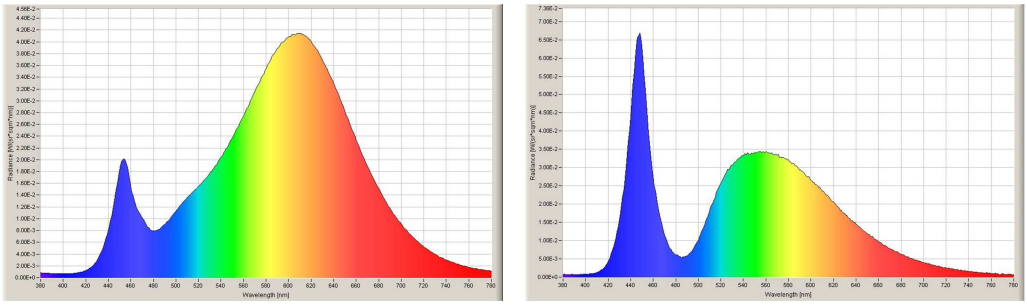

(a) (b)

Figure 4.8: Measured SPD of individual LED array (a) WW and (b) CW at rated supply voltage

The spectral composition of the composite light module is also measured when both the LED arrays at their full light output and presented in **Figure 4.9**.

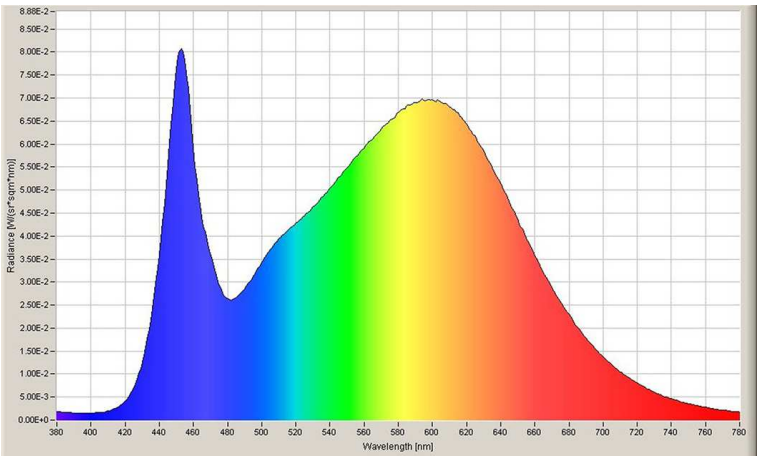

Figure 4.9: Spectral composition of the composite LED module at rated condition

Summary

The composite WLED module comprises of two WLED emitters of different spectral composition viz., warm white (WW) LED and cool white (CW) LED. The range of CCT of the developed module is 2840K - 5750K- the CCT values of the WW and CW LED arrays. The LED chips of each color are connected in series-parallel combinations and form an array. For proper mixing of emitted light, these two arrays are arranged alternatively and covered with a white diffuser. These two LED arrays are driven by two separate drivers of proper electrical specifications. The measured photometric parameters show that the light output from the individual LED array satisfies the target minimum lumen requirement (600 lm) and the CCT variation of the composite light module lies within the limit. The measured electrical parameters are close to the design values.

This composite LED module is used to evaluate the performance of the developed DLC and results are presented in **Chapter 5**. Using the same procedure another composite WLED module of higher power rating and wider CCT range is developed to study the performance of daylight-responsive DLS discussed in the **Chapter 6**.

Parts of the work presented in this chapter are reported in the following publications-

1. *Maiti PK, Roy B. 2017. Development and performance assessment of white LED dimmer. Journal of The Institution of Engineers (India): Series B. (Springer) 98(5): 461-466.*

2. *Maiti PK, Roy B. 27-29th November 2015. Performance evaluation of developed LED dimmer on WLED parameters: Photometric. Lux Pacifica 2015 Proceedings. 312-319.*

Chapter 5

Design and Development of Dynamic Lighting System

This chapter describes the step-wise design and development of a DLC which is the primary component of a DLS as described in **Chapter 3**. A DLS is realised by connecting the developed DLC electrically with the developed composite LED module. The control logic embedded in the DLC can be modified accordingly to drive the DLS for three operational modes viz., (1) variable illuminance at fixed CCT (similar to a conventional dimmer), (2) variable CCT at fixed illuminance (tunable CCT) and (3) variable CCT and variable illuminance (tunable light source). The control logic can be modified to vary the CCT and illuminance of the DLS either in steps or continuously to follow a preset time varying pattern. Finally, results of the experimental evaluation of the developed system are presented here.

5.1 Features and Control Schemes

In case of commercially available products, as discussed in **Section 3.2**, both the LED driver and the controller are integral parts of the system. In some products control signals act directly on the driver-cum-controller and in other products the control signals are fed to the dimmable driver to get the desired colour tuning. In the proposed system, the dynamic light controller (DLC) is electrically connected between the driver and the composite WLED module as shown in **Figure 5.1** and is able to control the power fed to the WLED module to control the light output and CCT.

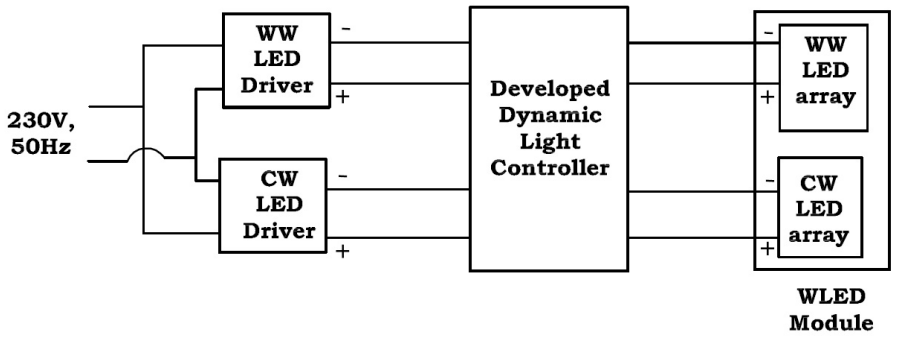

Figure 5.1: Block diagram of the dynamic lighting system (DLS) [Maiti and Roy 2018]

The unique features of the DLS are listed below-

I.A) The DLC is capable of controlling directly the power fed to the WLED module. Thus it is possible to bypass the driver if constant current DC power bus/supply of suitable rating is fed to the WLED module. Moreover, no dimmable driver is required for the operation of the DLS.

I.B) Single DLC is capable of controlling a number of WLED modules simultaneously; where the quantity of modules is restricted by the allowable voltage drop of the control signal generated by the DLC.

The single line diagram as represented in **Figure 5.2** explains the above two features.

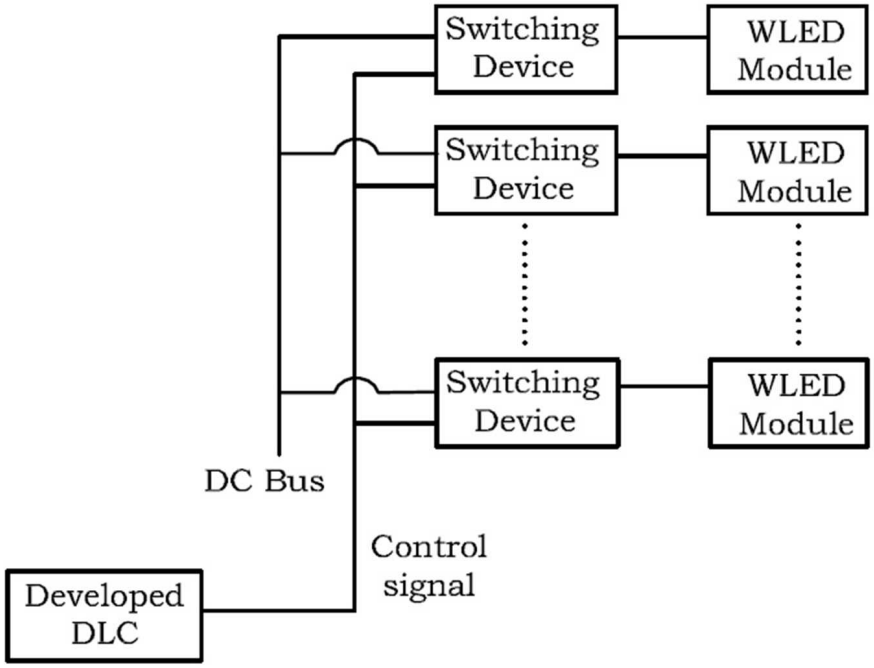

Figure 5.2: Single line diagram of the DC operated DLS [Maiti and Roy 2018]

II) Custom made time varying pattern of intensity and color can be reproduced by the developed DLS. The time varying pattern may be of two types, viz., step variation and continuous variation.

5.2 Background Theory

The function of DLC is to generate two control signals based on color mixing algorithm which in turn drives the WW and CW LED arrays at specified power level. So DLC controls light output (Φ)

from the two WLED arrays. Since illuminance (*E*) is directly proportional to the luminous flux (Φ), so color can be specified by (*x,y*) and *E*. The chromaticity coordinates of the blended color is modified as

$$x^b = \frac{x_1\frac{E_1}{y_1} + x_2\frac{E_2}{y_2}}{\frac{E_1}{y_1} + \frac{E_2}{y_2}} \quad and \quad y^b = \frac{E_1 + E_2}{\frac{E_1}{y_1} + \frac{E_2}{y_2}} \tag{5.1}$$

The blending of light output of two WLED arrays is executed using the following steps:-

Step 1 CCT values of the individual WLED array are measured using *CL-200* chromameter. Desired CCT points are set.

Step 2 The chromaticity coordinates (*x,y*) of individual WLED array and desired CCT points are calculated from corresponding CCT values.

Step 3 The blending ratio is calculated from (*x,y*) of the two WLED arrays and desired T_C point with the help of Grassman's color mixing law.

Step 4 The illuminance contribution of individual WLED array is calculated from blending ratio and desired illuminance level.

Step 5 Relationships between duty cycle and illuminance contribution of two WLED arrays are determined from experimentally measured values using MATLAB curve fitting tool.

Step 6 From the relationship as determined in **step 5**, the duty cycle of individual WLED array is calculated to get desired illuminance.

Step 7 Finally the individual WLED array is driven at computed duty cycle with the help of proposed dynamic light controller.

The execution details of each step are given in the following subsections. The instruments used for this work is listed in **Table 5.1** and the details are given in **Appendix A**.

Table 5.1: Instruments used for the experimentation

Sl. No.	Name of the Instrument
1	Agilent *MSO6014A* oscilloscope
2	GWINSTEK *APS-1102* programmable power source
3	Konica Minolta (CL-200) chromameter
4	PICKit3 burner
5	SONY IR TV remote

5.2.1 Measurement of source CCT

For this purpose, the composite LED module is mounted on a frame as shown in **Figure 5.3** and the *CL 200* chromameter is placed $1m$ below the source. The entire measurement is carried out in a dark room with rated power supply ($230V$, $50Hz$) by *APS-1102* power source. The CCT of the WW and CW LED arrays are measured as $2840K$ and $5750K$ respectively and corresponding electrical parameters are presented in **Table 4.5**.

Figure 5.3: Illuminance and CCT measurement setup of test WLED source [Maiti and Roy 2015]

5.2.2 Calculation of chromaticity coordinates from CCT

Grassman's color mixing law expresses resultant color in terms of chromaticity (x^b,y^b) [Murdoch 1985]. However, the desired color is expressed by set CCT point. Following Equations [Kim et al. 2006] are used to compute chromaticity from given CCT (T_C).

$$For\ \ 2222K \leq T_C \leq 4000K$$

$$x = -0.2661239\frac{10^9}{T_C^3} - 0.2343580\frac{10^6}{T_C^2} + 0.8776956\frac{10^3}{T_C} + 0.179910$$

$$y = -0.9549476x^3 - 1.37418593x^2 + 2.09137015x - 0.16748867 \tag{5.2}$$

$$For\ \ 4000K \leq T_C \leq 25000K$$

$$x = -3.0258469\frac{10^9}{T_C^3} + 2.1070379\frac{10^6}{T_C^2} + 0.2226347\frac{10^3}{T_C} + 0.240390$$

$$y = 3.0817580x^3 - 5.87338670x^2 + 3.75112997x - 0.37001483 \tag{5.3}$$

Chromaticity of WW LED array (x^W,y^W) and that of CW LED array (x^C,y^C) are computed from corresponding measured CCT values. The chromaticity of desired colors is calculated from the set CCT points.

5.2.3 Calculation of blending ratio

The blending ratio of illuminance contributed by the WW and CW LED arrays (E^W and E^C respectively) to get the desired CCT point can be found using **Eqn. 5.4** derived from Grassman's law of color mixing [Murdoch 1985].

$$x^b = \frac{x^W\frac{E^W}{y^W} + x^C\frac{E^C}{y^C}}{\frac{E^W}{y^W} + \frac{E^C}{y^C}}$$

$$so, \quad \frac{E^W}{E^C} = \frac{y^W(x^C - x^b)}{y^C(x^b - x^W)} \tag{5.4}$$

5.2.4 Calculation of illuminance contribution of two WLED arrays

Illuminance contribution of the two WLED arrays (E^W and E^C) depends on the blending ratio ($\frac{E^W}{E^C}$) and desired light level (E^d).

$$Let,\ \frac{E^W}{E^C} = M, \quad E^C \neq 0$$

$$so,\ E^W = ME^C \tag{5.5}$$

$$again,\ E^W + E^C = E^d$$

$$or,\ E^C = \frac{E^d}{M+1} \tag{5.6}$$

5.2.5 Determination of relationship between duty cycle and illuminance

To determine the relationship between duty cycle and illuminance of each WLED array, illuminance values at different dimming levels (duty cycles) are measured for both the WW and CW LED arrays. The illuminance values are measured at $1m$ vertical distance using the experimental setup shown in **Figure 5.3**. The duty cycles are varied with the IR remote from $0.6\mu s$ to $99.6\mu s$. The relation of duty cycle with illuminance is determined using MATLAB curve fitting tool from the above measured data. For WW LED array the best relation between duty cycle (DC^W) in time and corresponding illuminance (E^W) is expressed by a 9^{th} degree polynomial as represented by **Eqn. 5.7**.

$$DC^W = \sum_{i=1}^{10} P_i(\frac{E^W - E^{mean}}{E^{std}})^{(10-i)} \tag{5.7}$$

The mean E^{mean} and standard deviation E^{std} values are obtained from the measured illuminance (E^W) values of WW LED array and found as 168.4 *Lux* and 88.52 *Lux* respectively. The values of coefficients P_1-P_{10} with 95% confidence bounds are given in 2^{nd} column

of **Table 5.2**. The above fitted result gives lowest sum of squares due to error (SSE) value (7.692) and highest value of adjusted R-square (0.9998). The best fit plot is given in **Figure 5.4(a)**.

Table 5.2: Coefficients of best fit curve with 95% confidence bounds for individual WLED array [Maiti and Roy 2015]

Coefficient	WW LED array			CW LED array		
	Value	95% confidence		Value	95% confidence	
		Lower bound	Upper bound		Lower bound	Upper bound
P_1	0.5026	0.2709	0.7344	0.3071	0.2497	0.3644
P_2	0.8131	0.4882	1.1380	0.5277	0.4298	0.6256
P_3	-2.994	-4.401	-1.587	-2.36	-2.766	-1.954
P_4	-4.089	-5.729	-2.449	-3.426	-4.007	-2.844
P_5	7.467	4.448	10.49	7.122	6.101	8.143
P_6	7.141	4.474	9.808	7.391	6.288	8.494
P_7	-9.432	-12.01	-6.85	-10.46	-11.49	-9.439
P_8	2.346	0.8265	3.865	-0.3317	-1.045	0.3816
P_9	32.03	31.32	32.74	30.12	29.79	30.45
P_{10}	33.18	32.97	33.4	33.18	33.07	33.29

Similarly, for CW LED array the best relation between duty cycle (DC^C) in time and corresponding illuminance (E^C) is expressed by a 9^{th} degree polynomial as represented by **Eqn. 5.8**.

$$DC^C = \sum_{i=1}^{10} P_i \left(\frac{E^C - E^{mean}}{E^{std}}\right)^{(10-i)} \tag{5.8}$$

The mean E^{mean} and standard deviation E^{std} values are obtained from the measured illuminance (E^C) values of CW LED array and found as 173.9 *Lux* and 81.83 *Lux* respectively. The values of coefficients P_1-P_{10} with 95% confidence bounds are given in 3^{rd} column of **Table 5.2**. The above fitted result gives lowest SSE value (6.482) and highest value of adjusted R-square (0.9999). The best fit plot

is given in **Figure 5.4(b)**. The non-linear relationship between light output and duty cycle of forward injection current is explained by the relationship between radiative recombination rate with forward injection current [Schubert 2003; Žukauskas et al. 2002].

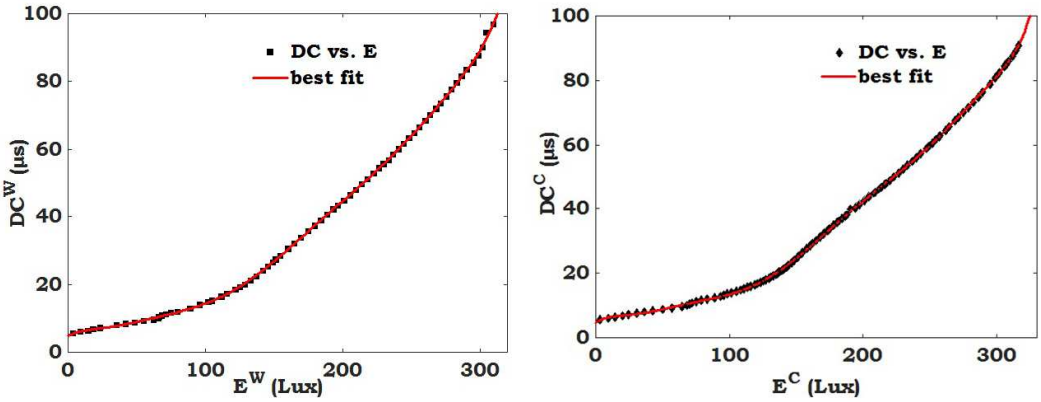

Figure 5.4: Best fit plots of (a) WW and (b) CW LED arrays [Maiti and Roy 2015]

5.2.6 Calculation of duty cycle for desired illuminance

The duty cycle of required dimming signal to get the desired illuminance is determined with the help of relationship between duty cycle and illuminance of individual WLED array. The duty cycle (DC^W) of dimming signal in time for the desired illuminance level (E^W) is calculated using **Eqn. 5.7** and the value of coefficients P_1-P_{10} from 2^{nd} column of **Table 5.2**.

Following the above mentioned procedure, the duty cycle (DC^C) of dimming signal in time for the desired illuminance level (E^C) from CW LED array is calculated using **Eqn. 5.8** and the value of coefficients P_1-P_{10} from 3^{rd} column of **Table 5.2**.

5.2.7 Injection of power at calculated duty cycle

After determining the duty cycles of the individual WLED arrays for the desired light scene, the dynamic light controller drives the individual WLED array with the respective computed duty cycle.

5.3 Design and Development of Dynamic Light Controller

The dynamic light controller (DLC) is the main functional module of the dynamic lighting system. The DLC adjusts the duty cycles of the two WLED arrays of the composite LED module to achieve desired light scene. The DLC is designed based on PWM dimming topology where SONY IR (Infra Red) remote keys are used to set desired light scene.

The block diagram representation of the DLC is shown in **Figure 5.5** and the main functional modules are listed below and details of each functional module are described in the following subsections.

1. Power supply (AC to DC converter)
2. IR transmitter (IR Remote)
3. IR receiver
4. IR decoder
5. PWM signal generator
6. Signal amplifier and switching device

5.3.1 Power supply

Some functional modules of the DLC used low DC (+5V & +12V) voltage. So it can not be connected directly to the 230V, 50Hz supply. The power supply module, shown in **Figure 5.6**, is basically a AC to DC converter and generates constant +5V and +12V DC supply from 230V, 50Hz supply.

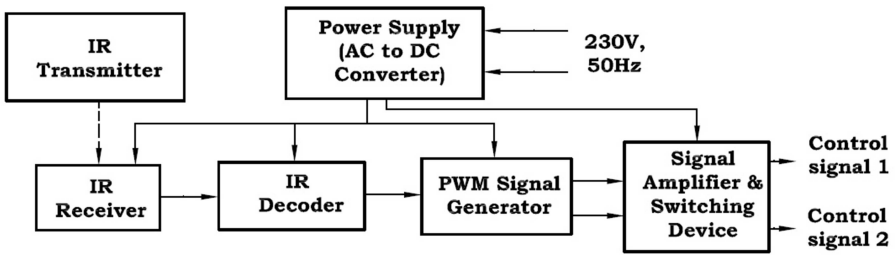

Figure 5.5: Block diagram of the dynamic light controller [Maiti and Roy 2015]

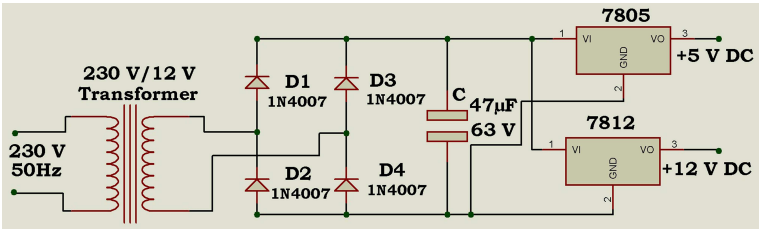

Figure 5.6: Circuit diagram (PROTEUS simulated) of power supply module [Maiti and Roy 2015]

5.3.2 IR transmitter

SONY IR remote,shown in **Figure A.9**, an external component of developed DLC, is used as IR transmitter to set the desired CCT points. SONY IR remote uses the 12 bits SIRC protocol [Nhivekar and Mudholkar 2011] as represented by typical pulse train in **Figure 5.7**.

The pulse train consists of 2.4 *ms* Header, 7 bit Command and 5 bit Address. Logical "1" and "0" are of 1.2 *ms* and 0.6 *ms* width respectively with a space of 0.6 *ms*. Commands are repeated every 45 *ms* for as long as the key on the remote is held down.

5.3.3 IR receiver

TSOP-1738 is used as an IR receiver to receive IR signal transmitted by SONY IR remote. This IR receiver demodulates the received IR signal so that it becomes compatible for decoding by the IR decoder. The demodulated pulse train is inversion of received pulse train.

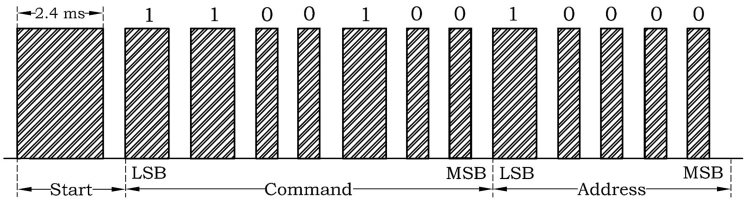

Figure 5.7: Typical pulse train of SIRC protocol [Nhivekar and Mudholkar 2011]

The **Figure 5.8** shows the application circuit connection of *TSOP-1738* as recommended by manufacturer [Anonymous 2001]. The V_S pin (pin2) is connected to +5V supply through a 100 Ω resistance. A 4.7μF capacitance is connected between pin1 and pin2. The resistance and capacitance are connected to suppress the supply disturbances.

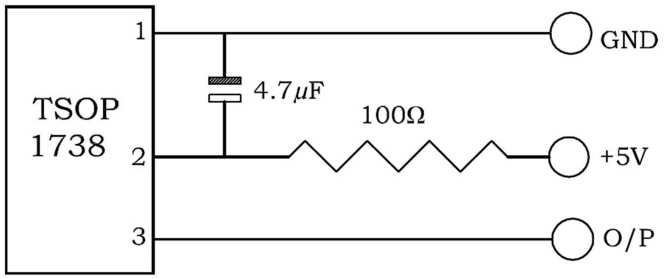

Figure 5.8: Application circuit of *TSOP-1738* as recommended by manufacturer [Anonymous 2001]

5.3.4 IR decoder

The demodulated frame as generated by IR receiver module is decoded to corresponding command data byte and address data byte with the help of IR decoder. Flowchart representing the proposed functional logic of decoder is shown in **Figure 5.9**.

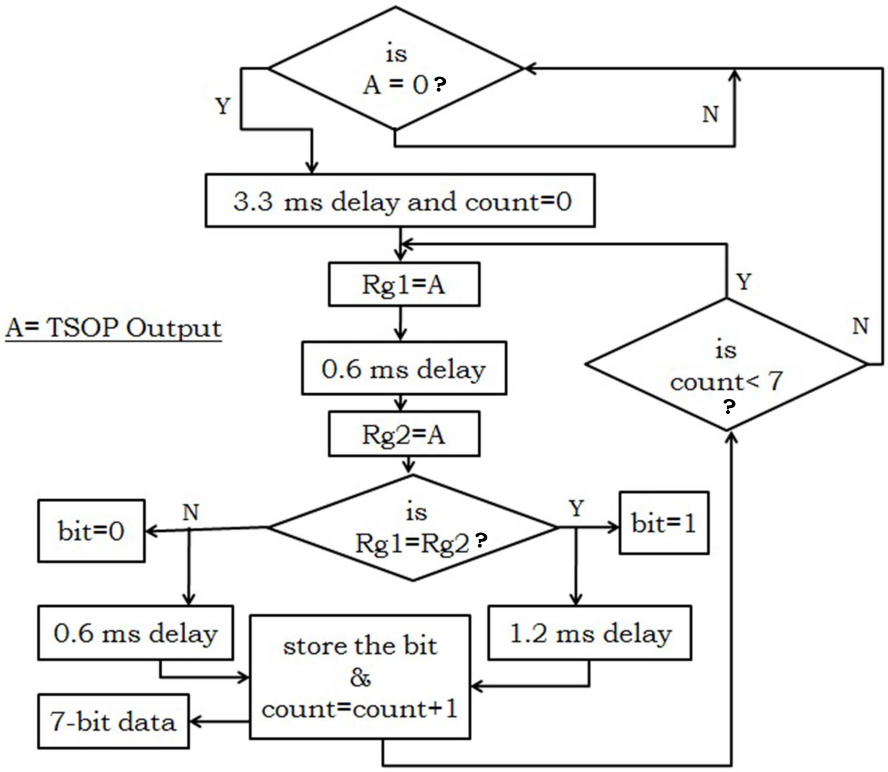

Figure 5.9: Flowchart for functional logic of IR decoder [Maiti and Roy 2015]

IR decoder is designed and fabricated using PIC *18F4550* microcontroller. The clock frequency is set at 10*MHz* by connecting a external crystal oscillator (*XTAL*) of 10*MHz* across *OSC1* and *OSC2* terminals of PIC along with two capacitors (22*pF*) *C1* and *C2* as shown in **Figure 5.10**. This value of clock frequency is required

to recognize the pulse train of SIRC protocol. The output (pin 3) of *TSOP-1738* is connected to the *RA2* pin (pin 4) of the PIC.

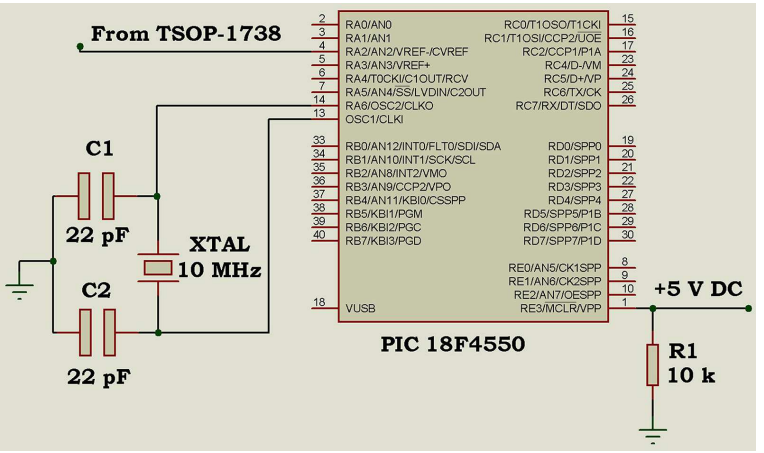

Figure 5.10: Circuit diagram (PROTEUS simulated) IR Decoder [Maiti and Roy 2015]

After execution of above functional logic, IR decoder stores 7-bit command as a consequence of pressing of any key of SONY IR remote. This stored bit pattern is then compared with predefined bit pattern, as provided by the manufacturer and shown in **Table B.1**, for identifying the pressed remote key.

5.3.5 PWM signal generator

CCP1 module of PIC *18F4550* is utilized as a standard capture/ compare/ PWM (CCP) module with Enhanced PWM capability to control both the WLED arrays with a single microcontroller through its dual PWM output channels. Other provisions of ECCP module viz., user-selectable polarity, dead-band control [Anonymous 2006; Mazidi et al. 2008] are also utilized in the developed DLC. Usage of different registers, calculation of PWM period, PWM duty cycle (in time) and delay are shown in **Appendix B**.

In dual PWM mode, the output from two output pins *P1A* and *P1B* are modulated with dead-band delay. The active high outputs of dual PWM mode with dead-band delay are shown in **Figure 5.11** [Anonymous 2006; Mazidi et al. 2008]. The figure explains that the *P1A* pin stays at high state for the duration equal to (duty cycle – delay) whereas *P1B* gives complementary PWM signal i.e. stays high for the duration equal to (PWM period – duty cycle – delay) and delay occurs at the signal transition from non-active state to active state.

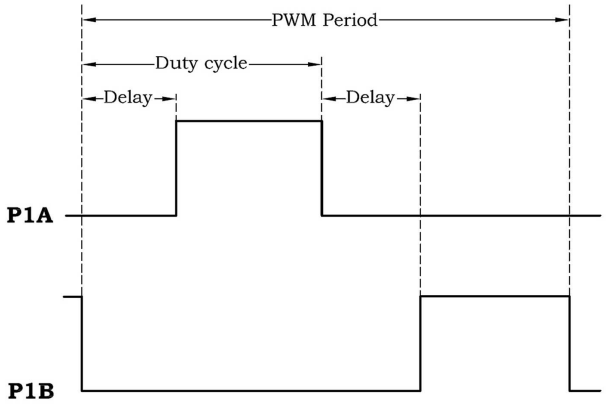

Figure 5.11: Typical dual PWM output of ECCP mode [Anonymous 2006; Mazidi et al. 2008]

Now the value of PWM frequency is found as 10 *kHz* (vide **Appendix B**) and a program for generation of 10 *kHz* dual PWM signal with 50μs duty cycle and 10μs delay is written in MPLAB IDE V8.88 software. The corresponding HEX file is loaded into the PIC *18F4550* microcontroller of the PWM signal generator shown in **Figure 5.12** with the help of PIC burner-PICKit3.

The PROTEUS simulated and measured waveform of dual PWM signal mode is presented in **Figure 5.13**. From the waveform it is cleared that output of *P1A* stays high for 40μs and output of *P1B* stays high for 40μs.

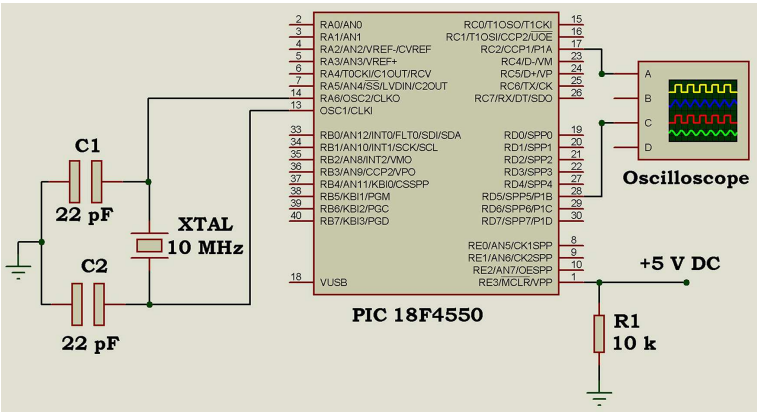

Figure 5.12: Circuit diagram (PROTEUS simulated) of PWM signal generator [Maiti and Roy 2015]

5.3.6 Signal amplifier and switching device

Light output of two WLED arrays are controlled by developed DLC through a switching device for each of them. The generated dual PWM signals are fed to the two separate switching devices to control the forward current of two WLED arrays respectively. In this work, *IRFP250N* is used as switching device which is an n-channel metal oxide silicon field effect transistor (MOSFET). The maximum gate-to-source voltage (V_{GS}) of this MOSFET is $\pm 20V$ [Anonymous 2000]. The output of PWM generator is insufficient for the operation of *IRFP250N* as PWM signal is toggled between $0V$ and $5V$. Therefore, an amplifier is needed to amplify the PWM signal to a level which is sufficient for the proper operation of the *IRFP250N*. This may be done using many low V_{GS} MOSFET available in the market and in that case use of amplifier can be avoided. In this work, *LM358P*, dual operational amplifier (OPAMP) [Anonymous 1976] is used to design a non-inverting amplifier. Each OPAMP module of *LM358P* is used to amplify each of the signals of dual PWM generator.

The output from *P1A* is connected to the non-inverting input (pin3) and the inverting input (pin2) is connected to ground through a

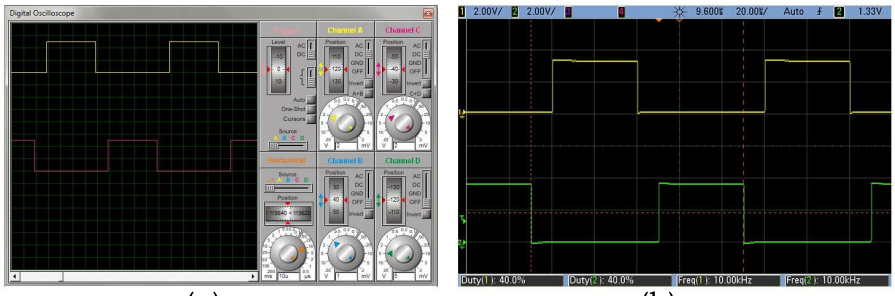

(a) (b)

Figure 5.13: (a) Simulated [Maiti and Roy 2015] (b) measured waveform of PWM signal generator in dual PWM mode

10 $k\Omega$ resistance. A 10$k\Omega$ resistance is also connected between the output (pin1) and inverting terminal (pin2) of the OPAMP module1 as shown in **Figure 5.14**. Similarly, another output from *P1B* is connected to the non-inverting input (pin5) and the inverting input (pin 6) is connected to ground through a 10 $k\Omega$ resistance. A 10 $k\Omega$ resistance is also connected between the output (pin7) and inverting terminal (pin 6) of the OPAMP module 2 (not shown in figure). The gain of the both amplifiers is 2.

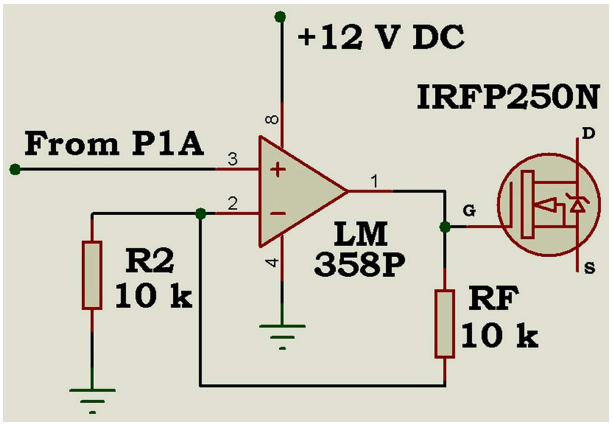

Figure 5.14: Circuit diagram (PROTEUS simulated) of signal amplifier and switching device [Maiti and Roy 2015]

The output of each amplifier is fed to gate (*G*) terminal of individual *IRFP250N*. The fabricated dynamic light controller and its components are shown in **Figure 5.15**.

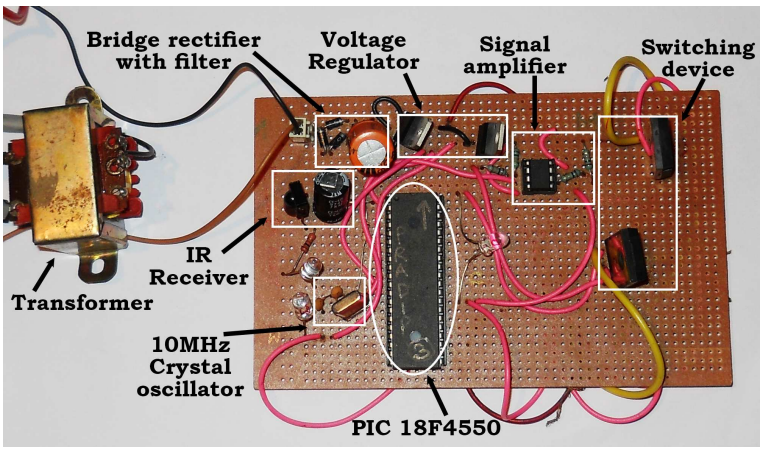

Figure 5.15: Components of fabricated DLC [Maiti and Roy 2015]

5.4 Working of DLC

The microcontroller of the developed DLC is programmed for the PWM signals of duty cycle DC^W and DC^C to dim the individual WLED array at desired illuminance. From the **Figure 5.11**, it is clear that the delay occurs twice in a single time period. In this work, the PWM period (T_{PWM}) is set at 100μs (10 *kHz* frequency). This 10 *kHz* frequency ensures no perceived flicker in the light produced by WLED source. So, the value of delay provided to get the PWM signals of duty cycle (in time) DC^W and DC^C is calculated as

$$Delay = \frac{T_{PWM} - (DC^W + DC^C)}{2}. \tag{5.9}$$

Now, the value of duty cycle (DC^W_{reg}) to be stored in the duty cycle register *DC1B9:DC1B0* to get PWM signals of duty cycle DC^W and

DC^C was calculated as

$$DC^W_{reg} = DC^W + Delay. \tag{5.10}$$

The (*ECCP1DEL*$< 6 : 0 >$) values are calculated using **Eqn. B.3** from the delay values for the corresponding desired light scene. A MATLAB program is developed based on the flowchart shown in **Figure 5.16** to compute the above parameters by considering the desired set points as input. This program generates the entire operational program in a notepad file for the microcontroller of the DLC. This notepad file is then converted into .HEX file using MPLAB IDE V8.88 software to embed into the microcontroller.

For each desired set point a sub-program is written within the main program. The SONY IR remote is used to change the sub-program. Each key of the remote indicates the one desired light scene.

The switching devices of the DLC are connected with the two WLED arrays as shown in **Figure 5.17** to drive the respective LED arrays of DLS with required duty cycles to achieve desired CCT and illuminance.

For the measurement of achieved light scene, the composite LED module is mounted on a frame and *CL-200* chromameter is placed at nadir of the luminaire at a distance of $1m$ as shown in **Figure 5.3**.

The control algorithm of dynamic light controller can be modified to obtain following modes of operation of DLS

- variable illuminance at fixed CCT (similar to a conventional dimmer)
- variable CCT at fixed illuminance (tunable CCT)
- variable CCT and variable illuminance (tunable light source)

These applications of the developed DLS are explained, in details, in the following sub-sections.

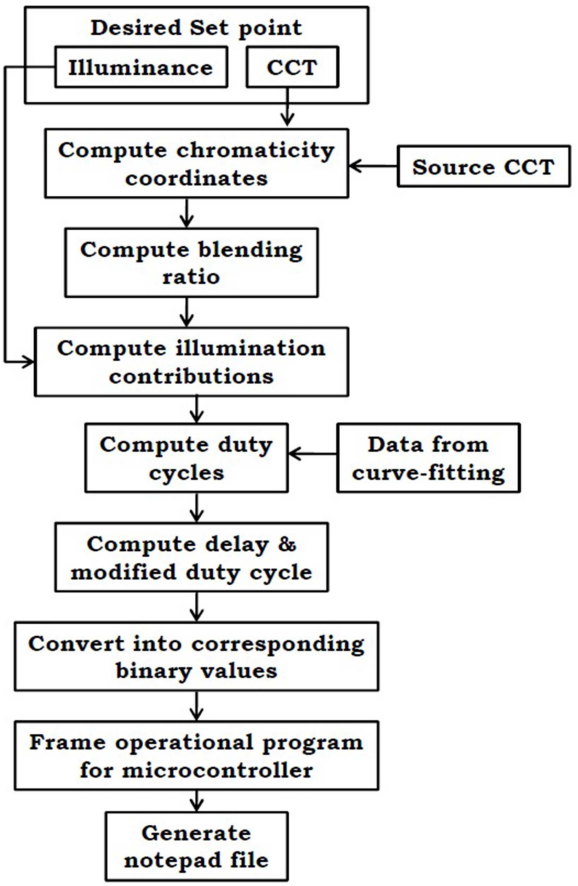

Figure 5.16: Flowchart of control algorithm for MATLAB program [Maiti and Roy 2018]

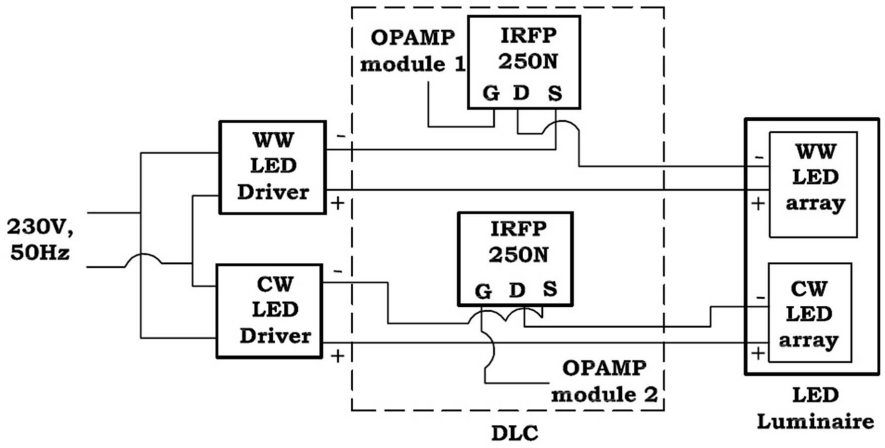

Figure 5.17: Connection of DLC with composite WLED luminaire [Maiti and Roy 2015]

5.4.1 DLS: Variable illuminance at fixed CCT

The DLC controls the light output of the individual WLED arrays of the composite LED module by controlling the power fed to the individual LED arrays. Hence the DLC can be programmed to control only the light output of the DLS by keeping its CCT constant. This operational mode is similar to that of a conventional dimmer. To do this, the DLC varies the duty cycles of both the WLED arrays proportionally. The DLC can vary the light output (Φ) either in steps or in continuous way as per the user requirements. For the step variations, the DLC changes the duty cycles of both the WLED arrays from one set value to another set value. Whereas, in case of continuous variation, the DLC increases or decreases the duty cycle of the individual LED arrays continuously to reduce or to increase the Φ respectively.

To drive the DLS as variable illuminance source, the DLC is programmed to vary the illuminance in steps for four illuminance values and this process is repeated for four CCT points. Experimental results are shown in **Table 5.3**.

Table 5.3: Experimental results of variable illuminance DLS

CCT point (K)	Desired E (Lux)	Measured CCT (K)	Measured E (Lux)	Variation CCT (K)	Variation E (Lux)
2900	300	2826	290	74	10
	200	2825	192.6	75	7.4
	150	2826	143.9	74	6.1
	100	2826	94.6	74	5.4
3800	300	3728	298.6	72	1.4
	200	3754	185.8	46	14.2
	150	3605	141.7	195	8.3
	100	3674	96.7	116	3.3
4700	300	4618	306.1	82	-6.1
	200	4641	199.2	59	0.8
	150	4587	155.3	113	-5.3
	100	4580	98.6	120	1.4
5600	300	5624	298.8	-24	1.2
	200	5645	196.1	-45	3.9
	150	5618	146.4	-18	3.6
	100	5580	106.3	20	-6.3

5.4.2 DLS: Variable CCT at fixed illuminance level

The DLC can be programmed to drive the DLS as variable CCT light source. In this case the CCT of the DLS varies by keeping the light output constant. The light level is set at 300 *Lux*. Desired CCT points of the variable CCT DLS, set from 3000K to 5600K with 200K regular interval, are achieved by mixing radiation from the two WLED arrays. However, two extreme CCT points are 2840K (for only WW LED array) and 5750K (for only CW LED array). The chromaticity coordinates are computed using **Eqns. 5.2** and **5.3**.

The 1^{st} and 2^{nd} column of **Table 5.4** represent the desired CCT points and corresponding computed chromaticity (x^b,y^b) respectively. The values of blending ratio ($\frac{E^W}{E^C}$) for each desired CCT point are

computed using **Eqn. 5.4** and presented in 3^{rd} column of **Table 5.4**.

Table 5.4: Computed chromaticity and blending ratio for the desired CCT points [Maiti and Roy 2015]

Desired CCT (*K*)	Chromaticity		Blending ratio (*M*)
	x^b	y^b	
2840	0.4483	0.4079	E^W=E^d
3000	0.4366	0.4042	11.35
3200	0.4232	0.3991	4.65
3400	0.4110	0.3936	2.74
3600	0.3999	0.3880	1.83
3800	0.3898	0.3824	1.30
4000	0.3805	0.3767	0.96
4200	0.3720	0.3713	0.72
4400	0.3643	0.3660	0.54
4600	0.3573	0.3610	0.40
4800	0.3509	0.3562	0.30
5000	0.3450	0.3516	0.21
5200	0.3396	0.3472	0.14
5400	0.3347	0.3430	0.08
5600	0.3301	0.3391	0.03
5750	0.3269	0.3363	E^C=E^d

For the desired CCT points, the illuminance contributions of the two WLED arrays (E^W and E^C) are calculated using **Eqns. 5.5** and **5.6** and given in 2^{nd} and 3^{rd} column of **Table 5.5** respectively.

The duty cycle (DC^W) of dimming signal in time for the desired illuminance level (E^W) of WW LED array presented in 2^{nd} column of **Table 5.5** is calculated using **Eqn. 5.7** and the value of coefficients P_1-P_{10} from 2^{nd} column of **Table 5.2**. The computed values are presented in 4^{th} column of **Table 5.5**.

Similarly the duty cycle (DC^C) of dimming signal in time for the

Table 5.5: Computed duty cycle and delay for the desired CCT points with constant illuminance [Maiti and Roy 2015]

Desired CCT (K)	E^W (*Lux*)	E^C (*Lux*)	DC^W (μs)	DC^C (μs)	$Delay$ (μs)	DC^W_{reg} (μs)
2840	300	0	87.64	4.54	3.91	91.6
3000	275.71	24.29	74.55	7.00	9.23	83.8
3200	246.90	53.10	61.68	9.09	14.62	76.3
3400	219.70	80.30	51.20	11.54	18.63	69.8
3600	194.03	105.97	42.20	14.21	21.79	64.0
3800	169.81	130.19	33.67	18.84	23.75	57.4
4000	146.92	153.08	25.94	25.69	24.18	50.1
4200	125.28	174.72	19.88	33.48	23.32	43.2
4400	105.20	194.80	15.90	40.71	21.69	37.6
4600	86.45	213.55	13.47	47.05	19.74	33.2
4800	68.93	231.07	11.84	52.89	17.64	29.5
5000	52.56	247.44	10.49	58.80	15.35	25.8
5200	37.26	262.74	9.39	64.97	12.82	22.2
5400	22.95	277.05	8.66	71.15	10.10	18.8
5600	9.55	290.45	7.97	77.03	7.50	15.5
5750	0	300	6.68	81.35	5.99	12.7

desired illuminance level (E^C) of CW LED array is calculated using **Eqn. 5.8** and the value of coefficients P_1-P_{10} from 3^{rd} column of **Table 5.2**. The computed values are presented in 5^{th} column of **Table 5.5**.

For the desired light scene, the values of *Delay* and DC^W_{reg} are calculated from the duty cycles DC^W and DC^C using **Eqns. 5.9** and **5.10** respectively and presented in 6^{th} and 7^{th} column of **Table 5.5** respectively. The (*ECCP1DEL*$< 6:0 >$) values are calculated using **Eqn. B.3** from the *Delay* values given in **Table 5.5** for the corresponding desired CCT points. The computed binary values are presented in 2^{nd} column of **Table 5.6**.

10-bit duty cycle (*CCPR1L:CCP1CON*$< 5:4 >$) values are calcu-

Table 5.6: Computed values of *ECCP1DEL*$< 6 : 0 >$, *CCPR1L*, *CCP1CON*$< 5 : 4 >$ [Maiti and Roy 2015]

Desired CCT (*K*)	*ECCP1DEL* $< 6 : 0 >$	*CCPR1L*	*CCP1CON* $< 5 : 4 >$
2840	0001010	11100101	00
3000	0010111	11010001	10
3200	0100101	10111110	11
3400	0101111	10101110	10
3600	0110110	10100000	00
3800	0111011	10001111	10
4000	0111100	01111101	01
4200	0111010	01101100	00
4400	0110110	01011110	00
4600	0110001	01010011	00
4800	0101100	01001001	11
5000	0100110	01000000	10
5200	0100000	00110111	10
5400	0011001	00101111	00
5600	0010011	00100110	11
5750	0001111	00011111	11

lated using **Eqn. B.2** from the DC_{reg}^{W} values given in **Table 5.5** for the corresponding desired CCT points. The computed values of *CCPR1L* and *CCP1CON*$< 5 : 4 >$ are presented in 3^{th} and 4^{th} column of **Table 5.6** respectively.

Experimental evaluation

The performance of the DLS as variable CCT at fixed illuminance level is experimentally evaluated with the setup as shown in **Figure 5.3**. CCT values are measured by CL-200 chromameter. The entire measurement is done at 230*V*, 50*Hz* supply from *APS-1102* programmable power source, in a dark room.

The microcontroller of DLC is programmed for the PWM signals

of duty cycle DC^W and DC^C to dim the individual WLED array at desired illuminance. For each desired CCT point a sub-program is written within the main program. The SONY IR remote is used to change the sub-program. Each key of the remote indicates the one desired CCT point. The remote keys and corresponding desired CCT points are shown in 1^{st} and 2^{nd} column of **Table 5.7** respectively.

Table 5.7: Desired CCT points as programmed with remote keys and corresponding measured values [Maiti and Roy 2015]

Key	Desired CCT (*K*)	Measured		Error CCT (*K*)
		CCT (*K*)	*E* (*Lux*)	
1	2840	2841	302.7	1
2	3000	2840	270.7	160
3	3200	3157	288.1	43
4	3400	3508	318.2	108
5	3600	3700	311.9	100
6	3800	3868	297.1	68
7	4000	4067	300.6	67
8	4200	4234	315.2	34
9	4400	4371	316.0	29
0	4600	4498	324.3	102
Volume+	4800	4699	319.2	101
Volume-	5000	4823	324.9	177
Channel+	5200	5132	316.5	68
Channel-	5400	5491	298.9	91
Mute	5600	5794	284.4	194
Power	5750	5794	292.5	44

The CCT of the DLS is varied by the SONY IR remote, shown in **Figure A.9** and corresponding measured CCT and illuminance values are presented in 3^{rd} and 4^{th} column of **Table 5.7** respectively. During measurement no flicker is perceived in the light produced by DLS at variable CCT points. The variations between desired

and measured CCT points are shown in **Figure 5.18**. From the 5^{th}

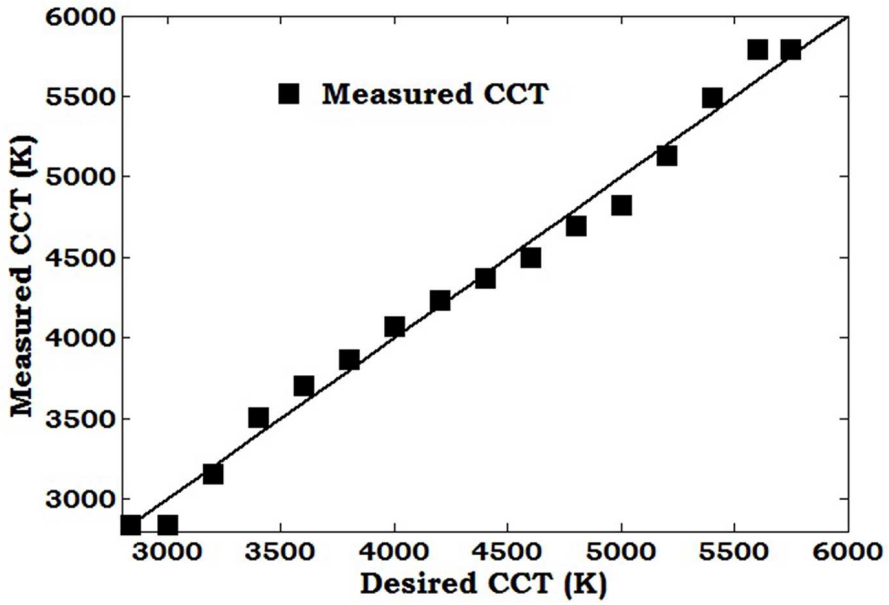

Figure 5.18: Measured CCT vs. desired CCT points of DLS [Maiti and Roy 2015]

column of **Table 5.7**, it is observed that the differences between desired and measured CCT points are lying in the range 1*K* to 194*K*. According to the study, [Anonymous 2008a; Chen et al. 2014] for warm white LED (2700*K*), the CCT variation within 145*K* is acceptable. For cool white LEDs these acceptable variations are limited to 355*K* for 5700*K* source and 510*K* for 6500*K* source. According to IS 3646 (Part 1) [Anonymous 1992], subjective effect of illuminance occurs only when the smallest significant difference of illuminance becomes higher than 1.5 times. The measured illuminance values at desired CCT points show small variation (-9.7% to +8.3%) with respect to desired value of 300 *Lux* as shown in **Figure 5.19**. Therefore, the above results confirm the satisfactory performance of the developed DLC to realize variable CCT dynamic lighting system.

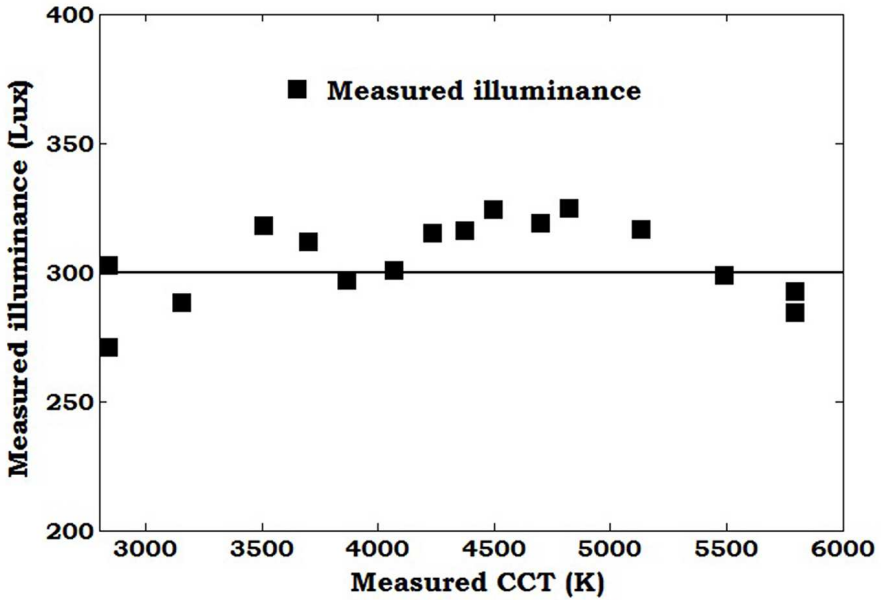

Figure 5.19: Measured illuminance vs. measured CCT for desired CCT points of variable CCT DLS [Maiti and Roy 2015]

5.4.3 DLS: Variable CCT and illuminance

The daylight integrated system demands light source of variable spectrum and light output. In the previous sub-section the developed DLC is programmed to drive the DLS as variable CCT light source. In this sub-section the developed DLC is upgraded to make the composite light module dynamic in term of quality and quantity. Hence the CCT and the light output of the developed DLS are to be variable with time of a day according to a preset protocol or as required, to follow patterns of daylight variation that support or enhance the natural rhythm of human's alertness. In this work the CCT and the light output of DLS are varied in two ways-

a. Step variation:

In this case, the CCT and the light output of the DLS are varied in steps. Some desired points of CCT and light output are set and

the DLC is programmed to achieve these set points. The desired CCT points are set from 2900*K* to 5600*K* with 900*K* regular interval.

The light levels are set at 300-200-150-100 *Lux*. The upper limit is set at 300 *Lux* since each LED array produces maximum 300 *Lux* at 1*m* vertical distance. Desired CCT points are achieved at minimum 100 *Lux* without flicker with the WLED module. Below 100 *Lux* flickering is observed at some of the CCT points. The *Lux* interval is set following the perceived interval of illuminance [Anonymous 1992]. Using the four CCT values and four illuminance (*E*) values sixteen possible combinations are considered as desired set points and presented in 3^{rd} column of **Table 5.8**. The **Figure 5.20** represents the value of CCT and Illuminance of the desired sixteen set points.

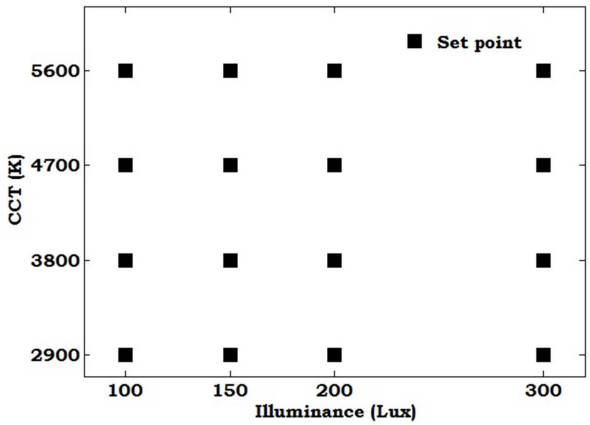

Figure 5.20: Desired set points of the DLS for step variation [Maiti and Roy 2018]

For step variation, a sub-program is written for each desired set point within the main program. SONY IR remote is used to change the sub-program. Each key of the remote indicates each set point. The desired set points and corresponding remote keys are shown in 1^{st} and 2^{nd} column of **Table 5.8** respectively.

Table 5.8: Step variation: remote keys for sixteen desired CCT and illuminance points and corresponding measured values with variation [Maiti and Roy 2018]

Set point	Remote key	Desired		Measured		Variation	
		CCT (*K*)	*E* (*Lux*)	CCT (*K*)	*E* (*Lux*)	CCT (%)	*E* (%)
1	1	2900	300	2882	305.3	0.62	1.77
2	2	3800	300	3739	304.5	1.61	1.50
3	3	4700	300	4665	309.1	0.74	3.03
4	4	5600	300	5588	306.4	0.21	2.13
5	5	2900	200	2869	200.5	1.07	0.25
6	6	3800	200	3801	206.9	0.03	3.45
7	7	4700	200	4530	219.0	3.62	9.50
8	8	5600	200	5551	206.4	0.88	3.20
9	9	2900	150	2852	147.8	1.66	1.47
10	0	3800	150	3769	148.1	0.82	1.27
11	Volume+	4700	150	4557	166.4	3.04	10.93
12	Volume-	5600	150	5575	154.8	0.45	3.20
13	Channel+	2900	100	2925	99.5	0.86	0.50
14	Channel-	3800	100	3679	115.6	3.18	15.60
15	Mute	4700	100	4505	114.5	4.15	14.50
16	Power	5600	100	5550	107.0	0.89	7.00

b. Continuous variation:

In this case, the CCT and light level of the DLS vary continuously to follow a preset pattern and the DLC is programmed to drive the DLS accordingly. **Figure 5.21** represents a desired pattern of the CCT and illuminance for a typical office environment for a working day (8am-6pm) [de Kort and Smolders 2010]. Here the time i.e. 10 hours is scaled down to 60 minutes and the maximum illuminance is also scaled down to 300 *Lux* for experimental purpose. From this pattern fourteen set points are selected to recognize the pattern. The values of CCT and illuminance (*E*) and the corresponding

time of those fourteen set points are presented in 3^{rd} and 2^{nd} column of **Table 5.9** respectively.

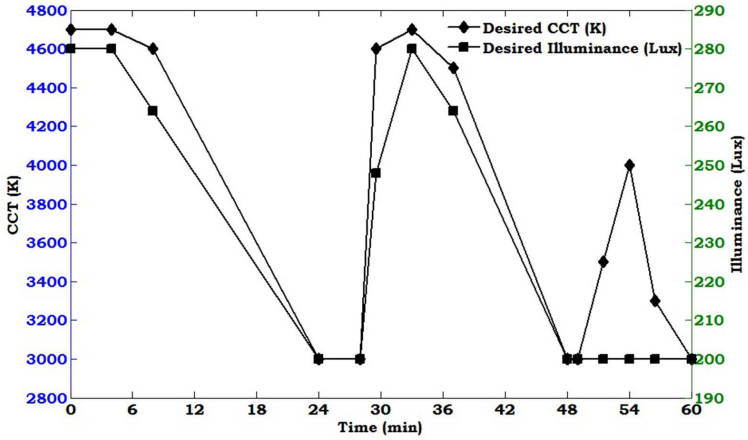

Figure 5.21: Desired patterns of CCT and illuminance for continuous variation [Maiti and Roy 2018]

For continuous variation, the value of *Delay* and DC_{reg}^{W} of the dual PWM signal are varied continuously with time to vary the duty cycles of the control signals 1 and 2. As a result the CCT and illuminance values are also varying continuously.

Experimental evaluation

The performance of the developed light controller to achieve the variable CCT and variable light output DLS, is measured with the experimental setup shown in **Figure 5.3**. The CCT and illuminance values are measured using CL-200 chromameter. The entire experimentation is done at rated supply (230*V*, 50*Hz*) from *APS-1102* programmable power source and in a dark room.

a. Step variation:

For step variation, the desired set points are activated by SONY IR remote keys and corresponding measured CCT and illuminance values are presented in 4^{th} column of **Table 5.8**. No flicker is perceived during measurement. Required duty cycles for both the WW and CW LED arrays are computed corresponding to the sixteen set points and accordingly DLC is programmed to generate PWM signals. DLC generated duty cycles are measured with digital storage oscilloscope (Agilent-*MSO6014A*) and they are almost equal to the desired duty cycles.

The desired and measured set points are presented in **Figure 5.22**. From the 5^{th} column of **Table 5.8**, it is observed that the differences between desired and measured CCT points are lying in the range $1K$ to $195K$. The measured illuminance values at desired set points show small variation (-15.6% to +1.47%) with respect to desired value. The percentage variations of measured CCT and illuminance values corresponding to sixteen set points are presented in **Figure 5.23**.

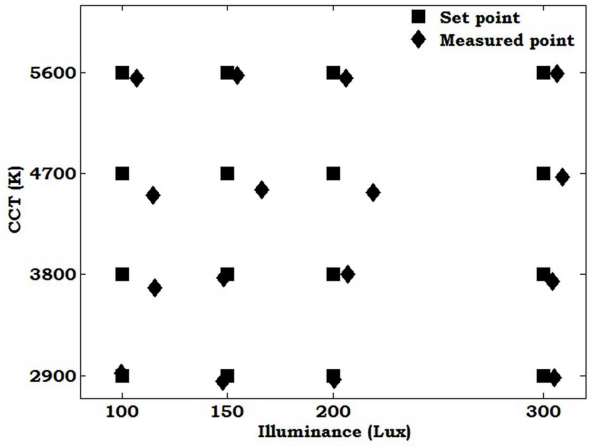

Figure 5.22: Step variation: measured CCT and illuminance values [Maiti and Roy 2018]

So the observed variations in CCT of step variation are within acceptable limit [Anonymous 2008a; Chen et al. 2014] and also the variation in illuminance is also low and visually not perceivable.

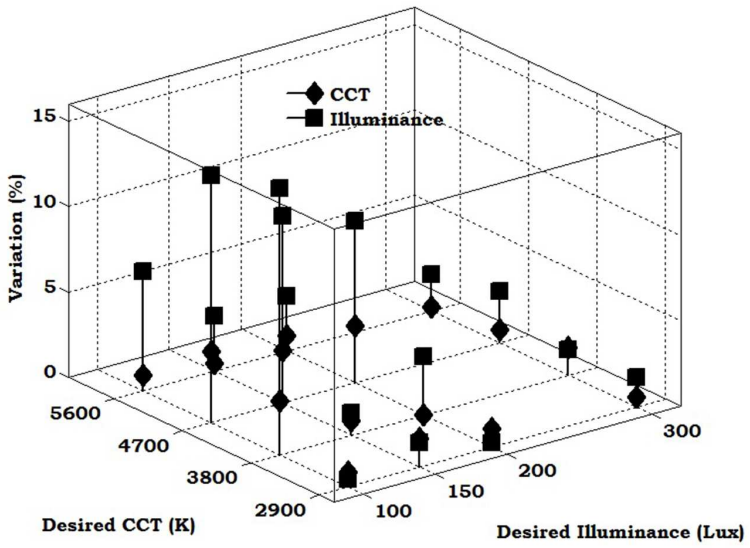

Figure 5.23: Step variation: percentage variation of measured CCT and illuminance values [Maiti and Roy 2018]

b. Continuous variation:

For continuous variation, the DLC drives the DLS to achieve the time varying desired pattern. Required duty cycles for both the WW and CW LED arrays are computed corresponding to the fourteen desired set points as presented in **Table 5.9** and accordingly DLC is programmed to generate PWM signals. The generated duty cycles are measured with Agilent-MSO6014A to test whether generated PWM signals follow the desired duty cycle patterns. **Figure 5.24 (a)** and **(b)** show patterns for desired and measured duty cycles for WW and CW LED arrays respectively. It is observed from these figures that the measured duty cycles show insignificant variation throughout the time span.

The performance of the DLS to test whether it follows the desired

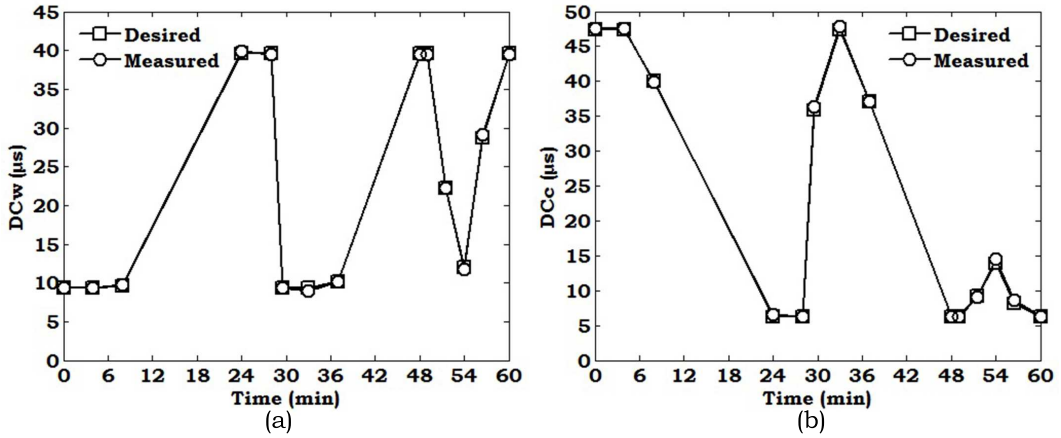

Figure 5.24: Continuous variation of duty cycle: measured and desired (a) WW LED arrays and (b) CW LED arrays [Maiti and Roy 2018]

variation of CCT and illuminance is evaluated through experimentation and repeated four times with the same initial condition to test repeatability of performance. Here also no flicker is perceived for the entire range of the desired pattern. The experimental results are presented in **Table 5.9**.

The desired and measured (average) CCT and illuminance patterns are shown in **Figure 5.25** and **Figure 5.26** respectively. The percentage variations are computed based on RMS error of four measured data-set and corresponding plots are presented in **Figure 5.27**.

Measured data shows significant variations of illuminance and CCT for the set points 11 and 13 corresponding to the lower CCT and lower illuminance points viz., 3500K and 3300K. These variations are explained by the deviations of lumen output from CW LED array at the duty cycles $< 10\%$ compared to estimated value.

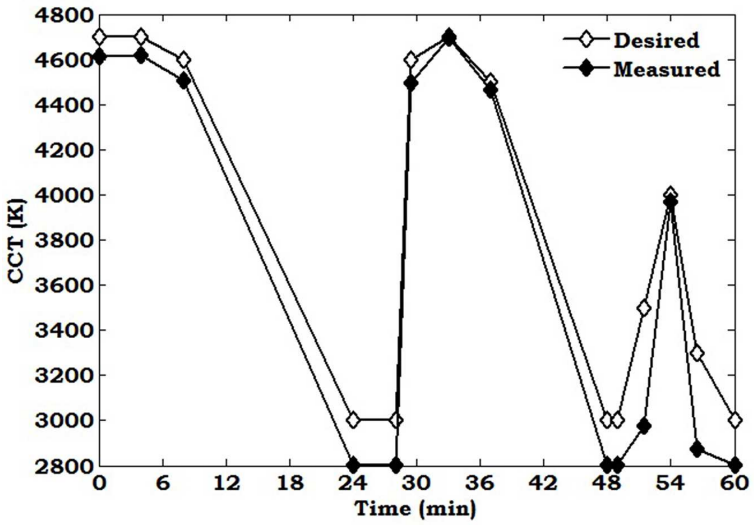

Figure 5.25: Continuous variation of CCT: measured average and desired [Maiti and Roy 2018]

Analysis of results

In this work the performance of the developed DLC is experimentally evaluated for both the step and continuous variation of CCT and illuminance from the DLS. The developed DLC is electrically integrated with the composite LED module and CCT and illuminance of DLS are measured at $1m$ vertical distance.

Step variation performance is tested with sixteen possible combinations of the four CCT values (range: 2900-5600K) and the four illuminance values (range: 100-300 *Lux*). Experimental result shows that all the sixteen set points are realized without any perceived flicker and observed variations of measured CCT points are within the limit of acceptable range and variations of the measured illuminance values are also very small ($<16\%$) and not visually perceivable [Anonymous 1992]. However, the developed DLC generates successfully the PWM signals of desired duty cycles.

Continuous variation performance is tested with a typical pattern

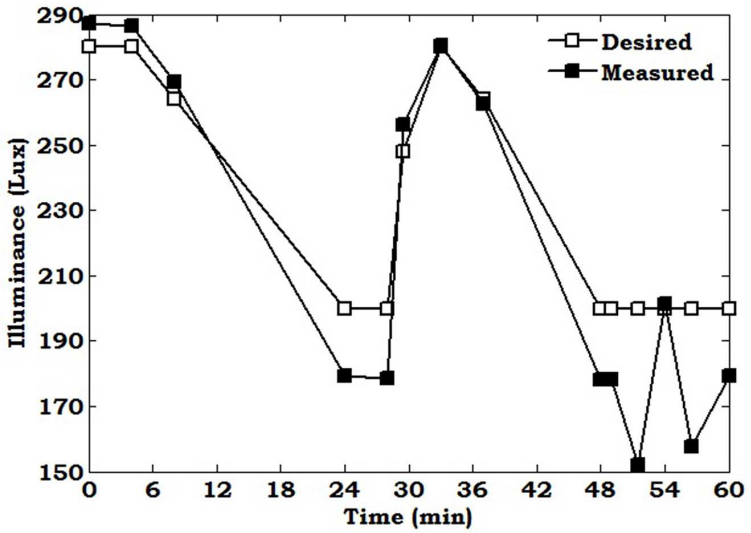

Figure 5.26: Continuous variation of illuminance: measured average and desired [Maiti and Roy 2018]

applicable for office lighting where CCT varies from 3000-4700K and illuminance varies from 200-280 *Lux* (scaled down). Satisfactory performance of the DLC is observed from its generated PWM signals of desired duty cycles. But for the DLS, significant variations are observed at two points of lower CCT values. Deviated light output from the CW LED array than the estimated output at lower duty cycles ($<$10 μs) results these variations.

Although the performance of the developed DLC is quite satisfactory, the satisfactory performance of the DLS depends on the light output of individual WLED array as per estimated values even at lower duty cycles.

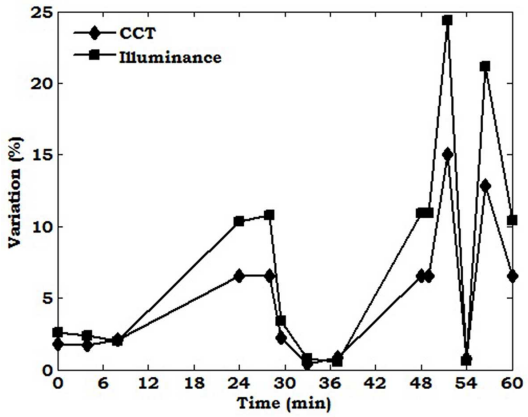

Figure 5.27: Continuous variation: percentage variation of measured average CCT and illuminance values [Maiti and Roy 2018]

Summary

In this chapter evaluation of a DLS is carried out with the developed DLC. Details of design and development of the system is presented. Step by step experimental evaluation is conducted to establish the working of embedded light control algorithm with the following sequences- (1) variable illuminance at fixed CCT, (2) variable CCT at fixed illuminance and (3) variable CCT and variable illuminance. The third mode of operation is tested for both the step variation and the continuous variation. The output of this chapter is utilised in **Chapter 6** to develop a daylight-responsive DLS.

Parts of the work presented in this chapter are reported in the following publications-

1. *Maiti PK, Roy B. 2018. Evaluation of a light controller for a LED-based dynamic light source. Lighting Research & Technology. (SAGE) 50(4): 571–582.*

2. *Maiti PK, Roy B. 2015. Development of dynamic light controller for variable CCT white-LED light source. LEUKOS. (Taylor & Francis) 11(4): 209-222.*

Table 5.9: Continuous variation: experimental results [Maiti and Roy 2018]

Set Point	Time (min)	Desired		Measured CCT (K)				Measured Illuminance (Lux)				Variation	
		CCT (K)	E (lx)	Run 1	Run 2	Run 3	Run 4	Run 1	Run 2	Run 3	Run 4	CCT (%)	E (%)
1	0	4700	280	4615	4617	4614	4617	288.5	286.7	287.0	286.9	1.8	2.6
2	4	4700	280	4613	4626	4617	4623	288.3	285.9	285.8	286.2	1.7	2.4
3	8	4600	264	4509	4504	4504	4505	269.3	269.4	269.1	269.3	2.1	2.0
4	24	3000	200	2805	2805	2804	2805	179.3	179.2	179.2	179.3	6.5	10.4
5	28	3000	200	2804	2804	2804	2804	178.5	178.4	178.4	178.5	6.5	10.8
6	30	4600	248	4488	4497	4501	4501	257.7	256.1	255.8	255.9	2.2	3.4
7	33	4700	280	4665	4700	4706	4706	284.2	279.5	279.1	279.3	0.4	0.8
8	37	4500	264	4467	4458	4463	4465	262.8	263.3	262.3	262.4	0.8	0.5
9	48	3000	200	2804	2804	2804	2804	178.3	178.0	178.2	178.2	6.5	10.9
10	49	3000	200	2804	2804	2804	2804	178.3	178.0	178.2	178.3	6.5	10.9
11	52	3500	200	2984	2967	2971	2977	168.1	146.4	146.6	147.3	15.0	24.4
12	54	4000	200	3974	3970	3966	3967	201.4	201.6	200.7	200.9	0.8	0.6
13	57	3300	200	2892	2873	2872	2867	158.8	157.4	157.5	157.0	12.9	21.2
14	60	3000	200	2804	2805	2804	2805	179.3	179.2	179.1	179.1	6.5	10.4

Chapter 6

Design and Development of Daylight-responsive Dynamic Lighting System

Daylight-integrated lighting system demands an artificial dynamic lighting system whose spectral composition and light output vary according to daylight. Dynamic lighting system (DLS) is developed and evaluated by experimental procedures as mentioned in **Chapter 5**. The DLS also successfully mimic a pre-defined time varying pattern of CCT and illuminance as presented in **Section 5.4.3**. Considering this feature a daylight-responsive DLS is designed and developed by means of two light control schemes- open-loop and closed-loop. One RGB color sensor, calibrated with *CL 200A* chromameter, is used in open-loop light control scheme to monitor the instantaneous daylight data at window plane. For closed-loop light control scheme, another calibrated RGB color sensor is used in the feedback path to monitor the output of the DLS and also to reduce the deviation between desired and measured data due to temperature variation and other physical process. Hardware prototype of both the light control schemes are developed, fabricated and subsequently performance is evaluated experimentally.

6.1 Daylight Color Sensor

The quality and quantity of daylight is dynamic in nature and vary as a result of weather conditions and position of the sun [Ashdown 2002] with time of a day, day of a month and season to season [de Kort and Smolders 2010; Pinho et al. 2013]. Hence it is required to monitor the dynamic daylight in terms of spectral composition (CCT) and global/diffuse horizontal illuminance. The CCT is very effective to characterize the spectral properties of a near-white light source.

In this study *TCS34725* RGB color sensor [Anonymous 2016a], sho-wn in **Figure 6.1**, is used as the daylight color sensor. The RGB color sensor returns data from four channels: red (*R*), green (*G*), blue (*B*) and clear (*C*) (non-filtered). The responses (*R,G,B*) from the red, green and blue channels are used to determine CCT of the instantaneous available daylight. The relative spectral responsivity of the four channels of the RGB color sensor is shown in **Figure 6.2**. The procedure to achieve CCT from these *R,G,B* values is to transfer the *R,G,B* responses to the CIE 1931 tistimulus values-*X,Y,Z*. Chromaticity coordinates (*x,y*) are calculated with tristimulus values (*X,Y,Z*) and *TCS34725* sensor is to be calibrated to map the sensor response (*R,G,B*) to the corresponding CIE tristimulus values (*X,Y,Z*). The **Figure 6.3** shows the overview of this process used for each step of transformation from (R,G,B) to CCT [Smith 2009].

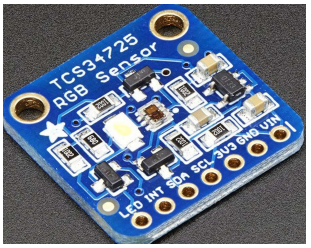

Figure 6.1: *TCS34725* RGB color sensor [Anonymous 2016a]

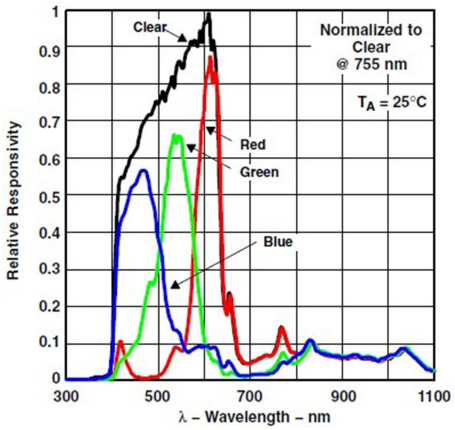

Figure 6.2: Relative spectral responsivity of four channels of *TCS34725* [Anonymous 2012a]

From the **Figure 6.3**, the tristimulus value (*X,Y,Z*) in the color space can be expressed mathematically in terms of (*R,G,B*) values of the light source and a 3×3 correlation matrix (**C**) as

$$\begin{bmatrix} X \\ Y \\ Z \end{bmatrix} = \mathbf{C} \begin{bmatrix} R \\ G \\ B \end{bmatrix} \quad or, \quad \mathbf{T} = \mathbf{CS} \tag{6.1}$$

$$where \quad \mathbf{T} = \begin{bmatrix} X \\ Y \\ Z \end{bmatrix}, \quad \mathbf{C} = \begin{bmatrix} c_{11} & c_{12} & c_{13} \\ c_{21} & c_{22} & c_{23} \\ c_{31} & c_{32} & c_{33} \end{bmatrix}, \quad \mathbf{S} = \begin{bmatrix} R \\ G \\ B \end{bmatrix}. \tag{6.2}$$

After calculating the tristimulus values, the chromaticity (*x,y*) is calculated using **Eqn. 6.3**.

$$x = \frac{X}{X+Y+Z} \quad and \quad y = \frac{Y}{X+Y+Z} \tag{6.3}$$

Finally, the CCT (T_C) is calculated from the (*x,y*) using McCamy's polynomial (**Eqn 6.4**) [Hernández-Andrés et al. 1999]. This model

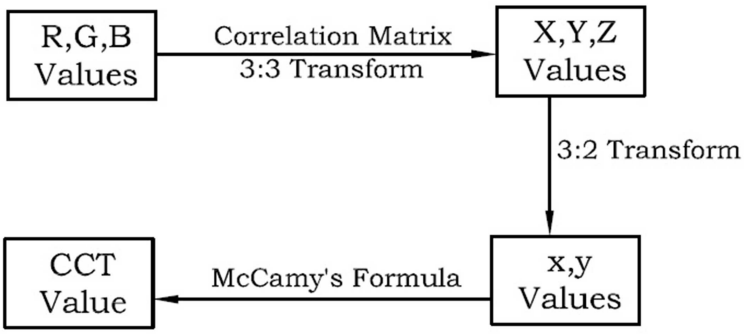

Figure 6.3: Overview of the CCT calculation process [Smith 2009]

is valid for the T_C range 2000 to 12500*K*.

$$T_C = 449n^3 + 3525n^2 + 6823.3n + 5520.33$$

$$where \quad n = \frac{x - 0.3320}{0.1858 - y} \tag{6.4}$$

The instruments used for the entire experimentation are listed in **Table 6.1** and their details are given in **Appendix A**.

Table 6.1: Instruments used for the experimentation

Sl. No.	Name of the Instrument
1	GWINSTEK *APS-1102* programmable power source
2	Integrating Sphere
3	Konica Minolta (*CL-200A*) chromameter
4	Yokogawa (*WT 210*) digital power meter

The coefficients of the correlation matrix are obtained from the RGB response signals of the *TCS34725* RGB sensor and corresponding tristimulus values measured with the help of *CL 200A* chromameter. For this purpose, the *R,G,B* values and corresponding *X,Y,Z* values are measured for three different CCT values viz., lower CCT, higher CCT and intermediate CCT point somewhere in the middle

range. At first, *R,G,B* values (R_L,G_L,B_L) and corresponding *X,Y,Z* (X_L,Y_L,Z_L) values are measured at lower CCT point as

$$\begin{pmatrix} R_L = 1350 \\ G_L = 798 \\ B_L = 602 \end{pmatrix} \quad and \quad \begin{pmatrix} X_L = 396.0 \\ Y_L = 357.3 \\ Z_L = 140.5 \end{pmatrix}. \tag{6.5}$$

Similarly at intermediate CCT point (R_I,G_I,B_I) and (X_I,Y_I,Z_I) values are measured as

$$\begin{pmatrix} R_I = 1112 \\ G_I = 1003 \\ B_I = 964 \end{pmatrix} \quad and \quad \begin{pmatrix} X_I = 376.5 \\ Y_I = 376.2 \\ Z_I = 302.2 \end{pmatrix} \tag{6.6}$$

and also at higher CCT point, the above values are measured as

$$\begin{pmatrix} R_H = 930 \\ G_H = 1006 \\ B_H = 1035 \end{pmatrix} \quad and \quad \begin{pmatrix} X_H = 339.4 \\ Y_H = 354.3 \\ Z_H = 345.3 \end{pmatrix}. \tag{6.7}$$

Hence the tristimulus matrix is defined as

$$\mathbf{T} = \begin{bmatrix} X_L & X_I & X_H \\ Y_L & Y_I & Y_H \\ Z_L & Z_I & Z_H \end{bmatrix}. \tag{6.8}$$

Similarly the *R,G,B* values from the response of the *TCS34725* RGB sensor are arranged in the sensor response matrix (**S**) as

$$\mathbf{S} = \begin{bmatrix} R_L & R_I & R_H \\ G_L & G_I & G_H \\ B_L & B_I & B_H \end{bmatrix}. \tag{6.9}$$

Hence the correlation matrix can be represented by **Eqn. 6.10**.

$$\mathbf{C} = \mathbf{T}\mathbf{S}^{-1}$$

$$or \quad \begin{bmatrix} c_{11} & c_{12} & c_{13} \\ c_{21} & c_{22} & c_{23} \\ c_{31} & c_{32} & c_{33} \end{bmatrix} = \begin{bmatrix} X_L & X_I & X_H \\ Y_L & Y_I & Y_H \\ Z_L & Z_I & Z_H \end{bmatrix} \begin{bmatrix} R_L & R_I & R_H \\ G_L & G_I & G_H \\ B_L & B_I & B_H \end{bmatrix}^{-1}$$

$$= \begin{bmatrix} 396.0 & 376.5 & 339.4 \\ 357.3 & 376.2 & 354.3 \\ 140.5 & 302.2 & 345.3 \end{bmatrix} \begin{bmatrix} 1350 & 1112 & 930 \\ 798 & 1003 & 1006 \\ 602 & 964 & 1035 \end{bmatrix}^{-1}$$

$$= \begin{bmatrix} 0.2355 & 0.0376 & 0.0797 \\ 0.1354 & 0.1958 & 0.0303 \\ -0.0587 & -0.0604 & 0.4451 \end{bmatrix} \tag{6.10}$$

The tristimulus values (*X,Y,Z*) of incident radiation on the color sensor can be determined from the measured *R,G,B* value and correlation matrix (***C***) using **Eqn. 6.11**.

$$\begin{bmatrix} X \\ Y \\ Z \end{bmatrix} = \begin{bmatrix} 0.2355 & 0.0376 & 0.0797 \\ 0.1354 & 0.1958 & 0.0303 \\ -0.0587 & -0.0604 & 0.4451 \end{bmatrix} \begin{bmatrix} R \\ G \\ B \end{bmatrix} \tag{6.11}$$

Once tristimulus values are determined, the CCT of the incident radiation is determined using **Eqns. 6.3** and **6.4**.

It is known that the tristimulus distribution function $\bar{y}_\lambda$ is exactly similar to the relative photopic spectral luminous efficiency curve $V(\lambda)$. Hence, any photometric parameter like luminous flux (Φ), luminance (*L*), or illuminance (*E*) is proportional to *Y*. So the measured illuminance (*E*) in *Lux* of the incident light can be obtained from **Eqn. 6.11** and expressed by **Eqn. 6.12**.

$$E = 0.1354R + 0.1958G + 0.0303B \tag{6.12}$$

6.2 Design Scheme: Open-loop and Closed-loop

The CCT and illuminance of daylight exhibit irregular variation, i.e. sometimes the variation is large and sometimes it is insignificant. These characteristics are taken into account to fix up the desirable characteristics of the proposed light controller, as mentioned below, to realize daylight-responsive DLS-

- to measure CCT and illuminance of external daylight at window plane of a room
- to vary CCT of daylight-responsive light source accordingly to match instantaneous measured daylight CCT
- to vary lumen output of daylight-responsive light source accordingly to follow measured daylight illuminance variation either in a similar pattern or in a reverse pattern.

It is desirable to adjust the emitted lumen output from the WLED arrays in response to the variation of available daylight only when the variations exceed preset limiting values; otherwise the emitted lumen output remain unchanged which results in system output unaltered.

In case of daylight–integrated dynamic lighting system, the DLS can be programmed to follow the dynamics of daylight by means of two control schemes- open loop and closed loop. In case of open-loop system, the DLS monitors the available instantaneous daylight and follows the CCT and illuminance based on pre-defined relationship between duty cycle and light output of WLED arrays. Whereas, in case of closed-loop system, along with the available instantaneous daylight data, the DLS also receives feedback of the achieved light scene through an internal color sensor to minimize the difference between the desired and achieved light scene in term of both CCT and illuminance.

6.2.1 Open-loop control scheme

One preliminary study is conducted to obtain daylight-responsive open-loop light controller based on radio-frequency (RF) communication between externally placed daylight sensor and light controller [Maiti et al. 2017]. In this control scheme, only light output of luminaires are allowed to control according to instantaneous available daylight level by a proposed control logic. This open-loop control logic is upgraded to obtain color tunable DLS.

The operational flowchart of the upgraded open-loop control scheme under continuous operation mode is shown in **Figure 6.4**. The detailed description is given below-

Step 1: after switching on the system, the DLS is driven for a predefined CCT (5000*K*) and illuminance (190 *Lux*) value with the corresponding duty cycles of the two WLED arrays. The upper and lower limit of $T^{\alpha}_{C,R}(t)$ and $E^{\alpha}_{R}(t)$ are set as T^{C}_{C}, T^{W}_{C} and E^{α}_{high}, E^{α}_{low} respectively which depend on the rated photometric parameters of

both WLED arrays.

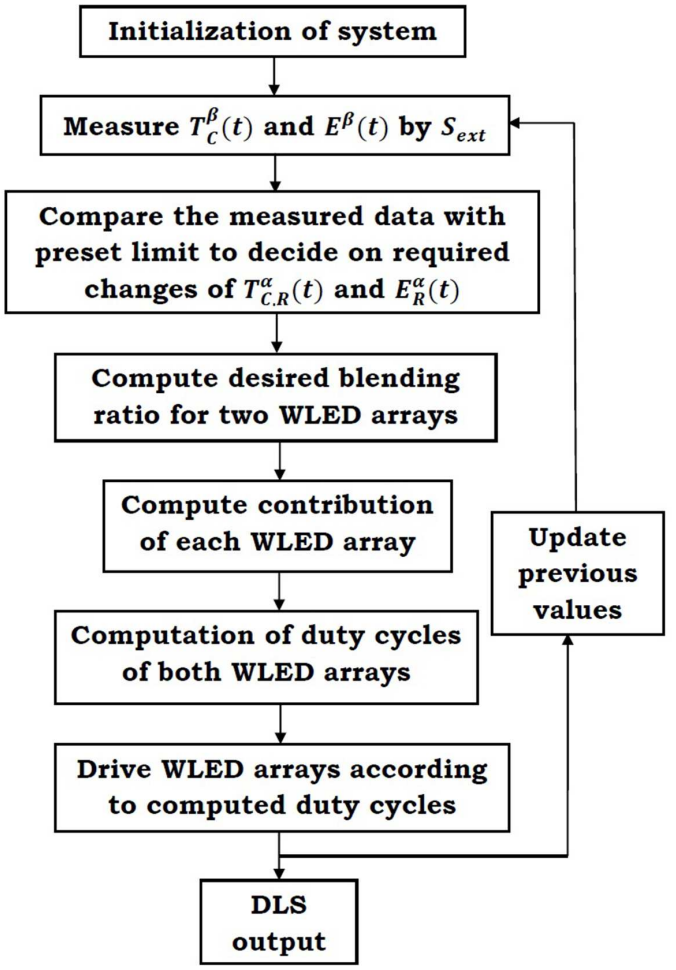

Figure 6.4: Operational flowchart of open-loop control scheme: Continuous operation mode

Step 2: after initialization, the daylight sensor S_{ext} measures $T_C^{\beta}(t)$ and $E^{\beta}(t)$ of available instantaneous daylight flux at the window plane.

Step 3: then the measured $T_C^{\beta}(t)$ and $E^{\beta}(t)$ values are checked as

to whether or not they lie within the upper and lower limits of CCT and illuminance respectively. When the $T_C^{\beta}(t)$ value is outside the limits then the $T_{C,R}^{\alpha}(t)$ value is updated as

$$\begin{aligned} T_{C,R}^{\alpha}(t) &= T_C^C, \qquad T_C^{\beta}(t) > T_C^C \\ &= T_C^W, \qquad T_C^{\beta}(t) < T_C^W. \end{aligned} \tag{6.13}$$

Otherwise the control scheme calculates the deviation in CCT as

$$\Delta T_C^{\beta} = |T_C^{\beta}(t) - T_C^{\beta}(t-1)| \tag{6.14}$$

and then updated the required values as

$$\begin{aligned} T_{C,R}^{\alpha}(t) &= T_C^{\beta}(t), \qquad \Delta T_C^{\beta} \geq 50K \\ &= T_{C,R}^{\alpha}(t-1), \quad \Delta T_C^{\beta} < 50K. \end{aligned} \tag{6.15}$$

Similarly, when $E^{\beta}(t)$ is outside the limits then $E_R^{\alpha}(t)$ value is updated as

$$\begin{aligned} E_R^{\alpha}(t) &= E_{low}^{\alpha}, \qquad E^{\beta}(t) > E_{high}^{\beta} \\ &= E_{high}^{\alpha}, \qquad E^{\beta}(t) < E_{low}^{\beta}. \end{aligned} \tag{6.16}$$

Otherwise, the percentage variation $E_{\delta}^{\beta}(t)$ and difference in percentage variation $\Delta E_{\delta}^{\beta}$ with respect to previous value are computed as

$$E_{\delta}^{\beta}(t) = \frac{E^{\beta}(t) - E_{avg}^{\beta}}{E_{avg}^{\beta}} \times 100$$

$$where \qquad E_{avg}^{\beta} = \frac{E_{high}^{\beta} + E_{low}^{\beta}}{2} \tag{6.17}$$

$$and \qquad \Delta E_{\delta}^{\beta} = E_{\delta}^{\beta}(t) - E_{\delta}^{\beta}(t-1) \tag{6.18}$$

and then calculates $E_R^{\alpha}(t)$ value as

$$\begin{aligned} E_R^{\alpha}(t) &= E_{avg}^{\alpha} - (E_{avg}^{\alpha} \times E_{\delta}^{\beta}(t)), \quad \Delta E_{\delta}^{\beta} \geq 0.5\% \ \ or \ \ \Delta E_{\delta}^{\beta} \leq -0.5\% \\ &= E_R^{\alpha}(t-1), \qquad -0.5\% < \Delta E_{\delta}^{\beta} < 0.5\% \end{aligned} \tag{6.19}$$

This calculated $E_R^{\alpha}(t)$ value is limited within the two limits- E_{high}^{α} and E_{low}^{α}. At initialization, $T_C^{\beta}(t-1)$, $E_R^{\alpha}(t-1)$ and $E_{\delta}^{\beta}(t-1)$ are assumed as 5000*K*, 0 *Lux* and 0% respectively.

Here the limiting values of ΔT_C^{β} and $\Delta E_{\delta}^{\beta}$ are set as 50*K* and 0.5% which are far below the acceptable limits of variation [Anonymous 1992, 2008a; Chen et al. 2014].

Step 4: the $T_{C,R}^{\alpha}(t)$ and $E_R^{\alpha}(t)$ values are achieved by proper mixing of luminous flux from the two WLED arrays in appropriate proportion [Maiti and Roy 2015, 2018; Murdoch 1985]. The ratio of luminous flux contributed by the WW to the luminous flux contributed by CW is termed as blending ratio [Maiti and Roy 2015] which is calculated based on Grassman's color mixing formula using the chromaticity of WW (x^W, y^W), CW (x^C, y^C) LED arrays and chromaticity $(x_R^{\alpha}, y_R^{\alpha})$ corresponding to required CCT value [Maiti and Roy 2015; Murdoch 1985]. The chromaticity $(x_R^{\alpha}, y_R^{\alpha})$ is updated as-

$$\begin{aligned} x_R^{\alpha} &= x^{\beta} \quad and \quad y_R^{\alpha} = y^{\beta}, \quad T_C^W < T_C^{\beta}(t) < T_C^C \\ x_R^{\alpha} &= x^W \quad and \quad y_R^{\alpha} = y^W, \quad T_C^{\beta}(t) \leq T_C^W \\ x_R^{\alpha} &= x^C \quad and \quad y_R^{\alpha} = y^C, \quad T_C^{\beta}(t) \geq T_C^C \end{aligned} \tag{6.20}$$

Step 5: the control scheme calculates the required illuminance contribution E_R^W and E_R^C of WW and CW respectively using the calculated blending ratio and $E_R^{\alpha}(t)$ [Maiti and Roy 2015].

Step 6: after computing the illuminance contribution of individual WLED array the light controller computes the duty cycles $DC^W(t)$ and $DC^C(t)$. The duty cycles corresponding to desired illuminances are computed from the experimentally evaluated relation between duty cycle and illuminance of individual WLED array of higher wattage and wider CCT range using the experimental procedure mentioned in **Section 5.2.5**. The corresponding experimental results are presented in **Section 6.3.1**.

Step 7: the light control scheme drives the two WLED arrays with respective calculated duty cycles fed to the switching devices con-

nected between each LED array and its driver and at the same time previous data are updated by current data.

To evaluate performance of the open-loop control scheme, $T^{\alpha}_{C,M}$ and E^{α}_{M} generated by the DLS are measured experimentally by a color sensor. A small delay is provided before measuring these data to stabilize the light source. After driving with the computed duty cycles the process is repeated from **step 2 to 7**.

6.2.2 Closed-loop control scheme

The open-loop control scheme has some inherent limitations due to absence of feedback such as-

- it is incapable of monitoring the instantaneous achieved CCT and illuminance
- it is incapable of addressing the effect of temperature variation on spectral composition and lumen output of WLEDs and also of lumen depreciation and spectral variation due to aging [Royer 2014].

To overcome the above limitations, closed-loop light control scheme is adopted to achieve daylight-responsive DLS. Here another RGB color sensor, S_{int} generates feedback signal by monitoring the CCT and illuminance of the achieved light scene produced by DLS. This closed-loop control scheme is capable of tuning the lamp system to cope up with the influence of ambient temperature variation as well as junction temperature and aging effect on spectral composition and lumen output of WLED modules.

The operational flowchart of the developed closed-loop light control scheme under continuous operation mode is shown in **Figure 6.5**. The detailed description of **step 1** to **5** are given in **Section 6.2.1** and remaining steps are given below-

Step 6: after computing the desired illuminance contribution of individual WLED array, the initial estimation of duty cycles $DC^{W}(t)$

and $DC^C(t)$ is done by linear approximation of the relationship between duty cycle and luminous flux.

Step 7: the light control scheme drives the two WLED arrays with respective calculated duty cycles fed to the switching devices connected between each LED array and its driver.

Step 8: the internal light sensor S_{int} measures $T^{\alpha}_{C,M}$ and E^{α}_{M} generated by the DLS. A small delay is provided for stabilization before measuring these data.

Step 9: after measuring $T^{\alpha}_{C,M}$ and E^{α}_{M}, the deviations in T_C and E are computed by

$$\begin{aligned} \Delta T^{\alpha}_{C} &= T^{\alpha}_{C,R}(t) - T^{\alpha}_{C,M} \\ and \quad \Delta E^{\alpha} &= E^{\alpha}_{R}(t) - E^{\alpha}_{M}. \end{aligned} \tag{6.21}$$

Step 10: the deviations are then compared with the tolerance values. If both the deviations are within the tolerance values then the control scheme updates previous values with the current values and then again repeats the process by measuring $T^{\beta}_{C}(t)$ and $E^{\beta}(t)$ using S_{ext} from Step 2.

A successive iteration method is applied to adjust the duty cycles of both the WLED arrays to bring down the deviations within the tolerances when any of the deviations are greater than the corresponding tolerance values. After adjusting the duty cycles the process is repeated from **step 7** to **10**.

In the method of successive iteration, the light control scheme compares the measured data with the desired data and changes the duty cycle of either WW or CW or the both, depending upon the values of ΔT^{α}_{C} and ΔE^{α} as discussed in **Table 6.2**.

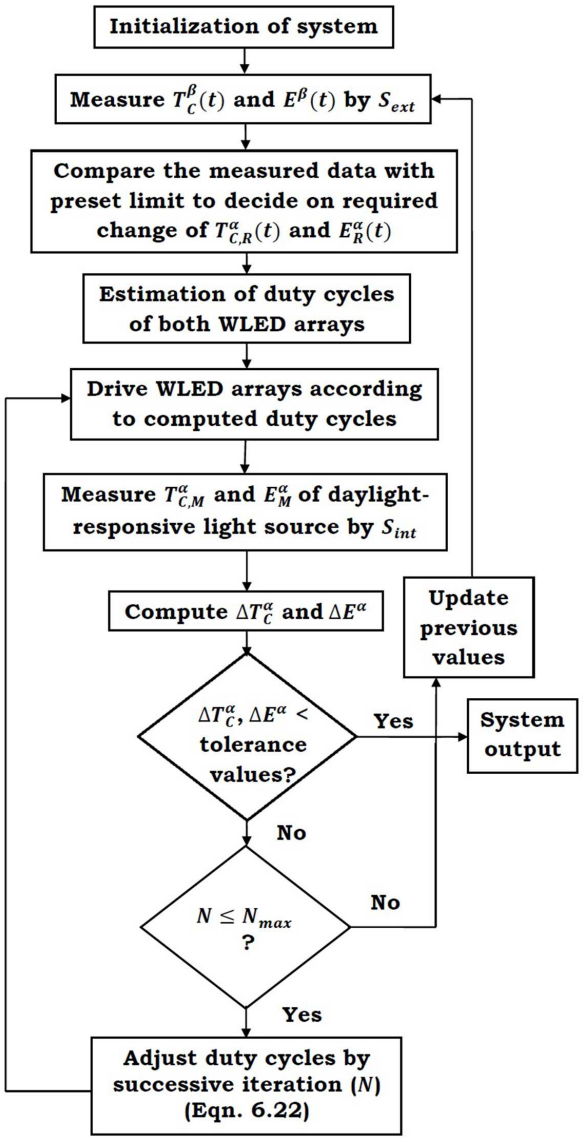

Figure 6.5: Operational flowchart of iterative closed-loop control scheme: Continuous operation mode

Table 6.2: Scheme of adjusting duty cycles in the successive iteration method

Possible case	Explanation	Action
$\Delta T_C^\alpha < 0$ $\Delta E^\alpha < 0$	Contribution of CW LED is more than the required value	Reduce the duty cycle of CW LED array
$\Delta T_C^\alpha > 0$ $\Delta E^\alpha > 0$	Contribution of CW LED is less than the required value	Increase the duty cycle of CW LED array
$\Delta T_C^\alpha < 0$ $\Delta E^\alpha > 0$	Contribution of WW LED is less than the required value	Increase the duty cycle of WW LED array
$\Delta T_C^\alpha > 0$ $\Delta E^\alpha < 0$	Contribution of WW LED is more than the required value	Reduce the duty cycle of WW LED array
$\Delta T_C^\alpha = 0$ $\Delta E^\alpha < 0$	Contribution of WW and CW LED are more than the required values	Reduce the duty cycles of both WW and LED arrays
$\Delta T_C^\alpha = 0$ $\Delta E^\alpha > 0$	Contribution of WW and CW LED are less than the required values	Increase the duty cycles of both WW and CW LED arrays
$\Delta T_C^\alpha < 0$ $\Delta E^\alpha = 0$	Contribution of WW LED is less than the required value whereas contribution of CW LED is more than the required value	Increase the duty cycle of WW LED array and reduce the duty cycle of CW LED array
$\Delta T_C^\alpha > 0$ $\Delta E^\alpha = 0$	Contribution of WW LED is more than the required value whereas contribution of CW LED is less than the required value	Reduce the duty cycle of WW LED array and increase the duty cycle of CW LED array

Hence the light controller modifies the two duty cycles (DC^W_{MOD} and DC^C_{MOD}) according to the action provided in 3^{rd} column of **Table 6.2** using **Eqn. 6.22**

$$\begin{aligned}
DC^W_{MOD} = DC^W(t) \quad \& \quad DC^C_{MOD} = (DC^C(t) - k), \\
when, \qquad \Delta T^\alpha_C < 0 \quad \& \quad \Delta E^\alpha < 0; \\
\\
DC^W_{MOD} = DC^W(t) \quad \& \quad DC^C_{MOD} = (DC^C(t) + k), \\
when, \qquad \Delta T^\alpha_C > 0 \quad \& \quad \Delta E^\alpha > 0; \\
\\
DC^W_{MOD} = (DC^W(t) + k) \quad \& \quad DC^C_{MOD} = DC^C(t), \\
when, \quad \Delta T^\alpha_C < 0 \quad \& \quad \Delta E^\alpha > 0; \\
\\
DC^W_{MOD} = (DC^W(t) - k) \quad \& \quad DC^C_{MOD} = DC^C(t), \\
when, \quad \Delta T^\alpha_C > 0 \quad \& \quad \Delta E^\alpha < 0; \\
\\
DC^W_{MOD} = (DC^W(t) - k) \quad \& \quad DC^C_{MOD} = (DC^C(t) - k), \\
when, \quad \Delta T^\alpha_C = 0 \quad \& \quad \Delta E^\alpha < 0; \\
\\
DC^W_{MOD} = (DC^W(t) + k) \quad \& \quad DC^C_{MOD} = (DC^C(t) + k), \\
when, \quad \Delta T^\alpha_C = 0 \quad \& \quad \Delta E^\alpha > 0; \\
\\
DC^W_{MOD} = (DC^W(t) + k) \quad \& \quad DC^C_{MOD} = (DC^C(t) - k), \\
when, \quad \Delta T^\alpha_C < 0 \quad \& \quad \Delta E^\alpha = 0; \\
\\
DC^W_{MOD} = (DC^W(t) - k) \quad \& \quad DC^C_{MOD} = (DC^C(t) + k), \\
when, \quad \Delta T^\alpha_C > 0 \quad \& \quad \Delta E^\alpha = 0;
\end{aligned} \tag{6.22}$$

where, $0 < k \leq 255$. This process will continue until the deviations are within the tolerance values or until the set maximum iteration N_{max} is reached. To avoid flickering of the DLS, while following continuous daylight variation, the value of *k* is taken equal to 0.3.

6.3 Open-loop DLS: Development and Evaluation

6.3.1 System description

Based on the open-loop light control scheme, an external photosensor based open-loop light controller is designed and developed to follow the dynamic pattern of daylight CCT and diffuse illuminance level. The test lamp system consists of two main functional module viz., open-loop light controller and daylight-responsive light source as shown in **Figure 6.6**. The open-loop light controller comprises of two main functional blocks viz., external daylight sensor (S_{ext}) and control unit. The control unit receives output from the S_{ext}, which monitors instantaneous daylight data ($T_C^{\beta}(t)$ and $E^{\beta}(t)$) at window plane and controls the power fed to the light source to follow variable $T_{C,R}^{\alpha}(t)$ and $E_R^{\alpha}(t)$.

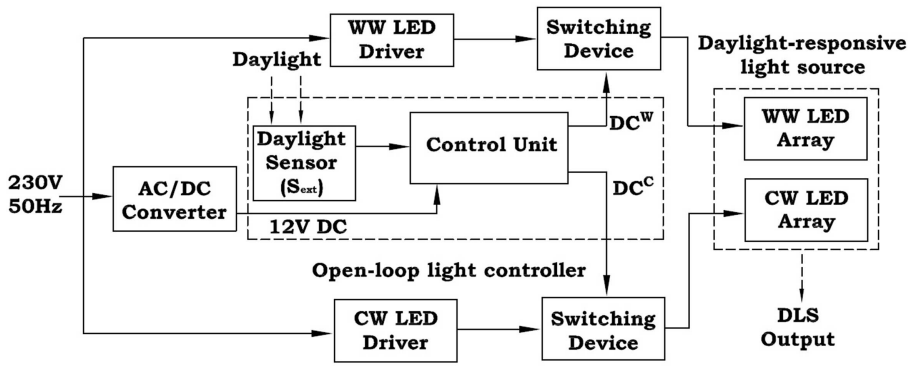

Figure 6.6: Block diagram representation of the proposed open-loop daylight-responsive DLS

A) Daylight sensor

One calibrated *TCS34725* RGB sensor (S_{ext}) is used to generate *R,G,B* values of incident daylight radiation at window plane and send the data to the control unit using I^2C protocol [Anonymous

2012a].

B) Control unit

A *ATmega328P* microcontroller based Arduino Uno is the primary component of the open-loop light controller and is used as the control unit [Anonymous 2018d]. This control unit receives signals from the RGB color sensor and converts it into corresponding CCT and illuminance values. When the measured data $T_C^{\beta}(t)$ and $E^{\beta}(t)$ show significant variation compared to previous values, then the control unit decides the target values $T_{C,R}^{\alpha}(t)$ and $E_R^{\alpha}(t)$, to be achieved by the DLS. Accordingly the control unit generates the required control signals (duty cycles) for the respective WLED arrays corresponding to the required CCT and illuminance values.

C) Daylight-responsive light source

WLED based composite light source of higher wattage and wider CCT range is developed for this purpose and stages of developent are described in **Section 4.4**. The electrical and photometric parameters of the fabricated WW and CW LED arrays are measured and presented in **Table 6.3**.

Table 6.3: Measured electrical and photometric parameters of daylight-responsive light source at rated supply voltage

Measured parameter		WW LED array	WW LED array
Electrical	V_T (*V*)	24.17	24.10
	I (*mA*)	603.4	609.4
	P (*W*)	14.58	14.68
Photometric	T_C (*K*)	2874	6350
	Φ (*lm*)	991	1142
Chromaticity	*x*	0.4447	0.3148
	y	0.4040	0.3358

The variation of illuminance of the individual WLED array of the

daylight-responsive light source with the duty cycle are experimentally measured and the relation between duty cycle and illuminance is determined by MATLAB curve fitting tool. For WW LED array, the best fit relation is a 9^{th} degree polynomial as represented by **Eqn. 5.7** where the values of E^{mean} and E^{std} are 175.1 *Lux* and 96.52 *Lux* respectively. The values of coefficients P_1-P_{10} with 95% confidence bounds are given in 2^{nd} column of **Table 6.4**. The above fitted result gives lowest SSE value (2.228) and highest value of adjusted R-square (1). The best fit plot is given in **Figure 6.7(a)**.

Table 6.4: Coefficients of best fit curve with 95% confidence bounds for individual WLED array of daylight-responsive light source

Coefficient	WW LED array			CW LED array		
	Value	95% confidence		Value	95% confidence	
		Lower bound	Upper bound		Lower bound	Upper bound
P_1	-0.225	-0.327	-0.1229	-0.4391	-0.58	0.2983
P_2	-0.4154	-0.5098	-0.321	-1.138	-1.377	-0.8994
P_3	0.8685	0.2083	1.529	1.33	0.5302	2.129
P_4	1.571	1.038	2.105	4.518	3.366	5.67
P_5	-1.173	-2.62	0.2735	-0.9961	-2.662	0.6701
P_6	-1.868	-2.829	-0.9072	-5.775	-7.558	-3.993
P_7	1.264	0.0362	2.492	1.215	-0.2347	2.664
P_8	4.078	3.482	4.675	10.93	9.977	11.89
P_9	73.51	37.17	73.84	73.87	73.45	74.29
P_{10}	125.9	125.8	126	120.9	120.8	121

Similarly for CW LED array, the best fit relation is also 9^{th} degree polynomial as represented by **Eqn. 5.8** where the values of E^{mean} and E^{std} are 255.1 *Lux* and 131 *Lux* respectively. The values of coefficients P_1-P_{10} with 95% confidence bounds are given in 2^{nd} column of **Table 6.4**. The above fitted result gives lowest SSE value (4.116) and highest value of adjusted R-square (1). The best fit plot is given in **Figure 6.7(b)**.

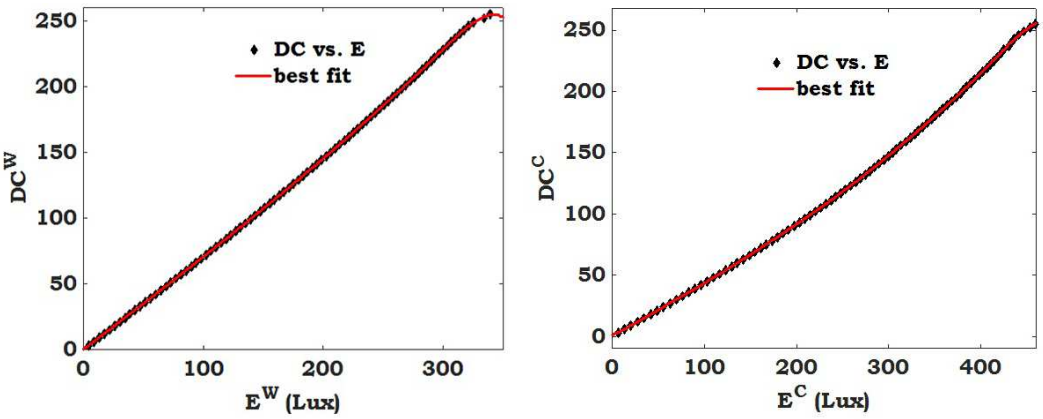

(a) (b)

Figure 6.7: best fit plots of (a) WW and (b) CW array of daylight-responsive light source

This daylight-responsive light source can follow the dynamic pattern of daylight CCT and illuminance within the range limited by CCT values and light output of its constituting LED arrays respectively as given below-

- T_C (*K*): 2874-6350
- *E* (*Lux*): 35-350

E is measured at a vertical distance of $1m$. The other features of the daylight-responsive light source are listed below-

- Variation mode: continuous
- Flicker: no perceived flicker

6.3.2 System development

The fabricated open-loop light controller is shown in **Figure 6.8**. *ATmega328P* based Arduino Uno is the primary component of the

light controller and used as the control unit. *TCS34725* RGB sensor is used as external daylight sensor which follow the I^2C protocol [Anonymous 2012a]. An Arduino (version 1.6.5) program is developed for the open-loop light control scheme by following the flowchart shown in **Figure 6.4** and embedded in the *ATmega328P* microcontroller of the Arduino Uno. After receiving the RGB data from S_{ext}, the control unit computes the required duty cycles for the two WLED arrays and accordingly generates two PWM signals (0-5V) separately at two PWM pins. These PWM signals are fed to the two separate switching devices connected between each WLED array and its driver. Here *BS 170*, n-channel MOSFET is used as the switching device [Anonymous 2017b]. For the proper functioning of the *BS 170*, the generated PWM signals (0-5V) are amplified to 0-12V using transistor (*BC 547B*) amplifier [Anonymous 2017a]. A real time clock (RTC) *DS3231* [Anonymous 2018a] and a Secure digital (SD) card module [Anonymous 2018b] are additionally connected with the Arduino Uno for real time monitoring and storing of the measured daylight data and also the measured indoor data. The technical specifications of components used to develop this open-loop light controller are presented in **Table 6.5**.

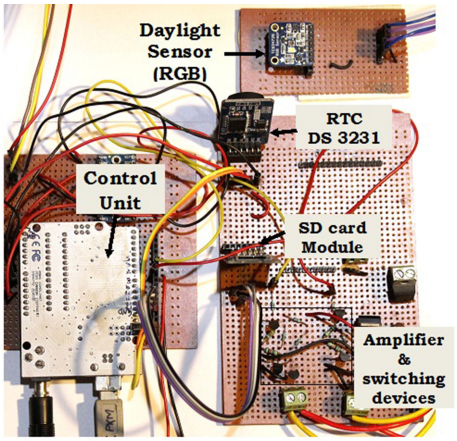

Figure 6.8: Fabricated open-loop light controller

Table 6.5: Technical specification of the system components

Component	Quantity	Specification
Arduino Uno	1	*ATmega328P* microcontroller, operating voltage: 5V, input voltage(recommended):7-12V DC, 14 digital I/O pins, 6 PWM pins, 6 analog pins, 16 *MHz* clock speed [Anonymous 2018d]
TCS34725 RGB color sensor	1	Red (R), Green (G), Blue (B), and Clear light sensing with IR blocking filter, very high sensitivity, 3,800,000:1 dynamic range [Anonymous 2012a]
Transistor (*BC 547B*)	4	n-p-n transistor, V_{CE}: 45V, V_{BE}: 5V, V_{CB}: 50V, I_C:100 mA [Anonymous 2017a]
MOSFET (*BS 170*)	2	n-channel, 500 mA, 60V [Anonymous 2017b]
Resistor	8 4	1$k\Omega$, 0.25W 10$k\Omega$, 0.25W
RTC *DS3231*	1	Fast (400kHz) I^2C interface, 3.3V operation, operating temperature ranges: Commercial ($0°$C to $+70°$C) and Industrial ($-40°$C to $+80°$C) [Anonymous 2018a]
SD card module	1	3.3/5V, SPI interface, micro SD compatible [Anonymous 2018b]

6.3.3 System evaluation

The performance of the developed open-loop light control scheme is experimentally evaluated through two testing procedures viz., laboratory testing and *in-situ* testing using the experimental setup shown in **Figure 6.9**.

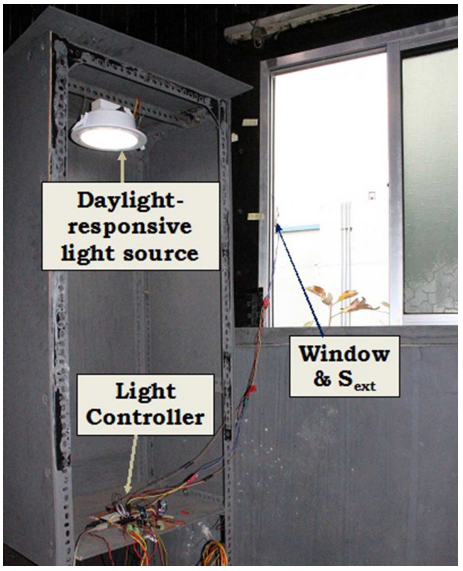

Figure 6.9: Experimental setup

Laboratory testing

In laboratory testing, the variable nature of daylight is simulated by an external light source comprised of one $6W$, $230V$ WW LED lamp and one $11W$, $230V$ CW CFL lamp supplied by GWINSTEK *APS-1102* programmable AC/DC power source. The performance is experimentally evaluated by sudden (step) variation of CCT and lumen output of the external light source at controlled environment. The open-loop light controller varies the duty cycles of both the LED arrays from current values towards required values in 300 steps with an in between delay of $50ms$ to eliminate possible

flickering effect. Another 15*s* delay time is introduced for the stabilization of output of DLS. Five preset combinations (set points) of $T_C^{\beta}(t)$ and $E^{\beta}(t)$, shown in 2^{nd} column of **Table 6.6**, are simulated and corresponding $T_{C,M}^{\alpha}$ and E_M^{α} are recorded after convergence to the required point. In set point 2, the CCT is increased in a step whereas in set point 3, the CCT value is suddenly decreased by keeping the illuminance value almost constant. Similarly in set point 4 the illuminance value is increased in a step, whereas in set point 5, illuminance is decreased sudenly by keeping CCT value constant. Subsequent step variation is simulated after convergence of the previous set point. The light sensor S_{ext}, placed below the external light source, feeds the data to the control unit. The values of E_{high}^{β} and E_{low}^{β} are set as 2000 *Lux* and 200 *Lux* respectively for the laboratory testing. The open-loop light controller varies the CCT of DLS in a similar pattern of the instantaneous external CCT and the illuminance in a reverse pattern of the variation of external illuminance. In response to the variation of external light scene, the required CCT and illuminance values are determined according to **Eqns. 6.13 - 6.15** and **6.16 - 6.19** respectively. The values of E_{high}^{α}, E_{low}^{α} and E_{avg}^{α} are set as 350 *Lux*, 35 *Lux* and 190 *Lux* respectively for the testing of open-loop light controller. The required and corresponding measured CCT and illuminance values of DLS generated indoor light scene are presented in 3^{rd} and 4^{th} column of **Table 6.6** respectively. The deviations of measured values from the required values are presented in 5^{th} column of the **Table 6.6**. It is already reported that chromaticity points slightly below the Planckian locus, i.e. negative D_{uv}, are more preferred [Ohno 2014]. Chromaticity deviation of DLS from the required CCT is expressed by D_{uv} [Ohno 2014] and the step size (n) of a MacAdam ellipse [Anonymous 2014a] to judge its compliance with the maximum allowable tolerance are calculated using **Eqns. 6.23** [Ohno 2014] and **6.24** [Anonymous 2014a] respectively where (u'_M,v'_M) and (u'_R,v'_R) are the chromaticity corresponding to measured and required CCT respectively.

$$D_{uv} = \sqrt{(u'_M - u'_R)^2 + (\frac{2}{3}v'_M - \frac{2}{3}v'_R)^2}.sgn(v'_M - v'_R)$$
$$where \quad sgn(v'_M - v'_R) = 1, \ (v'_M - v'_R) \geq 0$$
$$= -1, \ (v'_M - v'_R) < 0 \tag{6.23}$$

$$and \quad n = \frac{\sqrt{(u'_M - u'_R)^2 + (v'_M - v'_R)^2}}{0.0011} \tag{6.24}$$

The maximum deviation of the measured CCT is 99K which corresponds to 0.0017D_{uv} and D_{uv} values are found to be positive. These deviations lie within the maximum acceptable tolerance of a flexible CCT (2700-6500K) source [Anonymous 2008a]. Again, the step size 3, corresponding to maximum deviation in chromaticity, ensures acceptable colour deviation [Anonymous 2014a]. The maximum deviation in measured illuminance is found to be 7.8 *Lux*.

In-situ testing

The performance of the open-loop DLS under *in-situ* testing is carried out in a room of our laboratory with a single-sided and north-west facing window with a vertical obstruction (building) at a distance of 4m. The location of the measurement place is Kolkata, India (22.57° N, 88.36° E). S_{ext} is placed at the mid-height of window plane and the DLS within the experimental test setup. The values of E^{β}_{high} and E^{β}_{low} are set as 20000 *Lux* and 2000 *Lux* respectively for the *in-situ* testing based on several trial runs. The light controller varies the T_C and E of DLS according to **Eqns. 6.13 - 6.15** and **6.16 - 6.19** respectively as in the laboratory testing. The testing is conducted at time span *9:00 - 17:30* of different days in the month of May with partly cloudy sky conditions. The instantaneous values of T_C and E corresponding to external light scene, required light scene and measured internal light scene due to DLS are presented graphically in **Figure 6.10**. Internal light sensor measures CCT and illuminance of DLS generated light scene. To show whether the measured light scene due to DLS is highly correlated or loosely

Table 6.6: Laboratory test data of the open-loop DLS: measured CCT and illuminance values with deviations

Set point	External source (1)		Daylight-responsive DLS							
			Required (2)		Measured (3)		Deviation (2-3)			
	$T_C^{\beta}(t)$ (K)	$E^{\beta}(t)$ (Lux)	$T_{C,R}^{\alpha}(t)$ (K)	$E_R^{\alpha}(t)$ (Lux)	$T_{C,M}^{\alpha}$ (K)	E_M^{α} (Lux)	ΔT_C^{α} (K)	ΔE^{α} (Lux)	D_{uv}	Step Size (n)
1	3707	829.8	3707	236.7	3673	235.6	34	1.1	0.0011	2
2	6190	733.2	6190	253.4	6289	261.2	-99	-7.8	0.0017	3
3	3617	821.8	3617	238.0	3564	236.3	53	1.7	0.0014	2
4	3667	1839.8	3617	62.2	3592	60.0	25	2.2	0.0015	2
5	3690	800.7	3617	241.7	3577	239.9	40	1.8	0.0015	2

correlated with the required light scene, the correlation coefficient (*r*) values are calculated for CCT and illuminance where $-1 \leq r \leq 1$. *r* value of -1 implies a perfect negative relationship whereas *r* value of +1 implies a perfect positive relationship and *r* value of 0 implies no relationship between the required and measured values. For the above time span, *r* value between CCT of DLS ($T^{\alpha}_{C,M}$) and that of required light scene ($T^{\alpha}_{C,R}(t)$) is found to be 0.9944 whereas *r* value of the corresponding illuminance values is found to be 0.9998. The observed maximum deviations in measured CCT and illuminance are 280*K* and 9.9 *Lux*.

The target D_{uv} (D^{T}_{uv}) and the maximum allowable tolerance limits (D^{H}_{uv} and D^{L}_{uv}) for flexible CCT (2700-6500*K*) source are calculated using **Eqn. 6.25** [Anonymous 2008a] as

$$D^{T}_{uv} = \frac{57700}{T^{2}_{C}} - \frac{44.6}{T_{C}} + 0.0085$$
$$D^{H}_{uv} = D^{T}_{uv} + 0.006 \quad and \quad D^{L}_{uv} = D^{T}_{uv} - 0.006 \tag{6.25}$$

and shown in **Figure 6.11**. The solid line represents the D^{T}_{uv} value whereas the dashed represent the upper and lower limit of tolerance value. The overall D_{uv} values [Ohno 2014] are also calculated and shown in **Figure 6.11**.

The maximum deviation in CCT 280*K*, with respect to the required value of 6042*K*, is within the acceptable limit of CCT variation [Anonymous 2008a; Chen et al. 2014]. Whereas, the maximum deviation in illuminance is 9.9 *Lux* which is 4.7% of the required value of 210 *Lux* and far below the acceptable maximum deviation of illuminance [Anonymous 1992]. Moreover, out of 710 measured data points, 682 data points yield deviation in CCT $<$100*K* and 694 data points yield deviation in illuminance $<$5 *Lux* and above variations are within acceptable deviations [Anonymous 2008a].

These deviations and the r values establish the effectiveness of the proposed open-loop control algorithm as well as the satisfactory performance of the daylight-responsive open-loop light controller.

6.4 Closed-loop DLS: Development and Evaluation

6.4.1 System description

Based on the developed closed-loop light control scheme presented in **Section 6.2.2**, a light controller is designed to realize closed-loop DLS. The block diagram representation of the system is shown in **Figure 6.12**. Similar to open-loop DLS, the closed-loop DLS also comprises of two functional blocks viz., 1) closed-loop light controller and 2) daylight-responsive light source. The open-loop light controller is upgraded to the closed-loop light controller which comprises of three main functional blocks viz., external daylight sensor (S_{ext}), internal light sensor (S_{int}) and control unit. The control unit receives output from the S_{ext}, which monitors instantaneous daylight data ($T_C^{\beta}(t)$ and $E^{\beta}(t)$) at window plane and controls the power fed to the light source to follow variable $T_{C,R}^{\alpha}(t)$ and $E_R^{\alpha}(t)$. Whereas, S_{int}, in the feedback path, monitors both the instantaneous CCT and illuminance produced by the DLS. An I^2C multiplexer *TCA9548A* [Anonymous 2018c] is used for communication of the control unit with two light sensors S_{ext} and S_{int} by time division multiplexing because the light sensor *TCS34725* has a unique ID [Anonymous 2012a] and the control unit can not distinguish the signal output from the two sensors. The fabricated closed-loop light controller is shown in **Figure 6.13**. In the performance evaluation of the closed-loop DLS, the same daylight-responsive light source is used.

The features of the closed-loop daylight-responsive lamp system are listed below-

- Variation mode: continuous
- Convergence criteria: time- 15 *s* (maximum)
  T_C and E- $\pm$30*K* and $\pm$1 *Lux*
- Flicker: no perceived flicker

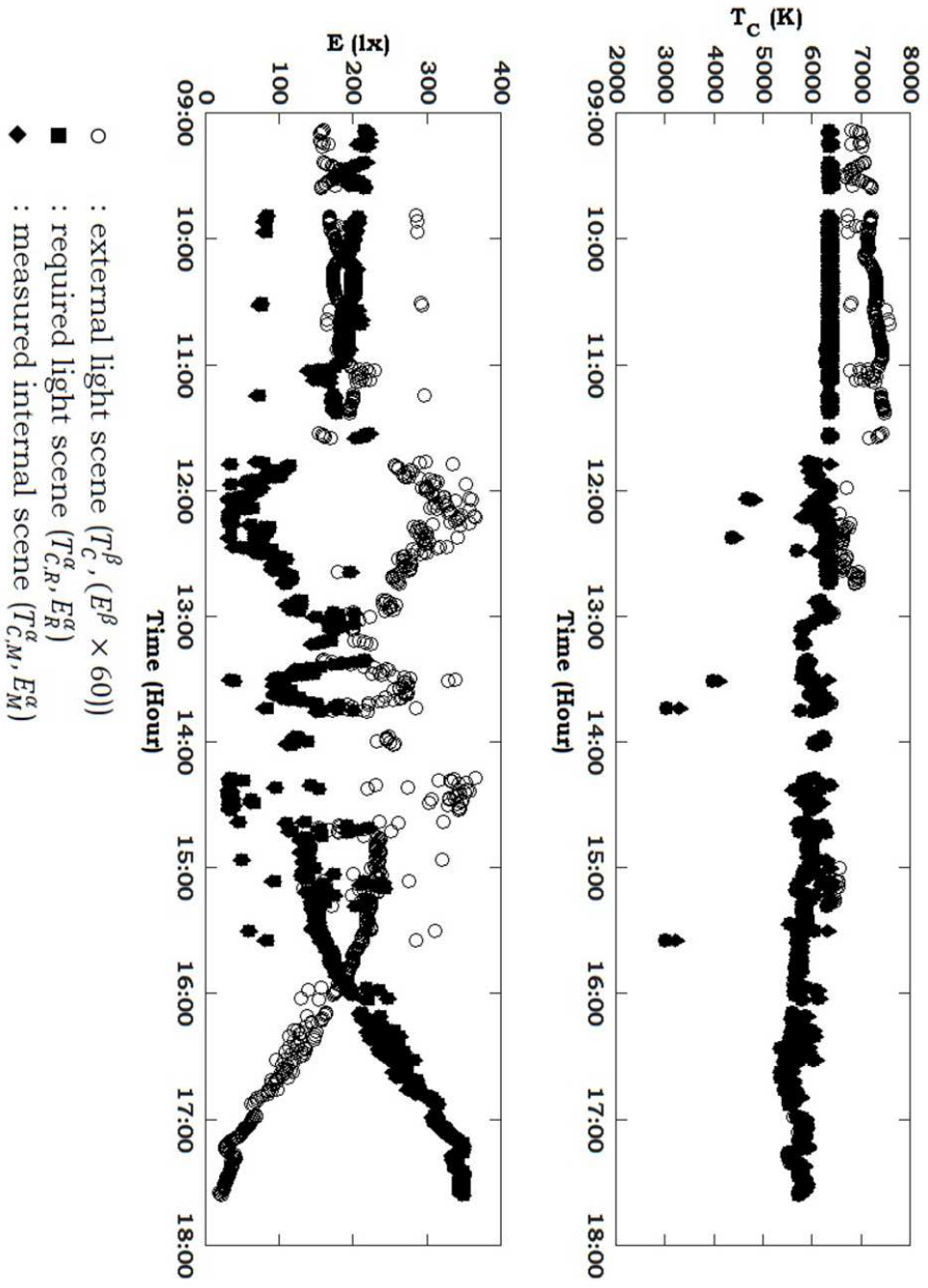

Figure 6.10: *In-situ* testing of the open-loop DLS

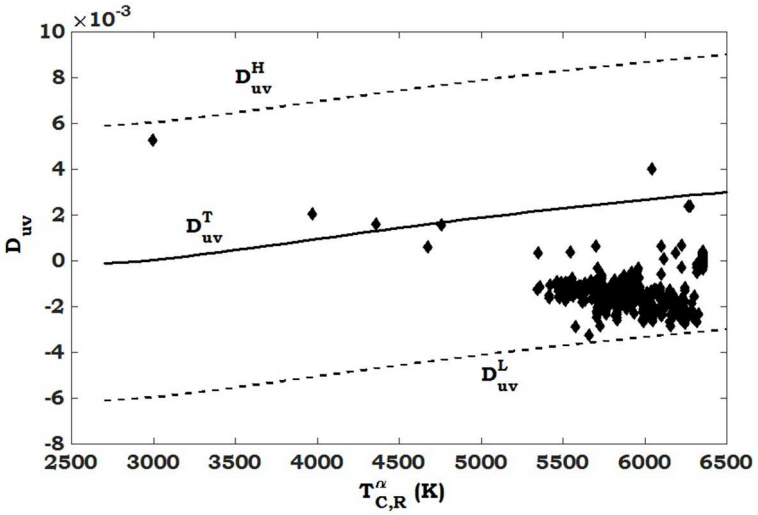

Figure 6.11: Overall chromaticity deviation (D_{uv}) of the open-loop DLS during in-situ testing

6.4.2 System evaluation

The performance of the developed closed-loop DLS is experimentally evaluated through two testing procedures viz., laboratory testing and *in-situ* testing using the expetimental test setup shown in **Figure 6.9**.

Laboratory testing

The performance of the closed-loop system is experimentally evaluated by sudden (step) variation of CCT and illuminance of the external light source at controlled environment similar to open-loop system. Here seven preset combinations of $T_C^{\beta}(t)$ and $E^{\beta}(t)$ as shown in 2^{nd} column of **Table 6.7**, are simulated and the time variations of $T_{C,M}^{\alpha}(t)$ and $E_M^{\alpha}(t)$ are recorded during the step-wise convergence to the required point. Subsequent step variation is simulated after convergence of the previous required point. In first 5 set points, test conditions similar to open-loop DLS are simulated. In set point 6, the CCT value is inceased and at the same time illuminance value is reduced suddenly wheareas in set point

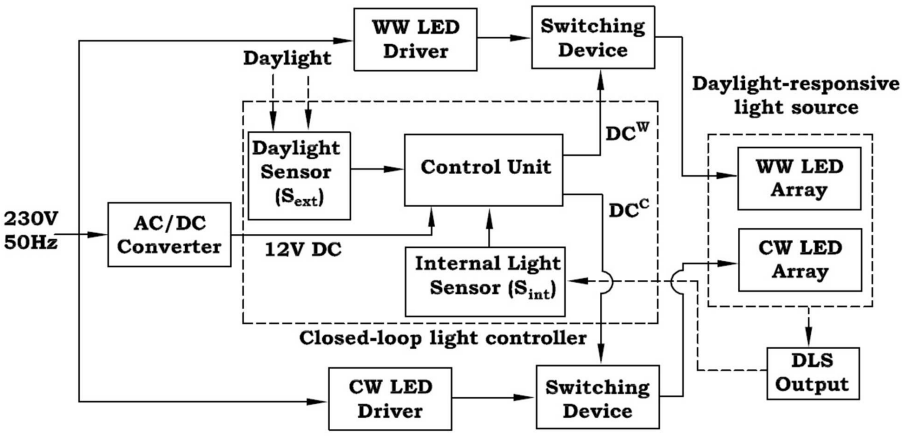

Figure 6.12: Block diagram representation of closed-loop daylight-responsive DLS

7 the reverse pattern of variation is simulated. The required values and corresponding measured values are presented in 3^{rd} and 4^{th} column of **Table 6.7**. The deviations in measured values from the required values are presented in 5^{th} column of the **Table 6.7**. The required convergence time varies between 7-15*s*. Chromaticity deviation of the DLS from the required CCT, expressed by D_{uv} [Ohno 2014] and step size (*n*) of MacAdam ellipse [Anonymous 2014a] are calculated using **Eqns. 6.23** [Ohno 2014] and **6.24** [Anonymous 2014a] respectively. The maximum deviation of the measured CCT is 25*K* which corresponds to 0.0025 D_{uv} and D_{uv} values are found to be positive. These deviations lie within the maximum acceptable tolerance of a flexible CCT (2700-6500*K*) source [Anonymous 2008a]. Again, the step size 4, corresponding to maximum deviation in chromaticity, ensures acceptable colour deviation [Anonymous 2014a]. The maximum deviation in measured illuminance is found to be 0.7 lx.

Figure 6.14 shows the variations of CCT and illuminance of the DLS with time to follow the preset step variation of external light source. Here time-variation of required and measured T_C and *E* due to DLS are plotted to show the progress of convergence towards

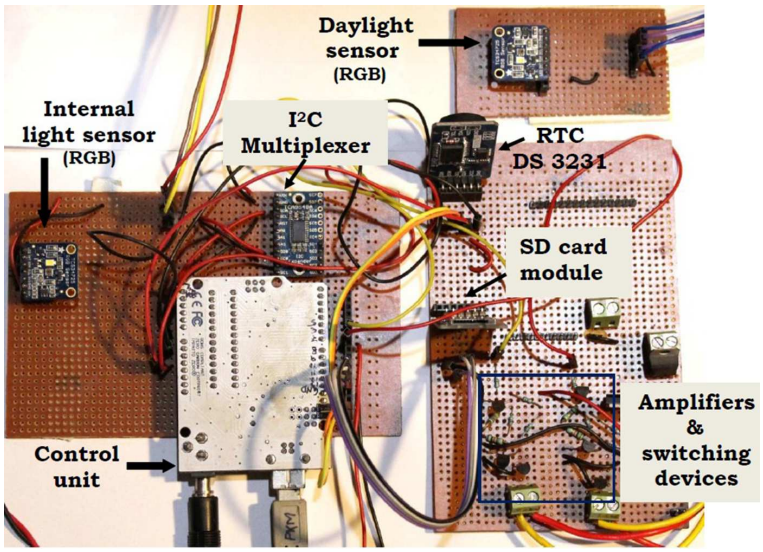

Figure 6.13: Fabricated closed-loop light controller

the preset combinations of T_C and E. At the initialization, CCT and illuminance generated by the DLS are 5000K and 190 *Lux* respectively as mentioned in **Section 6.2.1**. The first preset combination is achieved at about 12s; during convergence the $T^{\alpha}_{C,M}$ value gradually reduces towards required $T^{\alpha}_{C,R}$ while the E^{α}_{M} value overshoots the required value and then converges to the preset value. The overshoot occurs due to the initial estimation of duty cycle by linear approximation between duty cycle and lumen output of WLED. To avoid perceived flicker the duty cycles are varied in small step size with an in-between delay of few milliseconds while the output of DLS shifts from one set point to another set point, which result in convergence time of few seconds (7-15s).

The effectiveness of the proposed iterative closed-loop algorithm is thus demonstrated by the time propagation of convergence towards other preset combinations of T_C and E.

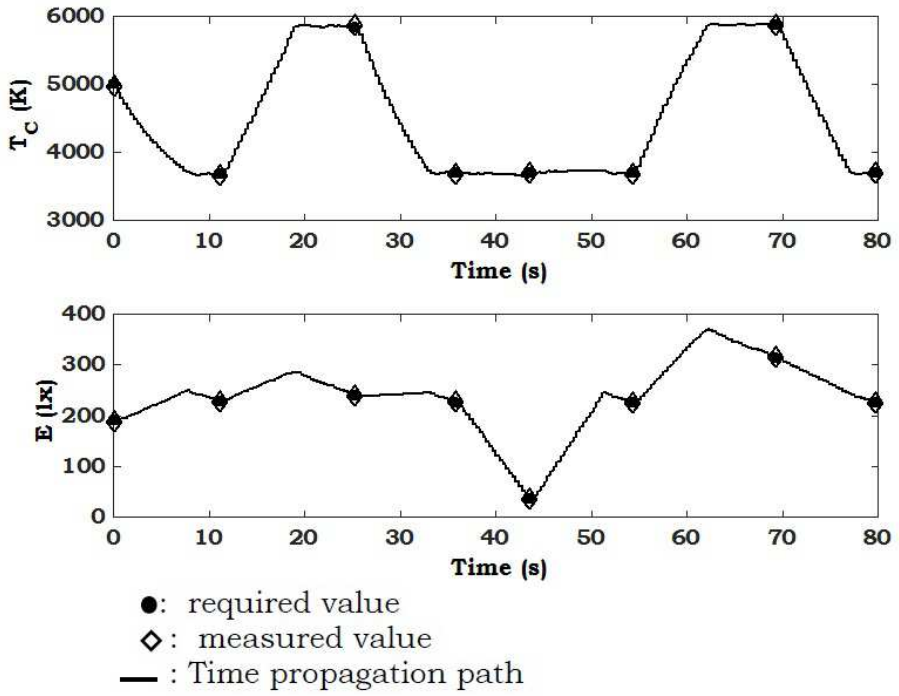

Figure 6.14: Laboratory testing of the closed-loop DLS

In-situ testing

Similar to open-loop system, the performance of the closed-loop DLS under *in-situ* testing is carried out in the same room with same settings. The testing is conducted at different times of different days in the month of November with partly cloudy sky conditions. The instantaneous values of T_C and E corresponding to external light scene, required light scene and measured internal light scene due to DLS are presented graphically in **Figure 6.15**. Three different time spans are chosen for performance evaluation during anti-meridian (9:00-10:00), meridian (11:30-12:30) and post-meridian (14:15-15:15) time slots. During above three time slots, CCT of internal light scene ($T^{\alpha}_{C,M}$) follow that of required light scene ($T^{\alpha}_{C,R}$) with a maximum deviation of 84K.

Table 6.7: Laboratory test data of the closed-loop DLS: measured CCT and illuminance values with deviations

Set point	Daylight-responsive DLS									
	External source (1)		Required (2)		Measured (3)			Deviation (2-3)		
	$T_C^{\beta}(t)$ (K)	$E^{\beta}(t)$ (Lux)	$T_{C,R}^{\alpha}(t)$ (K)	$E_R^{\alpha}(t)$ (Lux)	$T_{C,M}^{\alpha}$ (K)	E_M^{α} (Lux)	ΔT_C^{α} (K)	ΔE^{α} (Lux)	D_{uv}	Step Size (n)
1	3679	877.8	3707	228.4	3661	228.6	18	-0.2	0.0015	2
2	5841	815.4	6190	239.2	5866	239.4	-25	-0.3	0.0025	4
3	3700	889.4	3700	226.4	3676	226.8	24	-0.5	0.0016	3
4	3658	2000	3700	35.0	3690	35.2	10	-0.2	0.0017	3
5	3701	893.4	3700	225.7	3689	226.4	11	-0.7	0.0017	3
6	5863	380.8	5863	314.2	5871	314.9	-8	-0.6	0.0026	4
7	3701	889.4	3701	226.4	3693	226.5	8	-0.1	0.0019	3

The illuminance of the external light scene (E^{β}) gradually increases while that of internal light scene (E_M^{α}) gradually decreases during the time slot 9:00-10:00. The reverse pattern is observed for the time slot 14:15-15:15. However, during the time slot 11:30-12:30, E_M^{α} remains practically constant since E^{β} also remains more or less constant. To show whether the measured internal light scene due to the DLS is highly correlated or loosely correlated with the required light scene, the correlation coefficient (*r*) values are calculated for the above time slots and presented in **Table 6.8**.

The overall D_{uv} values [Ohno 2014] for the three time slots are also calculated and shown in **Figure 6.16** along with the target D_{uv} and the maximum allowable tolerance values. These calculated D_{uv} are within the acceptable tolerance limits. Overall maximum deviation between required and achieved illuminance is found to be 5 *Lux* which is 3.1% of the required value of 162 *Lux* and far below the acceptable maximum deviation of illuminance [Anonymous 1992]; whereas in case of CCT that is found to be 84*K* with respect to required value of 5689*K* and within the acceptable limit of CCT variation [Anonymous 2008a; Chen et al. 2014]. Maximum D_{uv} is found to be 0.0032 which corresponds to step size 4 of MacAdam ellipse. Moreover, out of 4658 measured data points, 4621 data points yield deviation in CCT within the tolerance value (30*K*) and 4608 data points yield deviation in illuminance within the tolerance value (1 *Lux*) which established the acceptable performance of the iterative closed-loop light control scheme.

Table 6.8: Correlation coefficient values for three time slots

Time slot	Correlation coefficient (*r*) value	
	CCT	Illuminance
9:00-10:00	0.7387	0.9976
11:30-12:30	0.7663	0.9592
14:15-15:15	0.9443	0.9995

The above deviations and the *r* values establish the effectiveness

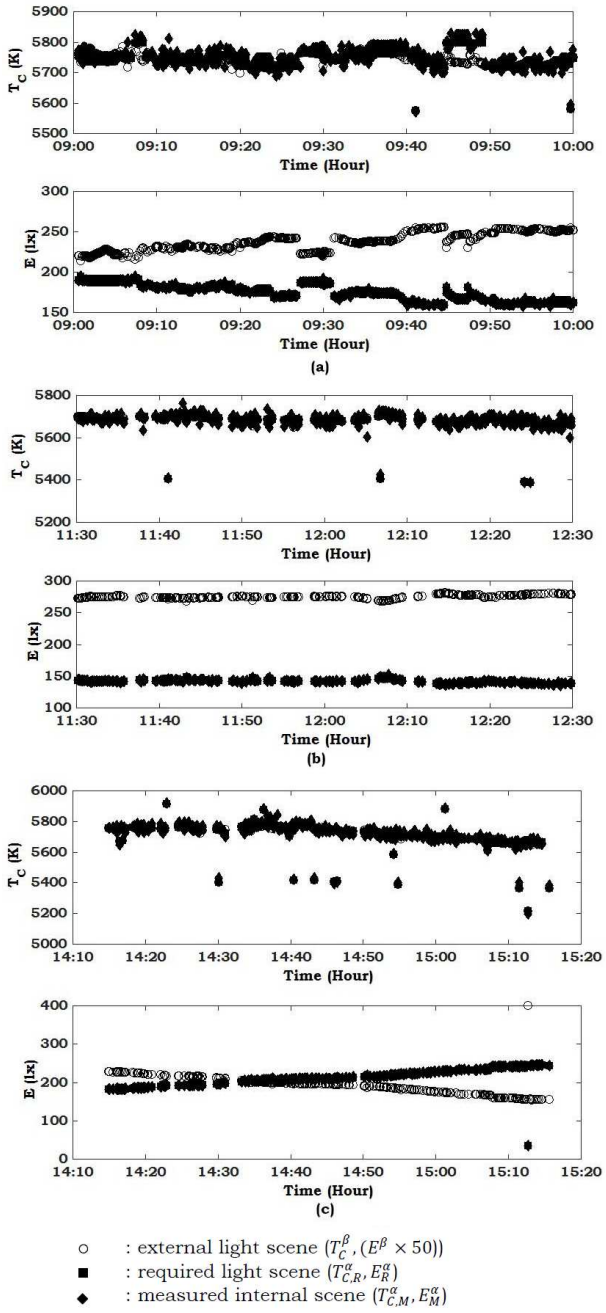

Figure 6.15: *In-situ* testing of the closed-loop DLS at different time interval (a) 9:00-10:00, (b) 11:30-12:30, (c) 14:15-15.15

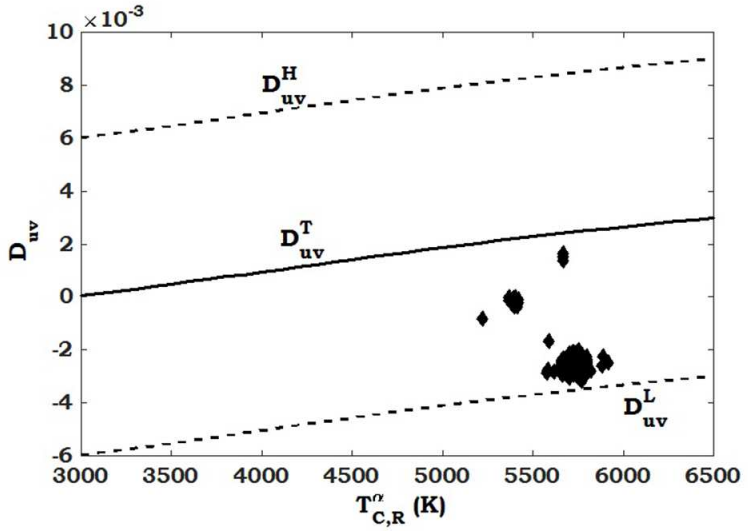

Figure 6.16: Overall chromaticity deviation (D_{uv}) of closed-loop DLS during in-situ testing

of the closed-loop light control algorithm as well as the satisfactory performance of the daylight responsive closed-loop light controller.

Summary

In this chapter, desired attributes of a daylight-responsive dynamic lighting system is realised by two light control schemes viz., open-loop and closed-loop. A RGB color sensor monitors the instantaneous daylight scene at window plane and accordingly tunes the DLS under open-loop light control scheme. In addition to this sensor, another RGB color sensor is used in feedback of the closed-loop system to monitor the internal light scene due to DLS. The RGB color sensors are calibrated with the *CL 200A* chromameter and a correlation matrix is developed to transform the measured *R,G,B* values into corresponding *X,Y,Z* values.

Apart from the instatntaneos tuning, the developed DLS is capable

of compensating the variation of light output due to rise in ambient temperature as well as junction temperature and also due to lumen depreciation over time.

Prototype DLS for both the control schemes are fabricated and the permormance is evaluated experimentally by laboratory testing and *in-situ* testing and found satisfactory performance.

Parts of the work presented in this chapter are reported in the following publications-

1. *Maiti PK, Roy B. 2019. Evaluation of a daylight-responsive, iterative, closed-loop light control scheme. Lighting Research & Technology. (SAGE). DOI: 10.1177/1477153519853318.*
2. *Maiti PK, Singh AD, Roy B. 2-3 Dec. 2017. Design and development of daylight responsive RF light controller. 2017 IEEE Calcutta Conference (CALCON). 309-313.*

Chapter 7

Conclusions and Future Scope

7.1 Conclusions

The daylight-integrated lighting system demands a special type of light source of tunable spectral composition and luminous flux in accordance with those of daylight available at the window plane or installed daylighting system. Variation of spectral composition of daylight results in variation of its correlated color temperature (CCT).

In this study the objective is set firstly to design and development of dynamic artificial lighting system whose spectral composition and light output vary according to variable CCT and illuminance of available external daylight. In the second stage of the study the objective is set to evaluate the developed system in terms of its performance to achieve desired output.

Accordingly the primary objective is subdivided in to two objectives viz., (1) development of dynamic lighting system and (2) its performance evaluation.

Attempts are made to design the target lighting system by using two types of LED chips of two different spectral compositions such that one emits yellowish-white (WW) and the other emits bluish-white (CW) light energy. **Chapter 4** describes the systematic design and development procedures followed to obtain a composite LED module – referred as lamp module of the target dynamic lighting system (DLS). This lamp module is tested to verify the compliance of the measured photometric parameters (CCT and lumen output) with those of the target values. The developed lamp system exhibits the range of CCT from 2840-5750*K* while the target range is 2700-6000*K*. On the other hand, it exhibits the range of lumen output from 0-648 *lm* while the target range is 0-600 *lm*. Since the differences of upper and lower limits of CCT are within the acceptable limits, the developed lamp module is found suitable for subsequent experimentation.

To operate the developed LED lamp module as a tunable lighting system, a light controller is designed and developed. **Chapter 5**

deals with the step-wise design and development procedure followed to obtain the desired light controller – referred as dynamic light controller (DLC). Light control logic of developed DLC is based on Grassman's color mixing law and hence the range of CCT variation of the test light source lies within the CCT values of the WW and the CW LEDs. A pulse width modulation (PWM) technique is applied to implement the light control logic and embedded in a PIC 18F4550 microcontroller to control the light output of two WLED arrays through enhanced PWM mode with dual PWM output. The developed controller is connected with the test light source and controllable by infrared (IR) remote within a distance of 4 *m*. Here the developed DLC is an integrated module consisting of an IR receiver, IR decoder, control signal (PWM) generator, amplifier, and switching device. Another study is made to control the developed system using RF communication. Performance evaluation of the developed DLC was carried out by driving the DLS for three operational modes viz., (1) variable illuminance at fixed CCT, (2) variable CCT at fixed illuminance and (3) variable CCT and variable illuminance. Under the first mode of operation, the DLC operates as a simple dimmer whereas under the second and third mode of operations, it operates as color-tunable light controller. Performance of the developed DLC is experimentally validated for a set of desired CCT points (2840–5750*K*) and constant illuminance (300 *Lux*) measured at a fixed distance. Measured CCT values show maximum deviation of 160*K* and 194*K* for warm white and cool white regions, respectively, compared to desired CCT points. On the other hand, the deviation of measured illuminance values lies within -9.7% to +8.3% with respect to set illuminance value of 300 *Lux*. Variations of measured CCT lie within the acceptable range. Experimental results establish the satisfactory performance of the developed DLC.

Furthermore, scope of modification in the embedded control logic is made available to operate under mode (3) to vary both the CCT and illuminance of the DLS either in steps or continuously to follow a pre-set time-varying pattern to generate dynamic light scene in an indoor environment. Step variation performance is tested with 16 possible combinations of four CCT values (range: 2900–5600*K*)

and four illuminance values (range: 100–300 *Lux*). Experimental result shows that all the 16 set points are realised without any perceived flicker and the observed variations of measured CCT points are within an acceptable range and the variations of the measured illuminance values are also very small ($<16\%$) and not visually perceivable. Thus, the developed DLC successfully generates the PWM signals for the desired duty cycles. On the other hand, continuous variation performance is tested with a typical pattern applicable for office lighting where CCT varies from 3000*K* to 4700*K* and illuminance varies from 200–280 *Lux* (scaled down). Satisfactory performance of the DLC is observed based on the generated PWM signals of the desired duty cycles. But for the dynamic light source, significant variations are observed at two points of lower CCT values. Deviated light output of the CW LED array from the estimated light output at lower duty cycles($<10\ \mu s$) causes these variations.

At the final stage of the system development, the developed DLS is upgraded accordingly to make it daylight responsive. It is achieved by two control schemes, viz., (1) open-loop and (2) closed-loop. **Chapter 6** describes the development and evaluation of these two control schemes.

Under the open-loop control scheme, the system functions primarily with the response signal of one RGB color sensor - daylight sensor (S_{ext}) to monitor the CCT and illuminance of available external daylight at window plane. Depending on the measured external light scene, the light controller estimates the required lumen contribution from the individual LED array to follow the instantaneous CCT of daylight and at the same time to respond to the variation of window plane illuminance in reverse pattern. Then corresponding duty cycles, computed from an experimentally evaluated empirical non-linear relationship between duty cycle and lumen output of individual LED array, are estimated for both the LED arrays. The performance of the developed open-loop light controller is experimentally evaluated by laboratory testing and in-situ testing. Under laboratory testing, the performance is tested with the sudden (step) variation of external CCT and illuminance. Here five test conditions are simulated using an external light source and cor-

responding output of DLS is measured. The maximum deviations in CCT, illuminance and chromaticity from the required values are found as 99*K*, 7.8 *Lux* and 0.0018 respectively. Under *in-situ* testing, the performance is evaluated with available natural daylight by placing the S_{ext} at mid-height of the window plane and maximum deviations in CCT, illuminance and chromaticity from the required values are found as 280*K*, 9.9 *Lux* and 0.0053 respectively. Moreover, out of 710 measured data points, 682 data points yield deviation in CCT $<$100*K* and 694 data points yield deviation in illuminance $<$5 *Lux*.

Under the closed-loop control scheme the system functions primarily with the response signals of two RGB color sensors, viz., daylight sensor to monitor daylight scene at window plane and internal light sensor to monitor the light scene created by the test lamp module. The control scheme controls the lumen delivery of individual LED arrays of the test lamp module by adjusting the duty cycles to follow the instantaneous external daylight CCT and at the same time variation of external illuminance in reverse pattern similar to open-loop system. Evaluation is conducted by laboratory testing and *in-situ* testing. The maximum deviations in CCT, illuminance and chromaticity from the required values under laboratory testing are found as 25*K*, 0.7 *Lux*, 0.0032. Under *in-situ* testing the maximum deviations are found to be 84*K*, 5 *Lux*, 0.0032 respectively. Moreover, out of 4658 measured data points, 4621 data points yield deviation in CCT within the tolerance value (30*K*) and 4608 data points yield deviation in illuminance within the tolerance value (1 *Lux*) which established the acceptable performance of the iterative closed-loop light control scheme.

One limitation of the developed system is required time of convergence to a desired point. The convergence time of the order of 10*s* is observed due to small size step variation of duty cycles with in-between delay which is necessary to avoid perceived flicker during continuous variation of CCT and illuminance.

The outcome of the present study is a WLED based daylight-responsive dynamic lighting system which is capable of tuning its lumen output as well as CCT by monitoring light level and CCT of available daylight at window plane.

7.2 Prospective Applications

The developed dynamic lighting control system has two prospective applications- energy saving through dimming of artificial light source and simulation of dynamics of daylight.

For daylight integrated lighting system where the useful daylight illuminance (UDI) is greater than the required light level, the application of the developed system is cost-effective and energy efficient. The developed lighting control system continuously adjusts the CCT of the artificial light sources to cope up with the dynamics of daylight. Apart from that, the developed control system dimmed the light output of the artificial light sources when the UDI is greater than the required light level. Hence a significant amount of electrical energy can be saved through the dimming of the artificial light sources.

The indoor spaces where the daylight availability is limited or even absent, the developed light control system is very effective to simulate the dynamics of daylight in the work space. This application of the developed system has no economical benefit but has biological and psychological impacts on the occupants. This aspect of the dynamic lighting system has been already discussed in Chapter 1.

7.3 Future Scope

This study can be extended to evaluate the developed system with a full scale daylight-integrated indoor lighting installation where the internal light sensor will be exposed to the lighting ambience contributed by both daylight coming through windows and artificial

light emitted by the developed lighting system. The daylight sensor used in this work, can measure the light level around 25000 *Lux*. If the sensor is exposed to direct sunlight, then the illuminance value exceeds the limit of the sensor. In that case, one suitable attenuator (here neutral density (ND) filter) is to be used over the sensor so that the incident radiation is reduced to the limiting value, here 25000 *Lux*. For example, the maximum value of the global illuminance at the window plane is around 100000 *Lux* for a typical sunny day during summer in Kolkata, when exposed to direct daylight. To use the light sensor *TCS34725* in the direct daylight, ND filter with optical density (OD) greater than 0.6 is to be placed over the sensor.

The performance of the developed system has been evaluated for north-west facing single window with a single light source. However, the system is capable of controlling simultaneously a number of light sources in a group, limited by the rating of the switching devices. It is also capable of processing signals from at most eight light sensors as *TCA9548A)* can handle eight I^2C modules. Furthermore, incorporation of another I^2C multiplexer will enable the system to communicate with more light sensors. This facilitates zone-specific control of light sources adjacent to windows with different orientations.

Furthermore, the DLS can be made circadian supportive by incorporating blue LED chip of suitable peak radiation wavelength with the WW and CW LED chips in the developed composite LED module. To judge the effectiveness of the circadian supportive light source, further study with a full-scale lighting installation is to be conducted.

Bibliography

HC Albu, L Halonen, E Tetri, F Pop, and D Beu. Luminous and power quality analysis of office building light sources. *Lighting Research & Technology*, 45(6):740–751, 2013. doi: 10.1177/1477153512455941.

Anonymous. *LM158, LM158A, LM258, LM258A,LM358, LM358A, LM358B, LM2904, LM2904B, LM2904V: Industry-Standard Dual Operational Amplifiers*. Texas Instrumentation, 1976. URL http://www.ti.com/lit/ds/symlink/lm358.pdf. Accessed 2014 June 15.

Anonymous. Code of practice for interior illumination, 1992. IS 3646: 1992, Part I.

Anonymous. *User's guide-AC Power Solotions-Agilent Models 6811B, 6812B and 6813B*. Agilent Technologies, 1998. URL http://ridl.cfd.rit.edu/products/manuals/agilent/power%20supplies/cd1/Model/6811usr.pdf. Acceesed 2015 March 15.

Anonymous. *IRFP250N HEXFET® Power MOSFET*. International Rectifier, 2000. URL http://pdf1.alldatasheet.com/datasheet-pdf/view/68504/IRF/IRFP250N.html. Accessed 2014 July 13.

Anonymous. *Vishay Telefunken photo modules for PCM remote control systems*. Vishay Inc, 2001. URL http://www.batronix.com/pdf/tsop17xx. pdf. Accessed 2013 September 1.

Anonymous. Ocular lighting effects on human physiology and behaviour. Technical Report 158, Commission Internationale de L'Eclairage, Vienna (Austria), 2004a.

Anonymous. Colorimetry. Tchnical Report CIE 15, Commission Internationale de L'Eclairage, 2004b. 3rd Edition.

Anonymous. *PIC 18F2455/2550/4450/4550 Data sheet*. Microchip Inc., 2006. URL http://ww1.microchip.com/downloads/en/devicedoc/39632c.pdf. Accessed 2012 July 31.

Anonymous. Specifications for the chromaticity of solid state lighting products, 2008a. ANSI_NEMA_ANSLG C78.377.

Anonymous. *InfiniiVision 6000 Series Oscilloscopes Data sheet*, 2008b. URL http://www.testequipmenthq.com/datasheets/Agilent-MSO6014A-Datasheet.pdf. Accessed 2017 July 20.

Anonymous. *Programmable AC/DC Power Source, APS-1102 User Manual*. GWINSTEK, 2009a. URL http://www.gwinstek.com.cn/upload/file/20181217052303947.pdf. Accessed 2015 April 28.

Anonymous. $PICKit^{TM}3$ *Programmer/Debuger User's Guide*. Microchip Technology Inc., 2009b. URL https://www.sparkfun.com/datasheets/Programmers/PICkit_3_User_Guide_51795A.pdf. Accessed 2015 January 20.

Anonymous. *WT210/WT230 Digital Power Meter User's Manual*, 4 edition, 2009c. URL http://www.yokogawa.co.jp/ftp/dist/ks/eusers/wt/ked5s/im/IM760401-01E_041.pdf. Accessed 2015 April 26.

Anonymous. *TCS3472 Color light-to-Digital converter with IR filter*. Texas Advanced Optoelectronic Solutions Inc., 2012a. URL https://cdn-shop.adafruit.com/datasheets/TCS34725.pdf. Accessed 2017 October 27.

Anonymous. *Chroma meter CL-200A instruction manual*. KONICA-MINOLTA, 2012b. URL https://www.konicaminolta.com/instruments/download/instruction_manual/light/pdf/cl-200a_instruction_eng.pdf. Accessed 2015 March 15.

Anonymous. Chromaticity difference specification for light sources. Tecnical Note 001, Commission Internationale de l'Eclairage, 2014a. CIE Tecnical Note 001.

Anonymous. *Exploring Dynamic Lighting Research and Design. Light Replicator and Penta System Specifications*. Telelumen®, 2014b. URL https://nebula.wsimg.com/58ad863a9e5c99c389e899bd6e25da2b?AccessKeyId=5A7A83F73522098C3E2F&disposition=0&alloworigin=1. Accessed 2016 November 18.

Anonymous. *Ketra® S38 Tunable Lamp*. Ketra®, 2015a. URL http://ledt8bulb.com/pdf/ketra-s38-spec-sheet.pdf. Accessed 2016 November 18.

Anonymous. *Operating Instructions specbos 1201 - Short Version*. JETI, 2015b. URL https://www.jeti.com/cms/index.php/instruments-55/radiometer/specbos/specbos-1211. Accessed 2016 March 29.

Anonymous. *Adafruit Color Sensors*. Adafruit Industries, 2016a. URL https://learn.adafruit.com/adafruit-color-sensors. Accessed 2018 December 20.

Anonymous. *Color Tuning with Lutron® Controls: Application Note#579*. Lutron®, 2016b. URL www.lutron.com/TechnicalDocumentLibrary/048579.pdf. Accessed 2016 September 27.

Anonymous. *Tunable White Light Engines for warm dimming and CCT tuning*. LuxiTune^{TM}, 2016c. URL www.ledengin.com/files/products/brochures/LuxiTune_Brochure.pdf. Accessed 2016 November 18.

Anonymous. *araya®[5] CTM 0ND and CTM 0TD Installation Guide*. Lumenetix Inc., 2016d. URL http://lumenetix.com/sites/default/files/Lumenetix_CTM0G3_InstallGuide_v3.pdf. Accessed 2016 November 18.

Anonymous. *araya®[5] Logic Module Tunable Color Round LED Arrays*. lumenetix Inc., 2016e. URL http://lumenetix.com/sites/default/files/Lumenetix_ ALM0%20G3+CTM2_SpecSheet_v1.pdf. Accessed 2016 November 18.

Anonymous. *Amplifier transistors BC546B, BC547A, B, C, BC548B, C*. ON Semiconductor, 6 edition, March 2017a. URL https://www.arduino.cc/documents/datasheets/BC547.pdf. Accessed 2018 November 27.

Anonymous. *Small Signal MOSFET- 500 mA, 60 Volts*. ON Semiconductor, 7 edition, November 2017b. URL https://www.onsemi.jp/PowerSolutions/document/BS170-D.PDF. Accessed 2018 November 27.

Anonymous. *DS3231 Extremely accurate I^2C-integrated RTC/TCXO/crystal*. maxim integrated, 2018a. URL https://datasheets.maximintegrated.com/en/ds/DS3231.pdf. Accessed 2018 November 27.

Anonymous. *Micro SD card breakout board tutorial*. Adafruit Industries, 2018b. URL https://cdn-learn.adafruit.com/downloads/pdf/adafruit-micro-sd-breakout-board-card-tutorial.pdf. Accessed 2018 November 27.

Anonymous. *Adafruit TCA9548A 1-to-8 I^2C multiplexer breakout*. Adafruit Industries, 2018c. URL https://learn.adafruit.com/adafruit-tca9548a-1-to-8-i2c-multiplexer-breakout. Accessed 2018 September 27.

Anonymous. *specification of Arduino Uno Rev3*. Arduino, 2018d. URL https://store.arduino.cc/usa/arduino-uno-rev3. Accessed 2018 October 27.

I Ashdown. Chromaticity and color temperature for architectural lighting. *Society of Photo-Optical Instrumentation Engineers*, 4776:51–60, 2002.

L Belia, F Bisegna, and G Spada. Lighting in indoor environments: Visual and non-visual effects of light sources with different spectral power distributions. *Building and Environment*, 46(10):1984–1992, 2011.

PR Boyce. Review: The impact of light in buildings on human health. *Indoor and Built Environment*, 19(1):8–20, 2010. doi: 10.1177/1420326x09358028.

PR Boyce. *Human Factors in Lighting*. CRC Press, 3rd edition, 2014. ISBN 978-1-43-987488-2.

GC Brainard, JP Hanifin, JM Greeson, B Byrne, G Glickman, E Gerner, and MD Rollag. Action spectrum for melatonin regulation in humans: evidence for a novel circadian photoreceptor. *Journal of Neuroscience*, 21(16):6405–6412, 2001.

M Canazei, P Dehoff, S Staggl, and W Pohl. Effects of dynamic ambient lighting on female permanent morning shift workers. *Lighting Research & Technology*, 46(2):140–156, 2014.

H-T Chen, S-C Tan, and S. Y. Hui. Color variation reduction of GaN-based white light-emitting diodes via peak-wavelength stabilization. *IEEE Transactions on Power Electronics*, 29(7):3709–3719, jul 2014. doi: 10.1109/tpel.2013.2281812.

H-T Chen, S-C Tan, and S. Y. Ron Hui. Nonlinear dimming and correlated color temperature control of bicolor white LED systems. *IEEE Transactions on Power Electronics*, 30(12):6934–6947, dec 2015. doi: 10.1109/tpel.2014.2384199.

I Chew, V Kalavally, CP Tan, and J Parkkinen. A spectrally tunable smart LED lighting system with closed-loop control. *IEEE Sensors Journal*, 16(11):4452–4459, jun 2016. doi: 10.1109/jsen.2016.2542265.

M Cole, H Clayton, and K Martin. Solid-state lighting: The new normal in lighting. *IEEE Transactions on Industry Applications*, 51(1):109–119, jan 2015. doi: 10.1109/tia.2014.2328790.

M.H. Crawford. LEDs for solid-state lighting: Performance challenges and recent advances. *IEEE Journal of Selected Topics in Quantum Electronics*, 15(4):1028–1040, jul 2009. doi: 10.1109/jstqe.2009.2013476.

G Curcio, L Piccardi, F Ferlazzo, A Maria, GC Burattini, and F Bisegna. LED lighting effect on sleep, sleepiness, mood and vigor. In *2016 IEEE 16th International Conference on Environment and Electrical Engineering (EEEIC)*, page 1540 – 1545. IEEE, June 2016.

YAW de Kort and KCHJ Smolders. Effects of dynamic lighting on office workers: First results of a field study with monthly alternating settings. *Lighting Research & Technology*, 42(3):345–360, 2010.

EE Dikel, JA Veitch, S Mancini, HH Xue, and JJ Valdés. Lighting-on-demand: Balancing occupant needs and energy savings. *Leukos*, 14(1):3–11, oct 2018. doi: 10.1080/15502724.2017.1373597.

F Dong and AC Sanderson. A dynamic adaptive field sampling approach for smart lighting control. *Lighting Research & Technology*, 46(5):593–614, 2014.

M Dyble, N Narendran, A Bierman, and T Klein. Impact of dimming white LEDs: Chromaticity shift due to different dimming methods. In *Fifth International Conference on Solid State Lighting*, volume 5941, pages 291–299. SPIE, 2005.

D Gacio, JM Alonso, J Garcia, L Campa, M Crespo, and M Rico-Secades. High frequency PWM dimming technique for high power factor converters in LED lighting. In *2010 Twenty-Fifth Annual IEEE Applied Power Electronics Conference and Exposition (APEC)*. IEEE, feb 2010. doi: 10.1109/apec.2010.5433585.

JM Gilman, ME Miller, and MR Grimaila. A simplified control system for a daylight-matched LED lamp. *Lighting Research & Technology*, 45(5):614–629, 2013.

J Hernández-Andrés, RL Lee, and J Romero. Calculating correlated color temperatures across the entire gamut of daylight and skylight chromaticities. *Applied Optics*, 38(27):5703–5709, 1999. doi: 10.1364/ao.38.005703.

J Hernández-Andrés, J Romero, JL Nieves, and RL Lee. Color and spectral analysis of daylight in southern europe. *Journal of the Optical Society of America A*, 18(6):1325–1335, 2001. doi: 10.1364/josaa.18.001325.

L Heschong. Daylighting and human performance. *ASHRAE Journal*, 44:65–67, 2002.

KW Houser, M Wei, A David, and MR Krames. Whiteness perception under LED illumination. *Leukos*, 10(3):165–180, apr 2014. doi: 10.1080/15502724.2014.902750.

HM Jung, JH Kim, BK Lee, and DW Yoo. A new PWM dimmer using two active switches for AC LED lamp. In *The 2010 International Power Electronics Conference*, pages 1547–1551, 2010.

I-T Kim, I-H Jang, A-S Choi, and M Sung. Brightness perception of white LED lights with different correlated colour temperatures. *Indoor and Built Environment*, 24(4):500–513, mar 2015. doi: 10.1177/1420326x14528732.

J-H Kim, J-H Jung, M-H Ryu, and J-W Baek. A simple dimmer using a MOSFET for AC driven lamp. In *IECON 2011 - 37th Annual Conference of the IEEE Industrial Electronics Society*. IEEE, nov 2011. doi: 10.1109/iecon.2011.6119608.

JK Kim and EF Schubert. Transcending the replacement paradigm of solid-state lighting. *Optics Express*, 16(26):21835, dec 2008. doi: 10.1364/oe.16.021835.

Y Kim, B Cho, B kang, and D Hong. Color temperature conversion system and method using the same, 2006. US Patent No.- US 7,024,034 B2.

MT Koroglu and KM Passino. Illumination balancing algorithm for smart lights. *IEEE Transactions on Control Systems Technology*, 22(2):557–567, mar 2014. doi: 10.1109/tcst.2013.2258399.

ATL Lee, H Chen, S-C Tan, and SY Ron Hui. Precise dimming and color control of LED systems based on color mixing. *IEEE Transactions on Power Electronics*, 31(1):65–80, jan 2016. doi: 10.1109/tpel.2015.2448641.

AJ Lewy, TA Wehr, FK Goodwin, DA Newsome, and SP Markey. Light suppresses melatonin secretion in humans. *Science*, 210 (4475):1267–1269, 1980.

B Li, Q Zhai, R Luo, and F Ying. Atmosphere perception of LED dynamic lighting with color varied in cool and warm hue. In *2016 13th China International Forum on Solid State Lighting (SSLChina)*, page 114–118. IEEE, nov 2016. doi: 10.1109/sslchina.2016.7804365.

M Li, K Chen, A Rupp, D Chu, and D Vangari. Luminous flux and current uniformity analysis in linear LED modules. *Leukos*, 11 (1):19–29, 2015.

K-C Lin and C-S Lin. The study of a novel control method of the mood lighting emulator. *Optics Communications*, 350:71–76, sep 2015. doi: 10.1016/j.optcom.2015.04.001.

Y Lu, W Li, W Xu, and Y Lin. Impacts of LED dynamic white lighting on atmosphere perception. *Lighting Research & Technology*, 0:1–16, jan 2019. doi: 10.1177/1477153518823833.

DL MacAdam. *Color Measurements: Theme and Variations*. Springer, 1985.

PK Maiti and B Roy. Development of dynamic light controller for variable CCT white LED light source. *Leukos*, 11(4):209–222, apr 2015. doi: 10.1080/15502724.2015.1011784.

PK Maiti and B Roy. Development and performance assessment of white LED dimmer. *Journal of The Institution of Engineers (India): Series B*, 98(5):461–466, 2017. doi: 10.1007/s40031-017-0275-7.

PK Maiti and B Roy. Evaluation of a light controller for a LED-based dynamic light source. *Lighting Research & Technology*, 50 (4):571–582, 2018. doi: 10.1177/1477153517690798.

PK Maiti, AD Singh, and B Roy. Design and development of daylight responsive RF light controller. In *2017 IEEE Calcutta Conference (CALCON)*. IEEE, dec 2017. doi: 10.1109/calcon.2017.8280745.

R Malik, KK Ray, and S Mazumdar. Wide-range, open-loop, CCT and illuminance control of an LED lamp using two-component color blending. *IEEE Transactions on Power Electronics*, 33(11): 9803–9818, nov 2018. doi: 10.1109/tpel.2017.2785684.

R Malik, K Ray, and S Mazumdar. A low-cost, wide-range, CCT-tunable, variable-illuminance LED lighting system. *Leukos*, pages 1–20, feb 2019. doi: 10.1080/15502724.2018.1541747.

MA Mazidi, RD Mckinlay, and D Causey. *PIC microcontroller and embedded systems-using assembly and C for PIC 18*. Pearson International Edition, New Jersey, 2008.

PR Mills, SC Tomkins, and LJM Schlangen. The effect of high correlated colour temperature office lighting on employee wellbeing and work performance. *Journal of Circadian Rhythms*, 5(2):1–9, jan 2007. doi: 10.1186/1740-3391-5-2.

M Mirvakili and VJ Koomson. High efficiency LED driver design for concurrent data transmission and PWM dimming control for indoor visible light communication. In *Photonics Society Summer Topical Meeting Series*, pages 132–133. IEEE, 2012.

T Morita and H Tokura. The influence of different wavelengths of light on human biological rhythms. *Applied Human Science*, 17 (3):91–96, 1998.

JB Murdoch. *Illumination engineering-from Edison's lamp to laser*. Macmillan Publishing Company, New York, 1st edition, 1985.

S Muthu, FJP Schuurmans, and MD Pashley. Red, green, and blue LEDs for white light illumination. *IEEE Journal of Selected Topics in Quantum Electronics*, 8(2):333–338, 2002. doi: 10.1109/2944.999188.

SK Ng, KH Loo, YM Lai, and CK Tse. Color control system for RGB LED with application to light sources suffering from prolonged aging. *IEEE Transactions on Industrial Electronics*, 61(4):1788–1798, apr 2014. doi: 10.1109/tie.2013.2267696.

GS Nhivekar and RR Mudholkar. Microcontroller based ir remote control signal decoder for home application. *Advances in Applied Science Research*, 2(4):410–416, 2011.

Y Ohno. Practical use and calculation of CCT and Duv. *Leukos*, 10 (1):47–55, 2014. doi: 10.1080/15502724.2014.839020.

A Pandharipande and D Caicedo. Adaptive illumination rendering in LED lighting systems. *IEEE Transactions on Systems, Man, and Cybernetics: Systems*, 43(5):1052–1062, sep 2013. doi: 10.1109/tsmca.2012.2231859.

A Pandharipande, D Caicedo, and X Wang. Sensor-driven wireless lighting control: System solutions and services for intelligent buildings. *IEEE Sensors Journal*, 14(12):4207–4215, dec 2014. doi: 10.1109/jsen.2014.2351775.

P Pinho, T Hytönen, M Rantanen, P Elomaa, and L Halonen. Dynamic control of supplemental lighting intensity in a greenhouse environment. *Lighting Research & Technology*, 45(3):295–304, 2013. doi: 10.1177/1477153512444064.

N. Pousset, B. Rougié, and A. Razet. Impact of current supply on LED colour. *Lighting Research & Technology*, 42(4):371–383, aug 2010. doi: 10.1177/1477153510373315.

JB Protzman and KW Houser. LEDs for general illumination: The state of the science. *Leukos*, 3(2):121–142, 2006.

MS Rea and JP Freyssinier. White lighting. *Color Research & Application*, 38(2):82–92, 2013.

MS Rea, MG Figueiro, and JD Bullough. Circadian photobiology: an emerging framework for lighting practice and research. *Lighting Research & Technology*, 34(3):177–187, sep 2002. doi: 10.1191/1365782802lt057oa.

RJ Reiter. Pineal gland interface between the photoperiodic environment and the endocrine system. *Trends Endocrinology Metabolism*, 2(1):13–19, 1991.

M Rüger, MCM Gordijn, DGM Beersma, BV, and S Daan. Time-of-day-dependent effects of bright light exposure on human psychophysiology: comparison of daytime and nighttime exposure. *American Journal of Physiology-Regulatory, Integrative and Comparative Physiology*, 290(5):R1413–R1420, may 2006. doi: 10.1152/ajpregu.00121.2005.

M Royer. Lumen maintenance and light loss factors: Consequences of current design practices for LEDs. *Leukos*, 10(2):77–86, 2014. doi: 10.1080/15502724.2013.855613.

FAJL Scheer and RM Buijs. Light affects morning salivary cortisol in humans. *The Journal of Clinical Endocrinology & Metabolism*, 84(9):3395–3398, sep 1999. doi: 10.1210/jcem.84.9.6102.

EF Schubert. *Light-emitting diodes*. Cambridge University Press, New York (NY), 1st edition, 2003.

J Smith. Calculating color temperature and illuminance using the taos tcs3414cs digital color sensor, 2009. URL `https://www.ams.com/ger/content/view/download/145158`. Designer's Notebook, pp. 1–7.

C-W Tang, B-J Huang, and S-P Ying. Illumination and color control in Red-Green-Blue Light-Emitting Diode. *IEEE Transactions on Power Electronics*, 29(9):4921–4937, sep 2014. doi: 10.1109/tpel.2013.2251428.

S Tang, V Kalavally, KY Ng, and J Parkkinen. Development of a prototype smart home intelligent lighting control architecture using sensors onboard a mobile computing system. *Energy and Buildings*, 138:368–376, mar 2017. doi: 10.1016/j.enbuild.2016.12.069.

Y Uhm, I Hong, G Kim, B Lee, and S Park. Design and implementation of power-aware LED light enabler with location-aware adaptive middleware and context-aware user pattern. *IEEE Transactions on Consumer Electronics*, 56(1):231–239, feb 2010. doi: 10.1109/tce.2010.5439150.

A Žukauskas, MS Shur, and R Gaska. *Introduction to solid-state lighting*. John Wiley & Sons, New York (NY), 1st edition, 2002.

WJM van Bommel. Non-visual biological effect of lighting and the practical meaning for lighting for work. *Applied Ergonomics*, 37 (4):461–466, jul 2006. doi: 10.1016/j.apergo.2006.04.009.

F-C Wang, C-W Tang, and B-J Huang. Multivariable robust control for a Red-Green-Blue LED lighting system. *IEEE Transactions on Power Electronics*, 25(2):417–428, feb 2010. doi: 10.1109/tpel.2009.2026476.

HH Wang, M Ronnier Luo, P Liu, Y Yang, Z Zheng, and X Liu. A study of atmosphere perception of dynamic coloured light. *Lighting Research & Technology*, 46(6):661–675, oct 2013. doi: 10.1177/1477153513506591.

AR Webb. Considerations for lighting in the built environment: Non-visual effects of light. *Energy and Buildings*, 38(7):721–727, jul 2006. doi: 10.1016/j.enbuild.2006.03.004.

C-C Wu, N-C Hu, J-N Chen, and H-I Chang. Parameterised LED current regulator for pulse width modulation switch delay for accurate colour mixing in multi-LED light sources. *Lighting Research & Technology*, 46(2):171–186, 2014. doi: 10.1177/1477153512469622.

QY Zhai, MR Luo, and XY Liu. The impact of illuminance and colour temperature on viewing fine art paintings under LED lighting. *Lighting Research & Technology*, 47(7):795–809, jul 2014. doi: 10.1177/1477153514541832.

Appendix A

Instruments Used for Experimentation

The technical specifications of the instruments (arranged in alphabetic order) used in this study have been listed below:

A.1 Chromameter

The Chromameter is used to measure the CCT and chromaticity coordinates of the different sources. It is also used to measure illuminance level and to calibrate the RGB color sensors. The details of the Chromameter as shown in **Figure A.1** are given below:

Maker's Name: KONIKA MINOLTA

Model Number: *CL 200*; *CL 200A*

Technical Specifications [Anonymous 2012b]:

Illuminance (E_V): 0.1-99990 *Lux*.
CCT (T_C): 2300-20000 *K*.

Figure A.1: *CL 200A* Chromameter

A.2 Digital Multimeter

The Digital Multimeter as shown in **Figure A.2** is used to measure the voltage, current and resistance values at various circuit points. It is also used to check the continuity of the fabricated circuits. The details of the Digital Multimeter used in this project are given below:

Maker's Name: METRAVI

Model Number: *METRA Hit 29S*

Technical Specifications:

0-1000*V* (both AC and DC)
0-300*mA*-10*A* (both AC and DC)

A.3 Digital Power Meter

The Digital Power Meter shown in **Figure A.3** is used to measure the voltage, current and power across the LED luminaire during

Figure A.2: METRAVI Digital Multimeter

the experiment. The details of the Digital Power Meter are given

Figure A.3: WT 210 Digital Power Meter

below:

Maker's Name: YOKOGAWA Electric Corporation

Model Number: *WT 210*

Technical Specifications [Anonymous 2009c]:

Instantaneous Maximum Allowable Input (1 period, for 20*ms*):
Peak value of 2.8*kV* or RMS value of 2.0*kV*, whichever is less.
Peak value of 450*A* or RMS value of 300*A*, whichever is less.

Continuous Maximum Allowable Input:
Peak value of 1.5*kV* or RMS value of 1.0*kV*, whichever is less.
Peak value of 100*A* or RMS value of 30*A*, whichever is less.

A.4 Integrating Sphere

The light output of the LED sources and also the composite LED module is measured using the Ulbricht type Integrating Sphere of diameter 2.5 *m* as shown in **Figure A.4**.

Figure A.4: Integrating Sphere

A.5 Isolation Transformer

The Isolation Transformer is used to isolate the ground of the oscilloscope from the common ground. If the isolation is not provided, then there is a chance of damage of oscilloscope due to circulation current in the ground wire. The details of the Isolation transformer are given below:

Figure A.5: Isolation Transformer

Maker's Name: Indusree, Kolkata

Model Number: *IS/00K20*

Technical Specifications:
1 phase, 50*Hz*, AN cooling, 500*VA*, 230*VAC*/*230VAC* (no load)

A.6 Oscilloscope

The Oscilloscope is used to study the waveforms at various junction points of the fabricated circuits. It is also used to analyse the PWM waveforms.

The details are given below:

Maker's Name: Agilent Technologies.

Model Number: *MSO6014A*

Technical Specifications [Anonymous 2008b]:
Number of Channels: 4
Bandwidth (-3dB): DC to 100*MHz*

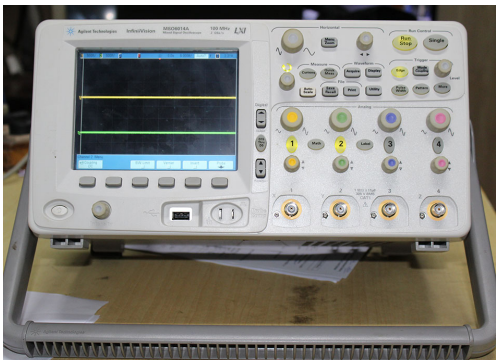

Figure A.6: *MSO6014A* Digital Storage Oscilloscope

Range: 1 *mV/div* to 5 *V/div* ($1M\Omega$)
Maximum Input: 90-264VAC_{RMS}
Input Power Frequency: CAT I- 300V_{rms} , 400V_{pk}, transient over voltage 1.6 kV_{pk}
CAT II- 100 V_{rms}, 400V_{pk}

A.7 PICKit3

The program that is written in *MPLAB IDE V8.88* software, loaded into microcontroller *PIC 18F4550* through an interface-burner. In this project *PICKit3* burner is used to load the program in *PIC*. The certain features of PICKit3 [Anonymous 2009b] are:

- Real-time Execution
- Built-in over-voltage/short circuit
- Low voltage to 5V (1.8-5V range)
- Diagnostic LEDs (power, active, status)
- Read/write program and data memory of microcontroller
- Erase of all memory types (EEPROM, ID, configuration and program) with verification

The *PICKit3* burner is shown in **Figure A.7** with its various parts labelled.

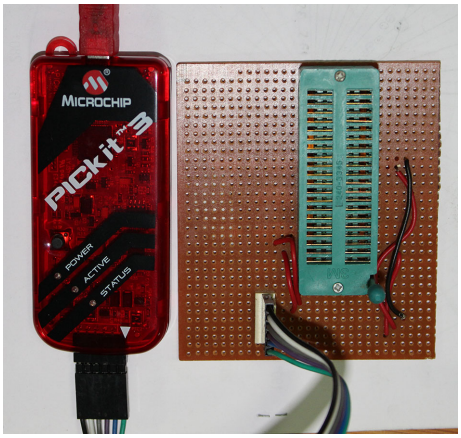

Figure A.7: PIC burner- PICKit3

A.8 Regulated AC Power Supply

Two regulated AC power supply are used to provide constant voltage, constant frequency supply. They are-

1. Agilent *6812B* AC Power Source/Analyser
2. GWINSTEK *APS-1102* Programmable AC/DC Power Source

The details of Agilent *6812B* AC Power Source/Analyser as shown in **Figure A.8(a)** are given below:

Maker's Name: Agilent Technologies

Model Number: *6812B*

Technical Specification [Anonymous 1998]:
0-230V_{rms}; 750*VA* (425V_{peak}; 40A_{peak})
The details of GWINSTEK *APS-1102* Programmable AC/DC Power

(a) (b)

Figure A.8: (a) *6812B* AC Power Source/Analyser and (b) *APS-1102* Programmable AC/DC Power Source

Source as shown in **Figure A.8(b)** are given below:

Maker's Name: GWINSTEK

Model Number: *APS-1102*

Technical Specifications [Anonymous 2009a]:
$100V_{rms}$ ($100V$ range) or $200V_{rms}$ ($200V$ range),
$1kVA$ (during AC $200V$ input)

A.9 SONY IR TV Remote

SONY IR TV remote as shown in **Figure A.9** is used in the performance evaluation of the developed DLS. Each key of this remote is assigned for a particular light scene. The sun-program written in the PIC*18F4550* microcontroller of the developed DLC. Some function keys and corresponding command in decimal value are presented in **Table B.1**.

Figure A.9: SONY IR TV Remote

A.10 Spectro Radiometer

For the measurement of spectral composition of different types of light sources the spectro-radiometer is used. In this study JETI *Specbos-1211* Spectro-Radiometer is used. The details are listed below-

Maker's Name: JETI

Model Number: *Specbos-1211*

Technical Specifications [Anonymous 2015b]:
Spectral Range: 350-1000 *nm*
Measuring range luminance: 0.1- 100000 cd/m^2
Measuring range illuminance: 2- 500000 *Lux*

Table A.1: SONY IR TV remote keys and corresponding command

Remote Key	Command (Decimal value)
1	0
2	1
3	2
4	3
5	4
6	5
7	6
8	7
9	8
0	9
Channel+	16
Channel-	17
Volume+	18
Volume-	19
Mute	20
Power	21

Figure A.10: Specbos-1211 Spectro-Radiometer

Appendix B

Usage of PIC 18F4550

Usage of *PIC 18F4550* registers are listed in **Table B.1**. **Eqns. B.1, B.2 and B.2** are used to calculate PWM period, duty cycle and delay in time respectively.

Table B.1: Usage of *PIC 18F4550* registers [Maiti and Roy 2015]

Register	Bit(s)	Usage
CCP1CON	$< 7:6 >$	Configuration of enhanced PWM functionality
	$< 5:4 >$	Storage of two LSBs of duty cycle
	$< 3:0 >$	Selection of polarity of PWM outputs
PR2	$< 7:0 >$	Storage of PWM period
CCPR1L	$< 7:0 >$	Storage of eight MSBs of duty cycle
ECCP1DEL	$< 7:0 >$	Storage of delay period

$$PWM\ \ Period = (PR2 + 1) \times 4 \times T_{OSC} \times N \tag{B.1}$$

$$Duty\ \ Cycle = (CCPR1L : CCP1CON < 5:4 >) \times T_{OSC} \times N \tag{B.2}$$

$$Delay\ \ Period = 4 \times T_{OSC} \times (ECCP1DEL < 6:0 >) \tag{B.3}$$

Where *N* and T_{OSC} are clock prescaler and inverse of oscillator frequency (F_{OSC}) respectively.

For N =1, F_{OSC}=10 *MHz* and *PR2*=249 the value of PWM period is calculated using **Eqn. B.1** as

$$PWM\ \ Period = (249 + 1) \times 4 \times \frac{1}{10} \times 1\ \ \mu s = 100 \mu s$$

$$Hence, \quad PWM\ \ Frequency = \frac{1}{PWM\ Period} = \frac{1}{100\ \ \mu s} = 10kHz.$$